Three-dimensional measurements of aerosol mixing state during CalNex using aircraft aerosol time-of-flight mass spectrometry

Final Report to California Air Resources Board
Contract No. 09-333

Prepared for
The California Air Resources Board and the California Environmental Protection Agency

September 16, 2013

Principal Investigator
Kimberly A. Prather

Contributors
John F. Cahill
Kaitlyn J. Suski
Alberto Cazorla
Cassandra J. Gaston

Department of Chemistry & Biochemistry
University of California San Diego
9500 Gilman Drive, MC 0314
La Jolla, CA 92093-0314

Disclaimer

The statements and conclusions in this Report are those of the contractor and not necessarily those of the California Air Resources Board. The mention of commercial products, their source, or their use in connection with material reported herein is not to be construed as actual or implied endorsement of such products.

Acknowledgements

This Report was submitted in fulfillment of ARB Contract No. 09-333, Three-dimensional measurements of aerosol mixing state during CalNex 2010 using aircraft aerosol time-of-flight mass spectrometry by the University of California, San Diego, under the sponsorship of the California Air Resources Board. Work was completed as of September 16, 2013. For ship measurements the authors would like to thank Derek Coffman, Drew Hamilton, and the entire crew of the R/V Atlantis for assistance during the CalNex field campaign. Chris Cappa is acknowledged for assistance with filtering out ship exhaust time periods. Dan Cziczo is acknowledged for assistance prior to the CalNex campaign. Eric J. Williams and Brian Lerner are acknowledged for use of NO_X and NO_Y data onboard the R/V Atlantis. We gratefully acknowledge the NOAA Air Resources Laboratory for the provision of the HYSPLIT transport model and READY website (http://ready.arl.noaa. gov/HYSPLIT.php). The authors also gratefully acknowledge the Southern California Coastal Ocean Observing System (SCCOOS) (www.sccoos.org/) for the provision of harmful algal bloom data. We would like to thank the field staff involved in the deployment of the G1 during CARES and CalWater. The deployment of the G-1 was funded by the Atmospheric Radiation Measurement (ARM) Program sponsored by the US Department of Energy (DOE), Office of Biological and Environmental Research (OBER) and the US DOE's Atmospheric System Research (ASR) Program under Contract DE-AC06-76RLO 1830 at PNNL for CARES, and by the California Energy Commission under contract CEC 500-09-043 and 500-09-032 for CalWater. The deployment of the Twin Otter during CalNex was supported by NOAA grant NA090AR4310128. We also would like to thank the people involved during the CalNex campaign, and especially to Haflidi Jonsson who provided useful insight with the optical measurements from the Twin Otter. We also would like to thank all the PI investigators and their staff for establishing and maintaining the AERONET sites used in this investigation. The entire Prather group is acknowledged for helpful comments and discussion.

Three-dimensional measurements of aerosol mixing state during CalNex 2010 using aircraft aerosol time-of-flight mass spectrometry

Table of Contents

List of Figures

List of Tables

Glossary of Abbreviations and Terms

λ^{-1}	Reciprocal wavelength
AAE	Absorption Ångström Exponent
A-ATOFMS	Aircraft-Aerosol time-of-flight mass spectrometer
AERONET	Aerosol robotic network
Aged Soot	Soot mixed with organic carbon
AM	Amine
AOD	Aerosol spectral optical depths
Art2a	Adaptive resonance theory
ATOFMS	Aerosol time-of-flight mass spectrometer
BB	Biomass burning
BIO	Biological
CalNex	Research at the Nexus of Air Quality and Climate Change
CARB	California Air Resources Board
CARES	Carbonaceous Aerosols and Radiative Effects Study
CCN	Cloud condensation nuclei
CEC	California Energy Commission
CIRPAS	Center for Interdisciplinary Remotely-Piloted Aircraft Studies
CN	Condensation nuclei
CPC	Condensation nuclei counter
D	Dust
DOE	Department of Energy
DOY	Day of year

dva	Vacuum aerodynamic diameter
EAE	Extinction Ångström Exponent
EC	Elemental carbon or soot
G-1	DOE Gulfstream–1
HMOC	High mass organic carbon
HP	Highly processes
HULIS	Humic-like substances
LA	Los Angeles
LB	Long Beach
MSA	Methanesulfonic acid
Nd:YAG	Neodymium-doped yttrium aluminum garnet
NOAA	National Oceanic and Atmospheric Administration
NoCal-1	Northern California-1
NoCal-2	Northern California-2
NPF	New particle formation
OC	Organic carbon
OS	Organosulfate
PCASP	Passive Cavity Aerosol Spectrometer Probe
PDT	Pacific daylight time (i.e. local)
PM2.5	Particulate matter < 2.5 µm
PSAP	Particle Soot Absorption Photometer
RH	Relative humidity
RPA	Relative peak area
SAE	Scattering Ångström Exponent
SOA	Secondary organic aerosol

SS	Sea salt
SSA	Single scattering albedo
UHSAS	Ultra-High Sensitivity Aerosol Spectrometer
UTC	Coordinated universal time
V-OC	Vanadium-organic carbon
YAADA	Yet Another ATOFMS Data Analyzer

Abstract

Particles in the atmosphere impact human health and climate. Knowledge of the sources of these aerosol particles, as well as how their physiochemical properties evolve once emitted, is key to accurately predict their impacts. As part of CalNex 2010, an aerosol time-of-flight mass spectrometer (ATOFMS) was used in ship and aircraft based measurements to obtain insight into the sources and properties of aerosol throughout California. Comparisons between this and other aircraft campaigns give a unique and unprecedented look into the different types of carbonaceous aerosol in California.

Carbonaceous particles were ubiquitous throughout the LA basin. The ports in Long Beach showed higher fractions of soot, from ships and local diesel traffic, compared to other areas. These particles underwent processing and acquired secondary species, such as ammonium and nitrate, rapidly after emission. Aerosol measured near the ports in Long Beach contained high amounts of sulfate and soot, relative to aerosol measured inland which contained more nitrate. In southern California, particulate secondary species were primarily nitrate rather than sulfate as encountered in northern California. Northern California sources were dominated by carbonaceous species produced by secondary biogenic compounds reacting with pollution, agricultural emissions, and traffic. Soot containing particles in northern California were generally much smaller (<100 nm) with less secondary coatings than in southern California. ATOFMS data were compared and validated against satellite optical retrievals. Secondary sources were classified well, but further improvement is needed for classification of primary sources. Six peer-reviewed scientific publications to date have used this dataset, highlighting that the results from the ATOFMS played an important role in improving our understanding of the sources of carbonaceous aerosols in California.

This page is blank intentionally.

Executive Summary

Background

Numerous studies over the last decade have utilized ground-based measurements to characterize aerosol chemical composition in California, yet these measurements do not fully capture the spatial variations of aerosol sources and processes, both regionally and vertically. These differences are critically important as the calculation of climate effects generally rely on the positioning of the aerosol regionally and in the atmospheric column. Properties such as radiative forcing and cloud activity (formation, modification, disintegration) need spatial resolution to be calculated accurately. The Research at the Nexus of Air Quality and Climate Change (CalNex) field campaign in 2010 was undertaken to better understand the regional impacts of different pollution sources in California. As part of this study, real-time, single particle mixing state aircraft and shipboard measurements were made. The extensive regional coverage provided by these studies allowed for unique insights into the variation of particle chemistry and sources in California.

Methods

The key instrument used in both aircraft and ship studies was an aerosol time-of-flight mass spectrometer (ATOFMS), which measures the size and chemical composition of individual particles in real time. Additional complementary instrumentation was on-board the aircraft and ship sampling platforms and each is discussed when mentioned or referenced. The mobile monitoring platforms included instrumentation for gas (SO_2, CO, O_3) and particulate (CPC, UF-CPC) measurements. Additionally, the CalNex data were supplemented with data from the routine ground-based air quality monitoring network.

Results and Conclusions

This project accomplished specific objectives specified for the CalNex campaign. Two published accounts utilize the extensive regional coverage provided by the CalNex study [*Cahill et al.*, 2012; *Gaston et al.*, 2012]. Using the ship ATOFMS data, important differences were observed between the northern and southern California port regions. Soot containing aerosol was found to represent the largest number fraction of submicron particles in the south, while organic carbon was more dominant in the north. Interestingly, much of the organic carbon in northern California was biogenic organic aerosols formed by local vegetation emissions mixing and reacting with local pollution. Soot particles at the Ports of Los Angeles and Long Beach were mixed with sulfate due primarily to freshly emitted shipping and port pollution. In northern California, amines and nitrate were more prevalent likely from local agricultural emissions. Using the aircraft-ATOFMS (A-ATOFMS) measurements during CalNex and CARES (Carbonaceous and Radiative Effects Study), comparisons of aerosol chemical composition over much broader regions in northern and southern California were possible. The results show a unique difference between port and regional aerosol characteristics. Nearly 88% of all A-ATOFMS measured

particles (100-1000 nm in diameter) were internally mixed with secondary species, with 96% and 75% of particles internally mixed with nitrate and/or sulfate in southern and northern California, respectively. Interestingly, the chemical composition was very different from that measured using CalNex ship measurements, providing unique contrast between measurements covering entire regions (i.e., aircraft) to those near port-influenced regions. In summary, northern California was dominated by biogenic, agriculture, and vehicle emissions and less aged than southern California PM. In contrast, southern California PM was dominated by vehicle and ship emissions with no evidence of biogenic organic species. Table 1 summarizes these findings.

Given the impact of soot on radiative forcing, calculations and the potential additional effects of organic coatings, understanding the spatial differences between these two species is important. Optical properties of an aerosol population, specifically the Absorption Ångström Exponent (AAE) and the Scattering Ångström Exponent (SAE), have become increasingly important, and have even been used to estimate aerosol chemistry [*Barnaba and Gobbi*, 2004; *Higurashi and Nakajima*, 2002; *Jeong and Li*, 2005; *Kaskaoutis et al.*, 2007; *Kaufman et al.*, 2005; *Kim et al.*, 2007; *Torres et al.*, 2005; *Yu et al.*, 2009]. The single particle and gas phase data provided by the CalNex study, as well as other studies in California between 2010 and 2011, were used to compare the chemical speciation using optical properties. Secondary sources were well-classified; however, emissions from primary sources, such as dust and fossil fuel, were often underestimated. As optical techniques are increasingly being used to estimate the composition of the aerosol, these results provide important insight into the limitations and improvements needed for these optical techniques.

Aircraft studies did not reach as high of altitudes as expected in the original proposal. Nevertheless, the differences in chemistry as a function of altitude were investigated. Soot was present in higher number fractions at low altitudes, while at altitudes near the boundary layer the aerosol had significant sulfate and nitrate present indicating the aerosol was more highly processed. Sulfate was the predominant secondary species seen at low altitudes, while nitrate was more prevelant at higher altitudes.

Region	Predominant Chemistry (ATOFMS)	Measurement
ports of Long Beach	Soot+Sulfate	Ship
inland Southern California	Soot+Nitrate	Air
Bay Area/Sacramento	Soot/OC+Amines/Nitrate	Ship
inland Northern California	Soot/OC+Sulfate	Air

Table 1: Summary of the predominant chemistry measured by the ATOFMS in regions measured by both ship and aircraft measurements

Body of Report

1.1 Introduction

1.1.1 Research Objectives

This project exploited the larger regional coverage provided by aircraft and ship-based measurements as part of the Research at the Nexus of Air Quality and Climate Change (CalNex) campaign and the unique single particle aerosol time-of-flight mass spectrometer (ATOFMS) to investigate the spatial (horizontal and vertical) variability in aerosol chemical composition. The immediate task was to compare the chemical composition of aerosols from northern and southern California with specific focus on the mixing state of carbonaceous aerosol such as soot and organic carbon. This aerosol project met one of the major goals of the CalNex program: to examine the air quality and climate effects of air pollution over California. Another objective was to examine how aerosol mixing state affects optical properties by incorporating and analyzing the collocated optical measurements during CalNex.

The aerosol mixing state provides a measure of how different chemical components are combined in an aerosol particle mixture. At the individual particle levels, mixing state refers to whether those components are internally mixed (i.e., homogeneous), externally mixed (i.e., each chemical is separate), or both. Ambient air usually contains a combination of both types, where there are external mixtures of particle types, like sea salt and soot, but those types are mixed with their own unique blend of other chemical species, like sulfate or nitrate. The cartoon in Figure 1 demonstrates these difference types of mixing states. Filter-based methods which collect and measure the composition of all particles at once must assume all particles have identical compositions (far left) and thus are internally mixed. In contrast, ATOFMS and other single particle methods measure the composition of each particle one by one. Knowing precisely the mixing state of a particle will ultimately help determine its chemically relevant properties. For example, a soot aerosol is highly absorbing, but in the presence of an organic coating this absorption can be enhanced beyond soot alone [*Moffet and Prather*, 2009]. Thus, prediction of the various effects of aerosols on climate depends upon knowledge of aerosol mixing state. Furthermore, the mixing state can be used to determine the original source of the aerosol as well as the degree of aging the aerosol has undergone in the atmosphere.

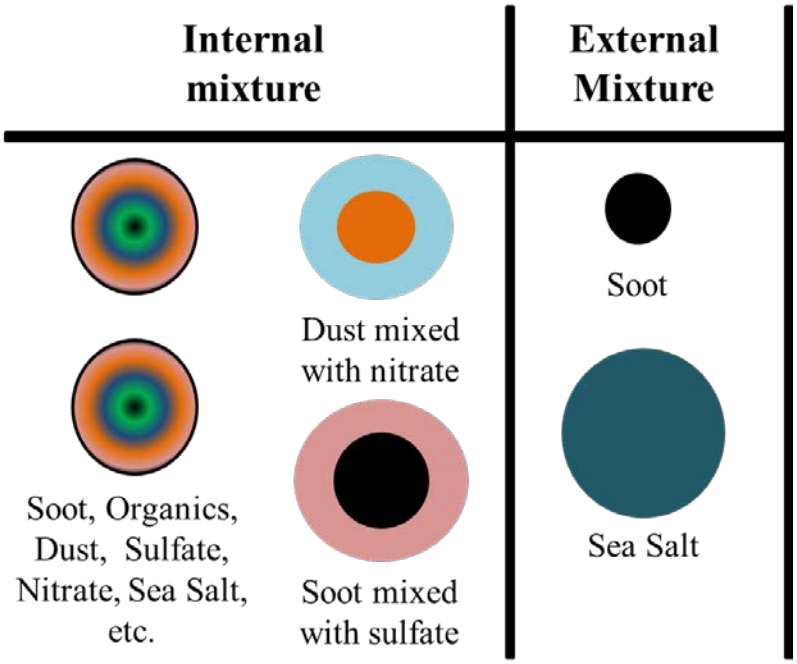

Figure 1: Exemplary cartoon of different aerosol mixing states and how they commonly appear in the atmosphere.

The goals for this project were adapted based on the limits of plane flight plans in the CalNex study, determined by the chief scientist. CalNex was comprised of ship and aircraft measurements between the dates, 14 May to 8 June 2010 and 5 May 2010 – 18 May 2010, respectively. Flights were generally limited to within the boundary layer (i.e., <1000 m). As such, it was not possible to obtain high altitude chemical data during the CalNex study. In general, the concentrations of aerosols at the highest altitudes were much lower, 1000-1500 particles/cm^3 compared to ~1700-2500 particles/cm^3, when above and within the boundary layer, respectively.

Interestingly, the amount of PM pollution encountered in northern California during the study period was much lower than that in southern California. This is shown in Figure 2 below.

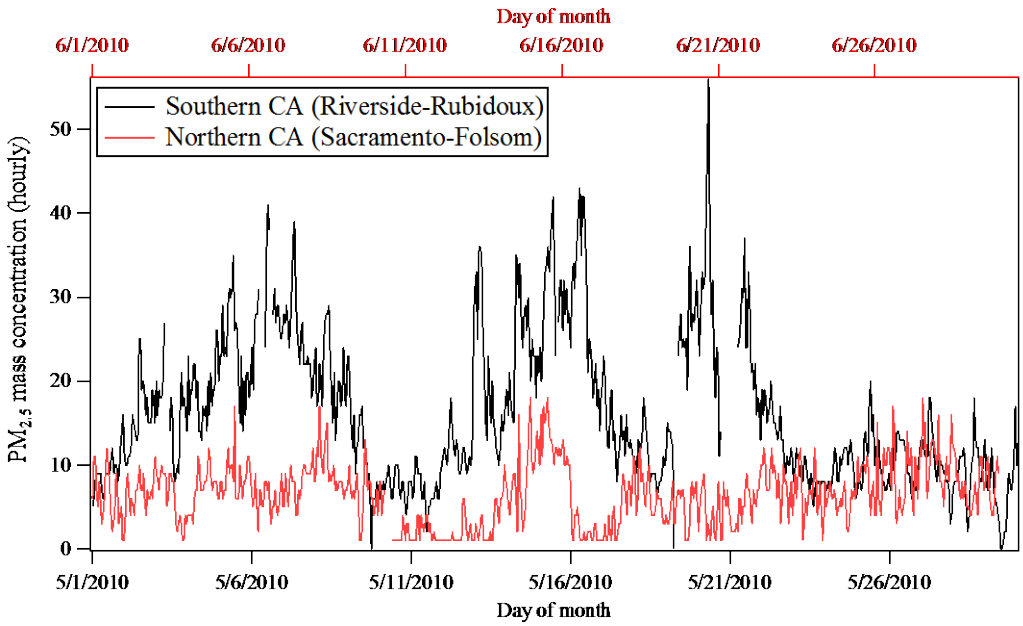

Figure 2: $PM_{2.5}$ mass concentration ($\mu g/m^3$) measured in northern (red) and southern (black) California.

In general, the pollution levels in northern California remained below 20 $\mu g/m^3$ whereas those in southern California approached 50 $\mu g/m^3$. Northern California particles had undergone far less processing and thus contained less secondary species. The soot particles in general were much smaller (<100 nm) in northern California except for the very end of the study in June when more nitrate and secondary species accumulated on the particles. Interestingly, a large contribution from biogenic emissions in the form of secondary organic species were detected in northern California. Southern California sources included ships and vehicles with higher amounts of ammonium and nitrate on the particles. It is not surprising the levels were so much higher in southern California as the population in the LA region is much larger than that of Sacramento. Thus, vehicle emissions are known to strongly impact air quality in southern California both in the form of primary as well as secondary aerosols.

Many of the original questions specified in the proposal were predicated on the initial plan that the flights would obtain high altitude data. However, high altitude flights were not performed during this study, and thus it was not possible to address some of the original questions proposed. However, the dataset obtained with the flights in CalNex was rich with information about the horizontal spatial gradients in aerosol sources and chemistry that is now being used to answer important questions about the major sources of aerosol pollution in the state of California. The overall goal of the proposal was, "… to obtain detailed data on aerosol size and chemical mixing state during CalNex in May 2010 and link it with measured optical and hygroscopic properties". The data collected during CalNex fulfills this over-arching goal. Specifically, the CalNex dataset was used to address the following questions:

1. What are the major sources contributing to black carbon or soot aerosols in California?
2. What are the differences in aerosol sources and secondary chemistry between northern and southern California?
3. What are the differences in chemical mixing state across the LA basin?
4. How accurate are the optical retrievals from satellite measurements?
5. What is vertical profile of chemical mixing state within and just above the boundary layer?
6. How does aerosol mixing state impact hygroscopic properties?

This report summarizes data obtained from both ship and aircraft measurements. The ATOFMS data were used in the publication of six peer-reviewed papers [*Cahill et al.*, 2012; *Cazorla et al.*, 2013; *Gaston et al.*, 2012; *Hersey et al.*, 2013; *Weiss-Penzias et al.*, 2013; *Zaveri et al.*, 2012]. The scope of these publications fulfills the broad array of questions to be answered in this project. As the scope of each result section of this report is sufficiently unique, a comprehensive introduction for each chapter is given below for the scientific questions to be addressed in that result. This layout was chosen to help the reader understand the specific objectives answered in each chapter.

1.1.2 The impact of shipping, agricultural, and urban emissions on single particle chemistry observed aboard the R/V Atlantis during CalNex

Atmospheric aerosols contribute to air pollution, have adverse effects on human health, and perturb the Earth's radiative balance [*Poschl*, 2005]; both aerosol size and composition play key, yet uncertain, roles in these effects. One aim of the Research at the Nexus of Air Quality and Climate Change (CalNex) field campaign was to elucidate the links between aerosols, air pollution, and climate in order to guide policies regarding emission regulations in California. Diverse particle sources impact California, including ships, vehicle exhaust, oil refineries, meat cooking, and animal husbandry and agricultural emissions. The Ports of Los Angeles (LA) and Long Beach (LB) are the busiest container ports in the United States, contributing high levels of ship and port emissions (e.g., trucks, trains, cranes, oil refinery emissions) to Southern California. Locations in inland Southern California (i.e., Riverside) and the Sacramento and San Joaquin Valley areas in Northern California are impacted by dairy farm and agricultural emissions leading to high mass concentrations of particulate matter that contain large fractions of secondary species [*Chen et al.*, 2007; *Chow et al.*, 2006b; *Docherty et al.*, 2008; *Grover et al.*, 2008; *Hughes et al.*, 2000; *Hughes et al.*, 2002; *Magliano et al.*, 1999; *Pastor et al.*, 2003; *Qin et al.*, 2012; *Sorooshian et al.*, 2008b]. Furthermore, biogenic emissions from forested regions such as the Sierra Nevada foothills and from marine biological activity along the California coast also contribute to the aerosol burden in California [*Creamean et al.*, 2011; *Gaston et al.*, 2010]. Assessing how these regional differences in particle sources and secondary atmospheric reactions impact the physicochemical properties of aerosols represents a key step in fulfilling the goals of the CalNex field campaign.

Single-particle mass spectrometry is well-suited for providing the high temporal resolution and mass spectral fingerprints necessary for distinguishing between diverse particle sources and assessing the impact of atmospheric processing (e.g., gas-to-particle partitioning, heterogeneous reactions, etc.) on particle size and chemistry [*Pratt and Prather*, 2011; *Sullivan and Prather*, 2005]. Aerosol time-of-flight mass spectrometry (ATOFMS), an on-line single-particle analysis technique, has been successfully used for the source apportionment of particulate matter in California for 17 years [*Ault et al.*, 2010; *Creamean et al.*, 2011; *Gaston et al.*, 2010; *Hughes et al.*, 2000; *Moffet et al.*, 2008; *Noble and Prather*, 1996; *Pastor et al.*, 2003; *Pratt and Prather*, 2009; *Qin et al.*, 2012; *Toner et al.*, 2008; *Whiteaker et al.*, 2002]. Herein we present real-time measurements of single-particle composition and size using ATOFMS during the CalNex campaign onboard the R/V Atlantis sampling platform. Atmospheric measurements were made off the California coast, targeting specific sources, including the Ports of LA and LB, continental outflow from the LA basin, and emissions from northern California, including the inland Sacramento area. This paper describes the significant differences observed in single-particle mixing state and the emission sources between these regions. The implications of these findings are also discussed.

1.1.3 The mixing state of carbonaceous aerosol particles in northern and southern California measured during CARES and CalNex 2010

Carbonaceous aerosols, comprised of soot and/or organic carbon (OC), affect climate directly through scattering and absorbing radiation and indirectly by influencing cloud formation, albedo, and lifetime [*Ackerman et al.*, 2000; *Poschl*, 2005; *Ramanathan et al.*, 2007; *Rosenfeld and Givati*, 2006]. Soot, formed by incomplete combustion processes, is strongly absorbing and hence plays a key role in affecting climate through radiative forcing [*Jacobson et al.*, 2000; *Kanakidou et al.*, 2005; *Ramanathan and Carmichael*, 2008; *Solomon et al.*, 2007]. OC from vehicular, biogenic, and biomass burning emissions, as well as from secondary aerosol formation, can exhibit a wide range of optical properties that depend on the mixing state of particles [*Hand and Malm*, 2007; *Jacobson et al.*, 2000; *Kanakidou et al.*, 2005; *Rudich et al.*, 2007]. Soot and OC particles can form internal mixtures with one another as well as other secondary species, such as nitrate, sulfate, and ammonium, which strongly affect their optical and physical properties [*Moffet et al.*, 2010; *Prather et al.*, 2008; *Spencer and Prather*, 2006].

Internal mixtures of OC and soot increase the absorption coefficient, leading to greater radiative forcing than predicted for either species alone [*Moffet and Prather*, 2009; *Schnaiter et al.*, 2005; *Schwarz et al.*, 2008]. For example, Schnaiter et al. [2005] measured absorption amplification factors of 1.8 to 2.1 times higher for soot with coatings than without and similarly, Moffet and Prather [2009] found an absorption enhancement of 1.6 for soot particles coated with OC and secondary species over pure soot. Previous studies have determined that water soluble coatings, such as sulfuric acid, lead to enhanced absorption over that of externally-mixed particles [*Khalizov et al.*, 2009; *Naoe et al.*, 2009]. In addition to absorption enhancement, coatings can alter particle hygroscopicity, which in turn affects the particle's optical and physical properties, as particles that are more hygroscopic will absorb more water, scatter radiation more efficiently, and have a higher potential to become cloud condensation nuclei (CCN) [*Hand and Malm*, 2007;

Mochida et al., 2006; *Wang et al.*, 2010]. Laboratory and field studies show altered hygroscopicity for photochemically aged soot, due in part to the condensation of secondary species [*Cappa et al.*, 2011; *Furutani et al.*, 2008; *Petters et al.*, 2006; *Wang et al.*, 2010]. For example, Petters et al. [2006] observed that as hydrophobic soot particles age they can become hydrophilic due to the addition of a sulfate or nitrate coating. Wang et al. [2010] determined that nitrate partitioned onto aerosols leads to increased CCN activity. Multiple studies have shown that particles can acquire coatings rapidly, sometimes in only a few hours; hence, the amount of ambient particles existing as internal mixtures may represent a sizable fraction of total ambient aerosols [*Jacobson*, 2001; *Moffet and Prather*, 2009; *Riemer et al.*, 2010; *Wang et al.*, 2010]. In addition, the aerosol optical and CCN activation properties may be sensitive to the degree of internal mixing even after 1 to 2 days [*Zaveri et al.*, 2010].

Despite the importance of mixing state on particle optical and physical properties, atmospheric models generally represent the particle population as an internal mixture [*Koch et al.*, 2011]. Chung and Seinfeld [2002] found a difference of ~0.4 W/m^2 in radiative forcing depending on if internal or external mixing state was used. Jacobson estimated that global radiative forcing of soot increases by a factor of 2.9 when varied from an external to an internal mixture [*Jacobson*, 2001]. Additionally, numerous studies have shown the sensitivity of climate to large aerosol perturbations [*Kloster et al.*, 2010; *Leibensperger et al.*, 2012; *Mickley et al.*, 2012; *Solomon et al.*, 2007]. The potentially large effect on radiative forcing calculations due to mixing state of the aerosols necessitates empirical measurements to determine the extent of soot and non-absorbing species, such as OC, present in the atmosphere as internal or external mixtures.

Single particle mixing state is gradually becoming a more prevalent measurement in field studies [*Brands et al.*, 2010; *Gard et al.*, 1997; *Murphy and Thomson*, 1995; *Zelenyuk and Imre*, 2005]. Ground-based measurements have shown the large variability in the mixing state of carbonaceous aerosols, even within just California [*Chow et al.*, 2006b; *Chow et al.*, 1993]. For example, Qin et al. [2012] found carbonaceous aerosols in Riverside, California were internally mixed with sulfate from photochemical processing during the summer, while nitrate was the dominant secondary species in the fall due to semi-volatile partitioning of ammonium nitrate. In Bakersfield, California, carbonaceous aerosols were found to be internally mixed with ammonium, nitrate, and sulfate from partitioning of ammonium nitrate and ammonium sulfate [*Whiteaker et al.*, 2002]. An inherent limitation in ground-based measurements is the susceptibility of a single sampling site to local sources. Aircraft sampling can cover large areas over short timescales, providing measurements that are indicative of an entire region and therefore may be more useful for evaluation of model predictions over large areas. Relatively few aircraft studies to date have measured single particle mixing state [*Murphy et al.*, 2007; *Pratt and Prather*, 2010; *Zelenyuk et al.*, 2010]. Herein, *in situ* measurements of carbonaceous aerosol mixing state were determined using an aircraft-aerosol time-of-flight mass spectrometer (A-ATOFMS) over two major aircraft campaigns in California during the late spring and early summer of 2010 to elucidate: 1) the fraction of carbonaceous particles that are internally and externally mixed and 2) the differences in mixing state of carbonaceous particles between the two regions studied.

The Research at the Nexus of Air Quality and Climate Change (CalNex) campaign primarily sampled aerosols over southern California, with the goal of understanding the role of particle composition on air quality and climate change (www.esrl.noaa.gov/csd/calnex/). A large area of

northern California was characterized during the Carbonaceous Aerosols and Radiative Effects Study (CARES), a study that sought to follow the evolution of soot as particles are transported from fresh urban sources in Sacramento into the more remote Sierra Nevada foothills (campaign.arm.gov/cares/). These two studies overlapped, with CalNex beginning in May and CARES in June of 2010, and provide an assessment of particle mixing states throughout much of California during late spring and early summer.

1.1.4 Relating aerosol absorption due to soot, organic carbon, and dust to emission sources determined from in-situ chemical measurements

Atmospheric aerosol particles are one of the most variable components of the Earth's atmosphere, and affect the Earth's radiative balance and climate directly by absorbing and scattering solar radiation [*Haywood and Shine*, 1995; *Solomon et al.*, 2007], and indirectly by acting as cloud condensation nuclei, changing the microphysical properties of clouds [*Kaufman et al.*, 2005; *Solomon et al.*, 2007].

Carbonaceous particles (elemental carbon, EC, and organic carbon, OC) and mineral dust are the most strongly absorbing aerosol particles. The absorbing fraction of carbonaceous aerosols has been estimated as the second largest contributor to global warming [*Jacobson et al.*, 2000; *Ramanathan and Carmichael*, 2008]. However, the absorbing properties strongly depend on the mixing state of the particles [*Bond and Bergstrom*, 2006; *Schnaiter et al.*, 2005]. Further, current model estimates of aerosol forcing ascribe solar absorption entirely to EC, treating the organic fraction (OC) as scattering [*Koch et al.*, 2007; *Myhre et al.*, 2008] and therefore may be underestimating the aerosol warming potential. Though this is a reasonable assumption in regions dominated by fossil fuel combustion, not only does carbon from all emission sources contain both elemental and organic fractions [*Chow et al.*, 2009], but non-soot OC, particularly that emitted from biomass burning processes has a significant absorbing component at short wavelengths that may be comparable to the EC absorption[*Andreae and Gelencser*, 2006; *Hoffer et al.*, 2006; *Jacobson*, 1999; *Kirchstetter et al.*, 2004; *Magi et al.*, 2009]. A separation of the total aerosol absorption into different source specific chemical species is therefore essential, both for constraining the large uncertainties in current aerosol forcing estimates [*Solomon et al.*, 2007] and for informing emissions based control policy. Detailed studies of the chemical composition and size distribution of aerosol particles, and how they relate to the optical properties is therefore essential to evaluate their impact on climate.

Russell at al. [2010] highlighted that many recent studies have shown the persistent connections between aerosol absorbing species and the wavelength dependence of absorption. Thus, numerous studies have classified absorbing aerosol types from optical properties measured on ground stations [*Coen et al.*, 2004; *Dubovik et al.*, 2002; *Eck et al.*, 1999; *Fialho et al.*, 2005; *Giles et al.*, 2012; *Giles et al.*, 2011; *Kalapureddy et al.*, 2009; *Meloni et al.*, 2006; *Mielonen et al.*, 2009] and from satellites [*Barnaba and Gobbi*, 2004; *Higurashi and Nakajima*, 2002; *Jeong and Li*, 2005; *Kaskaoutis et al.*, 2007; *Kaufman et al.*, 2005; *Kim et al.*, 2007; *Torres et al.*, 2005; *Yu et al.*, 2009]. In this study, in-situ optical properties and single particle chemical composition measured during three aircraft field campaigns are combined in order to validate a methodology for the estimation of absorbing aerosol types using spectral optical properties. In addition, this approach is extended and applied to a longer term remote sensing optical measurements database (i.e., AERONET [*Holben et al.*, 1998], using data from California stations).

1.1.5 Characterization of single particle chemistry over the enitre LA Basin using aircraft measurements during CalNex

Carbonaceous aerosols have numerous effects on climate, whether by directly and indirectly affecting it [*Ackerman et al.*, 2000; *Poschl*, 2005; *Ramanathan et al.*, 2007; *Rosenfeld and Givati*, 2006]. The chemical identity (or mixing state) directly relates to the potential affects the aerosol can have on climate. For example, Soot, formed by incomplete combustion processes, is strongly absorbing [*Jacobson et al.*, 2000; *Kanakidou et al.*, 2005; *Ramanathan and Carmichael*, 2008; *Solomon et al.*, 2007] while organic carbon has many optical properties [*Hand and Malm*, 2007; *Jacobson et al.*, 2000; *Kanakidou et al.*, 2005; *Rudich et al.*, 2007]. The major sources of these particles, and areas where they are localized can help to predict potential forcing and health affects in the region. Hence, identification of the chemical mixing state resolved in space is important for prediction of their potential effects.

The sources and chemical composition of aerosols vary greatly both spatially and vertically. As described in 1.1.3, an inherent limitation to ground-based studies is the susceptibility of one particular sampling site to local sources. Aircraft sampling can cover large areas over short timescales, providing measurements that are indicative of an entire region and therefore may be more useful for evaluation of model predictions over large areas. Herein, *in situ* measurements of carbonaceous aerosol mixing state were determined using an aircraft-aerosol time-of-flight mass spectrometer (A-ATOFMS) flown during CalNex. This dataset was analyzed in detail to determine differences in chemical mixing state within separate regions of the LA basin, determine the size resolved chemistry observed during CalNex, as well as probe the vertical mixing state of aerosols. The aircraft data provide an unprecedented view of the chemical mixing state and sources of aerosols within the LA Basin.

1.1.6 Summary of Chapters

1.1.6.1 Introduction

The ATOFMS instrumentation and CalNex study are introduced. The objectives and motivations of the study are described along with the project deliverables. The instrumental technique, as well as the data analysis procedure, is presented. A brief summary of each chapter of the report is included.

1.1.6.2 Materials and Methods

The aerosol time-of-flight mass spectrometer is introduced. Common data analysis techniques used in the following chapters are described.

1.1.6.3 Results and Conclusions

Chapter 1 discusses the similarities and differences of particle mixing state as measured by ATOFMS ship-based measurements. Heterogeneous reactivity, water uptake, and cloud-forming abilities depend on the mixing state of the aerosol. Determining the dominant sources and secondary species in a region is extremely important for accurate climate forcing calculations. Port-influenced regions can have dramatically different aerosol composition compared to the surrounding region. This chapter describes the mixing states of the aerosols in these regions.

The ship-based measurements covered a large range of California, from Los Angeles to Sacramento. In Southern California, particles containing soot made up the largest fraction of submicron particles while organic carbon containing particles comprised the largest fraction of submicron number concentrations in Northern California. The mixing state of these carbonaceous particle types varied during the cruise with sulfate being more prevalent on soot-containing particles in Southern California due to the influence of fresh shipping and port emissions in addition to contributions from marine biogenic emissions. Contributions from secondary organic aerosol species, including amines, and nitrate were more prevalent in Northern California, as well as during time periods impacted by agricultural emissions. These regional differences and changes in the mixing state and sources of particles have implications for heterogeneous reactivity, water uptake, and cloud-nucleating abilities for aerosols in California.

The content of Chapter 2 is similar to Chapter 1 but discusses aircraft measurements. The shipboard measurements in Chapter 1 were highly impacted by port and ship emissions. The CalNex and CARES (Carbonaceous Aerosol and Radiative Effects Study) aircraft campaigns were used collectively to provide aerosol mixing state measurements over extremely large regions of Northern and Southern California. In Southern California, the aerosol was primarily soot mixed with nitrate while in the north, there was a significantly higher fraction of organic carbon mixed with sulfate. Single particle peak ratios show that there is large heterogeneity of sources and composition in Southern California; meaning that a significant number of particles were mixed with high amounts of sulfate as well as nitrate. In Northern California nearly all particles were heavily mixed with sulfate. These associations have implications for the water uptake properties in the respective regions.

In Chapter 3, the chemical speciation from AERONET sites based on the Absorption Ångström Exponent (AAE) and the Scattering Ångström Exponent (SAE) are compared to ATOFMS-measured mixing states across three aircraft campaigns. Optical properties are increasingly being used to provide insights into chemical composition; however, before these techniques can be broadly utilized, comparisons with direct measurements are necessary. The aircraft campaigns of CalNex, CARES, and CalWater were used to validate the methodology used for the estimates of aerosol chemistry using optical properties. The method was found to underestimate primary sources but classified secondary sources well. Dust sources were also misclassified in some cases. These results help to improve the classification procedure for aerosol compositions determined via optical properties.

Chapter 4 discusses the aircraft dataset obtained for CalNex in more detail. The chemical mixing state is described as a function of size, altitude, and region. Different particulate chemistry was seen depending upon the area of the LA basin being sampled. Soot from port emissions was observed near Long Beach, with a notable increase in the fractions of soot and soot-OC particles in this area. In addition, secondary species associated with these particles differed than particles measured in the rest of CalNex, containing higher peak ratios of sulfate compared to nitrate. A

chemically resolved vertical profile obtained during CalNex shows higher number fractions of soot aerosol at lower altitudes, while at altitudes near to the boundary layer have higher fractions of HP particles, indicating that particles acquire significant amounts of sulfate and nitrate as they increase in altitude. Upon closer examination, nitrate and sulfate containing number fractions actually cross as altitude increases, with nitrate resulting in a higher number fraction than sulfate at higher altitudes. ATOFMS data are compared with in flight hygroscopicity data. Sub-saturated hygroscopicity and super-saturated hygroscopicity parameters showed opposite trends for both biomass influenced and non-biomass influenced periods. This could be a result of organic coatings on these particles leading to reduced water uptake.

While some of the original questions of the proposal could not be answered, due to aircraft limitations in going to high altitudes, the results described in this report accomplished the main objective of the proposal, "… to obtain detailed data on aerosol size and chemical mixing state during CalNex in May 2010 and link it with measured optical and hygroscopic properties". ATOFMS data obtained in the CalNex study were used in the publication of six peer-reviewed papers in atmospheric journals [*Cahill et al.*, 2012; *Cazorla et al.*, 2013; *Gaston et al.*, 2012; *Hersey et al.*, 2013; *Weiss-Penzias et al.*, 2013; *Zaveri et al.*, 2012].

1.2 Materials and Methods

1.2.1 Instrumentation

Measurements by the aerosol time-of-flight mass spectrometer (ATOFMS) are the primary data resource used in this report. The ATOFMS acquires single particle chemical composition (i.e. the aerosol mixing state) and size in real time. A detailed description of the ATOFMS and aircraft-ATOFMS (A-ATOFMS) has been reported previously [*Gard et al.*, 1997; *Pratt et al.*, 2009b]; only a brief description is provided here. Figure 3 identifies the key components of the ATOFMS and A-ATOFMS. Aerosols first enter the instrument and are focused into a narrow beam where they enter a low pressure region and are accelerated to their terminal aerodynamic velocities. They then pass through two 532nm scattering lasers (JDSU, Crystal Laser) spaced 6cm apart, which provide a measurement of the aerosol terminal velocity. The velocity is then used to calculate the size of the particle, via calibration of particles of known size, and to time the firing of a third ionization laser (266nm Nd:YAG, Quantel) which ablates and ionizes the particle at ~0.5-1.5mJ per pulse. A dual time-of-flight mass spectrometer collects the ions and outputs a positive and negative mass spectrum for each individual particle. The particle source is determined using positive spectra, while negative spectra typically provide information on the secondary species and chemical processing that the particle has undergone [*Guazzotti et al.*, 2001; *Noble and Prather*, 1996; *Prather et al.*, 2008]. Mass spectra are calibrated against known standards. It should be noted that if particles do not absorb the ionization laser wavelength, 266nm, the particle will not be ionized. This causes certain known particle types, for example ammonium sulfate, to be missing from ATOFMS data (though most other particle types can be sampled). Relative fractions presented later in this report should be interpreted as the fraction of

ATOFMS particles sampled, not necessarily all particles; however, particles within the size range of the ATOMFS are typically mixed with absorbing species, such as nitrate and carbon, thus it is unlikely that many particle types are not measured. The fraction of particles that are ionized, or hit rate, is an indicator of periods containing particles types that are invisible to the laser. During the course of the studies used in this report, the hit rate was relatively constant so it is unlikely that the ATOMFS is missing a large fraction of particle types.

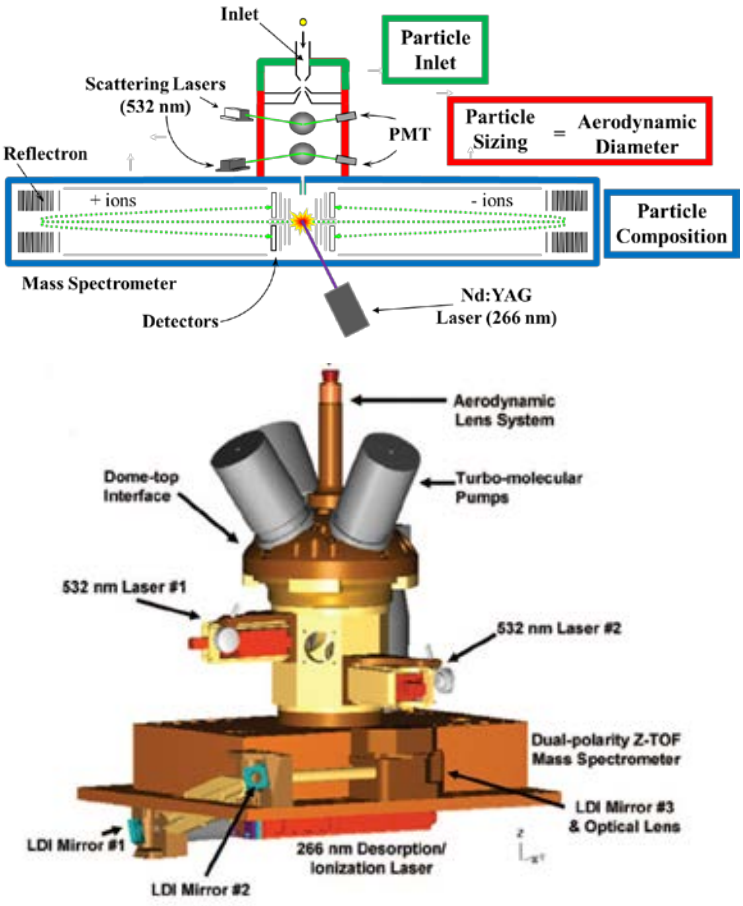

Figure 3: Schematic representation of the typical ATOFMS (top) and aircraft-ATOFMS (bottom) used in this report.

The standard ATOFMS can measure particles across the size range of ~200-3000 nm, while the A-ATOFMS has a smaller size range of ~200-1000 nm. The aircraft instrument utilizes an aerodynamic lens system that is significantly more efficient at transmitting particles than the typical converging nozzle used in a normal ATOFMS. Note that the difference in sizes transmitted by the ATOFMS instruments results in different chemistry and sources probed, with more supermicron particles being sampled by the standard ATOFMS used for ship measurements. This may result in some differences between the two instruments even when sampling within the same region.

It should be noted that the ATOFMS data is very different than standard PM2.5 measurements. First, the ATOFMS measures particle number rather than particle mass; however, spectral peak area can be used to relate qualitatively with particle mass. All fractions in this report are based on particle number fraction, unless otherwise noted. Second, the ATOFMS has a different size range (discussed above) than PM2.5 measurements. This could lead to discrepancies when size dependent chemistry is occurring in an area.

1.2.2 Data Analysis and Techniques

The ATOFMS can easily collect spectra on thousands of particles during a study. User analysis of individual spectra quickly becomes unmanageable, and alternate methods of analysis must be used. Particle mass spectra are loaded into Matlab (The MathWorks, Inc.) using the YAADA toolkit for Matlab (www.yaada.org). Then an adaptive resonance theory (ART-2a) algorithm groups spectra with similar peak patterns and intensities into clusters. New clusters are created if the dot product of a spectrum and a cluster does not pass a given threshold denoted as the vigilance factor (typically having a value of 0.80). Additional details on the analysis technique are provided elsewhere, [*Allen*, 2002; *Rebotier and Prather*, 2007; *Song et al.*, 1999]. The algorithm outputs a manageable number of clusters, indicative of spectra obtained throughout a whole study. Clusters are then identified manually and attributed to specific species based on previous studies. Mass spectral peaks are identified according to the most probable ions at a given mass-to-charge (*m/z*) ratio.

1.2.2.1 Interpretation of mass spectra

ATOFMS mass spectra contain a wealth of chemical information about a single particle. However, this detail can make interpretation and correlations with outside measurements difficult. The presence and intensities of specific ions in a mass spectrum is dependent upon the concentration of the chemical species, ionization laser intensity, and the presence of all chemical components on the particle, known as matrix effects. Matrix effects can suppress or enhance certain peaks based on the electron affinities or ionization potentials of all ions for negative and positive ions, respectively. Because of this, mass spectral peaks are not generally quantitative; however the intensity of the peaks is generally qualitatively representative of ion concentration. Additionally using relative mass spectral peak intensities (i.e. fractional intensities) helps to mitigate discrepancies caused by matrix effects and hence is typically used over absolute peak areas. In the case of the CalNex, the vast majority of particles were carbonaceous and so have similar matrices. Further, carbon containing ions typically have high ionization potentials making the matrix effects for these particles relatively small (as compared to metal containing particles like sea salt). Additionally, because most particles were carbonaceous the matrix effects between different particles would be similar. This allows for comparisons of relative peak areas to comment on increased or decreased content of specific species on particles.

1.2.2.2 Goal of specific data analysis

As has been demonstrated above, ATOMFS mass spectra can be extremely complex. There are many ways ATOFMS data can be analyzed depending on the scientific question. For example, one can cluster particles based on source (i.e. Soot), or on secondary species (i.e. nitrate/sulfate containing), or even both (i.e. Soot-Nitrate or Soot-Sulfate)? Hence, each chapter has a unique designation of particle types in order to better address each of the specific questions of this project. To help the reader understand how the data were generated for each section, a method

and materials section has been included with each result chapter to describe the specific data analysis procedures used within each chapter.

1.3 Results

1.3.1.1 The Impact of Shipping, Agricultural, And Urban Emissions On Single Particle Chemistry Observed Aboard The R/V Atlantis During Calnex

1.3.1.2 Materials and Methods

1.3.1.2.1 Aerosol Measurements: ATOFMS

The size-resolved chemical composition of individual aerosol particles from 0.2 to 3.0 μm aerodynamic diameter was measured in real time using aerosol time-of-flight mass spectrometry (ATOFMS). The operating principles of the ATOFMS have been described previously [*Gard et al.*, 1997; *Prather et al.*, 1994]. Briefly, particles are sampled through a converging nozzle inlet into a differentially pumped vacuum chamber causing particles to be accelerated to a size-dependent terminal velocity. Particles next enter the sizing region of the instrument consisting of two continuous wave (532 nm) lasers separated by a fixed distance. The time taken to traverse the laser beams is recorded giving the terminal velocity of the particle, which is used to calculate the aerodynamic diameter of the particle. The particle velocity is also used to time the firing of a Q-switched neodymium:yttrium/aluminum/garnet (Nd:YAG) laser (266 nm) operating at ~1.2 mJ laser power that simultaneously desorbs and ionizes compounds from individual particles creating positive and negative ions, which are analyzed in a dual polarity time-of-flight mass spectrometer. Particle detection efficiencies are dependent on the ability of particles to interact with the 266 nm radiation [*Dall'Osto et al.*, 2006; *Qin et al.*, 2006; *Wenzel et al.*, 2003]. Dual-polarity spectra provide complementary information regarding the source (e.g., ships versus sea salt) and age of the particle (e.g., fresh versus reacted sea salt) [*Guazzotti et al.*, 2001; *Noble and Prather*, 1996]. A lack of negative ion spectra indicates the presence of tightly bound particle phase water, which suppresses negative ions produced by laser desorption/ionization [*Neubauer et al.*, 1997; *Neubauer et al.*, 1998]. Conditioning particles to 60% relative humidity (RH) decreases some of this water, thus increasing the formation of negative ion spectra.

The YAADA software toolkit was used to import ion peak lists into MATLAB v 6.5.1 (The MathWorks, Inc.) for processing of ATOFMS data [*Allen*, 2002]. Single particle mass spectra were then analyzed using a clustering algorithm (ART-2a), which groups spectra together with similar characteristics into distinct "clusters" [*Song et al.*, 1999]. These "clusters" are then merged into distinct particle types based on the prevalent mass spectral ions and intensities, which are indicative of particle sources and chemistry [*Noble and Prather*, 1996]. The prevalence of these particle types was averaged into 1 h time bins and separated into submicron (0.2–1.0 μm) and supermicron (1.0–3.0 μm) particles. Each ion peak assignment presented in this paper corresponds to the most likely ion produced at a given mass-to-charge (*m/z*). Particle types described herein are defined by characteristic ion peaks and/or possible sources and do not reflect all of the species present within a particular particle class.

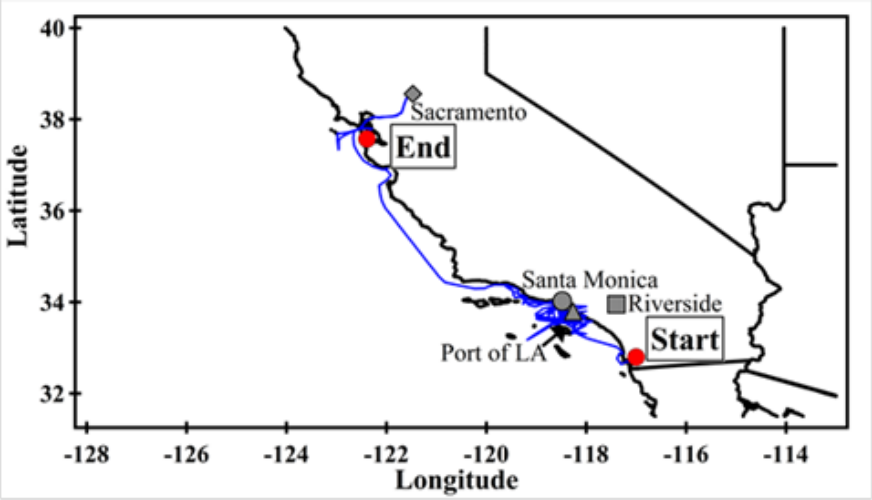

Figure 4: Cruise track for the R/V Atlantis (blue line) along the California coast during CalNex. The Port of Los Angeles (grey triangle), the Santa Monica area (grey dot), Riverside area (grey square) and the Sacramento area (grey diamond) are shown along with the start and end points of the cruise.

1.3.1.3 Results and Discussion

Temporal variations of single-particle measurements were analyzed to discern differences in particle composition between sources in southern and northern California. The temporal variability of the most frequently observed particle types detected by ATOFMS as well as the latitudinal position of the ship is shown in Figures 5a and 5b for submicron and supermicron particles, respectively. Several patterns in single-particle mixing state were identified based on differences in particle source, meteorological conditions, and aging processes. To illustrate this, six distinct time periods are identified by colored boxes in Figure 5; the time periods are defined as Riverside Transport (Period 1, boxed in red), Stagnant / Ports Transport (Period 2, boxed in black), Marine/Coastal Transport (Period 3, boxed in cyan), Ports of Los Angeles/Long Beach (LA/LB) (Period 4, boxed in green), Inland/Valley Transport (Period 5, boxed in orange), and Bay Area/Sacramento (Period 6, boxed in purple). The following sections provide a detailed comparison and discussion of the gas-phase species and meteorological conditions, prevalent particle types and sources, the mixing state of carbonaceous particles, and the secondary particulate species present during each time period.

1.3.1.3.1 Characteristics of Each Period

During the Riverside, Stagnant/Ports, and Marine/Coastal Transport periods, measurements took place along the Southern California coast focusing on emissions from the LA Basin, whereas measurements during the Ports of LA/LB period were entirely performed in the Ports of LA and LB and surrounding shipping lanes. During the Inland/Valley Transport period, measurements extended farther north to include the Santa Barbara region; the Bay Area/Sacramento period measurements were made in Northern California when the ship remained in the Deep Water Channel/Sacramento region for three days. Table 2 shows the corresponding dates and

meteorological and gas phase measurements for each time period. Figure 6 shows the 48 h air mass back trajectories at the 500m height [*Draxler and Rolph*, 2011] for each time period to highlight differences in air mass transport conditions. The Stagnant/Ports and Ports of LA/LB periods were heavily influenced by emissions from the Ports of LA/LB while the Riverside, Stagnant/Ports, Inland/Valley, and Bay Area/Sacramento periods were influenced by agricultural and urban emissions from Riverside and/or the Central Valley. The Marine/Coastal Transport period was influenced by oceanic emissions and serves as a background period.

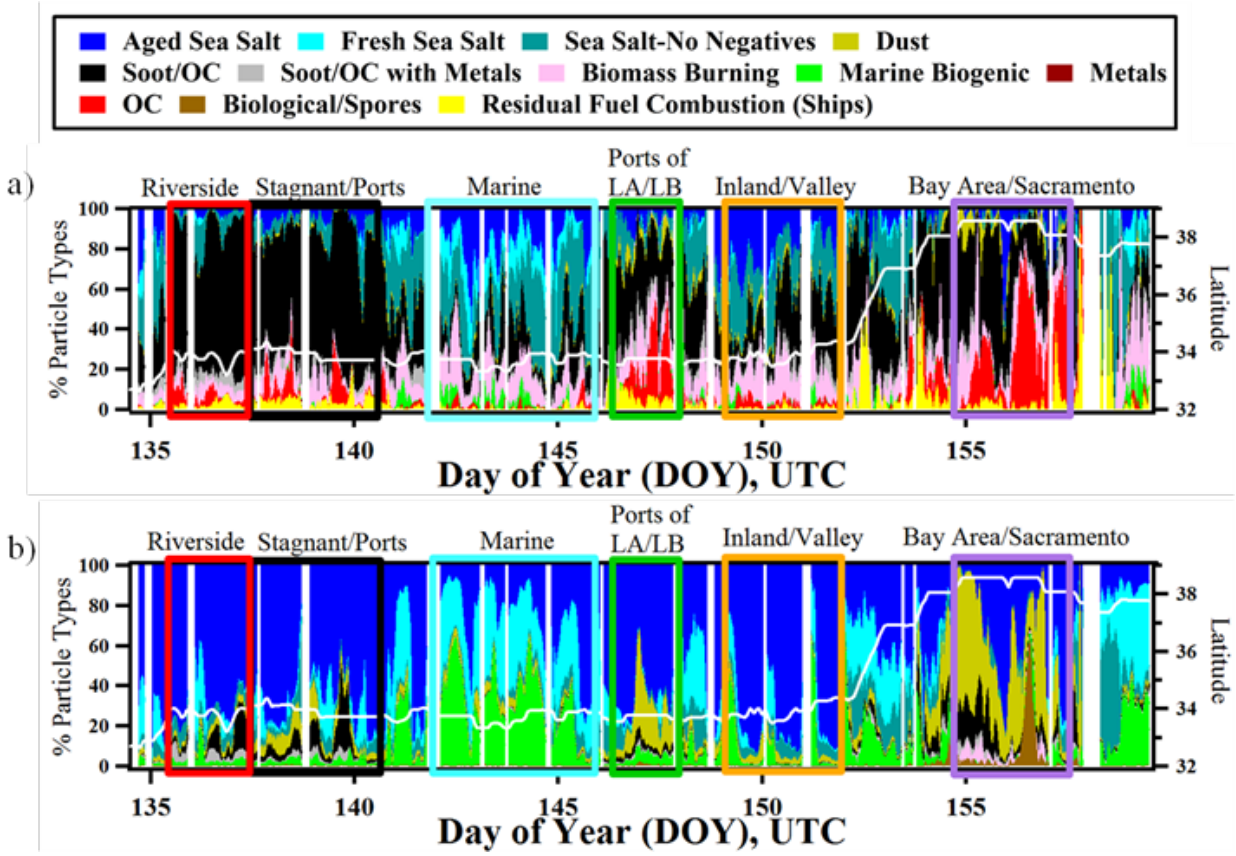

Figure 5: Hourly temporal profile of single-particle mixing-state observed by ATOFMS in UTC as a function of day of year (DOY) and latitude (white line). The top (a) and bottom (b) panels show the single-particle chemistry for submicron particles (0.2-1.0 μm) and supermicron particles (1.0-3.0 μm), respectively. Colored boxes highlight six different periods when differences in particle composition were observed due to different meteorological conditions, gas-phase concentrations, and aging processes.

Period	Location/Air Mass	Day of Year (DOY)	Date and Time (UTC)	Latitude	Longitude	Wind Speed (m/s)	RH (%)	Air Temp (°C)	Radon (mBq/m^3)	SO_2 (ppbv)	Ozone (ppbv)	Toluene/ Benzene
1	Riverside	135.5–137.375	5/15/2010 12:00 to 5/17/2010 9:00	33.14°N to 34.02°N	118.33°W to 119.22°W	2.93	89	13.2	2500	0.07	47.1	N/A
2	Stagnant/Ports	137.375–140.5	5/17/2010 9:00 to 5/20/2010 12:00	33.67°N to 34.38°N	118.22°W to 119.69°W	3.86	91	13.4	1060	0.06	39.0	0.40
3	Marine/Coastal	142–146	5/22/2010 0:00 to 5/26/2010 0:00	33.31°N to 33.95°N	118.07°W to 118.93°W	5.18	72	13.9	1550	0.14	35.1	0.85
4	Ports of LA/LB	146.33–147.875	5/26/2010 8:00 to 5/27/2010 21:00	33.53°N to 33.77°N	118.1°W to 118.5°W	2.40	73	16.0	740	3.40	29.3	1.89
5	Inland/Valley	149–151.875	5/29/2010 0:00 to 5/31/2010 21:00	33.5°N to 34.4°N	118.17°W to 119.85°W	3.29	83	15.2	3200	0.45	43.6	0.84
6	Bay Area/ Sacramento	154.625–157.625	6/3/2010 15:00 to 6/6/2010 15:00	38.02°N to 38.56°N	121.55°W to 122.16°W	4.53	69	20.9	1550	0.42	22.8	1.74

[a]Day of year (DOY), date and time (UTC), latitudinal and longitudinal range, average meteorological conditions (wind speed, RH, air temperature), and average gas-phase concentrations (radon, SO_2, ozone, and the toluene/benzene ratio) for measurements made during each of the six different time periods are highlighted. Dates are formatted as month/day/year.

Table 2: Meteorological and Gas Phase Data for Six Different Air Mass Transport Conditions.

Day of Year (DOY), date and time (UTC), latitudinal and longitudinal range, average meteorological conditions (wind speed, RH, air temperature), and average gas-phase concentrations (radon, SO_2, ozone, and the toluene/benzene ratio) for measurements made during each of the six different time periods are highlighted

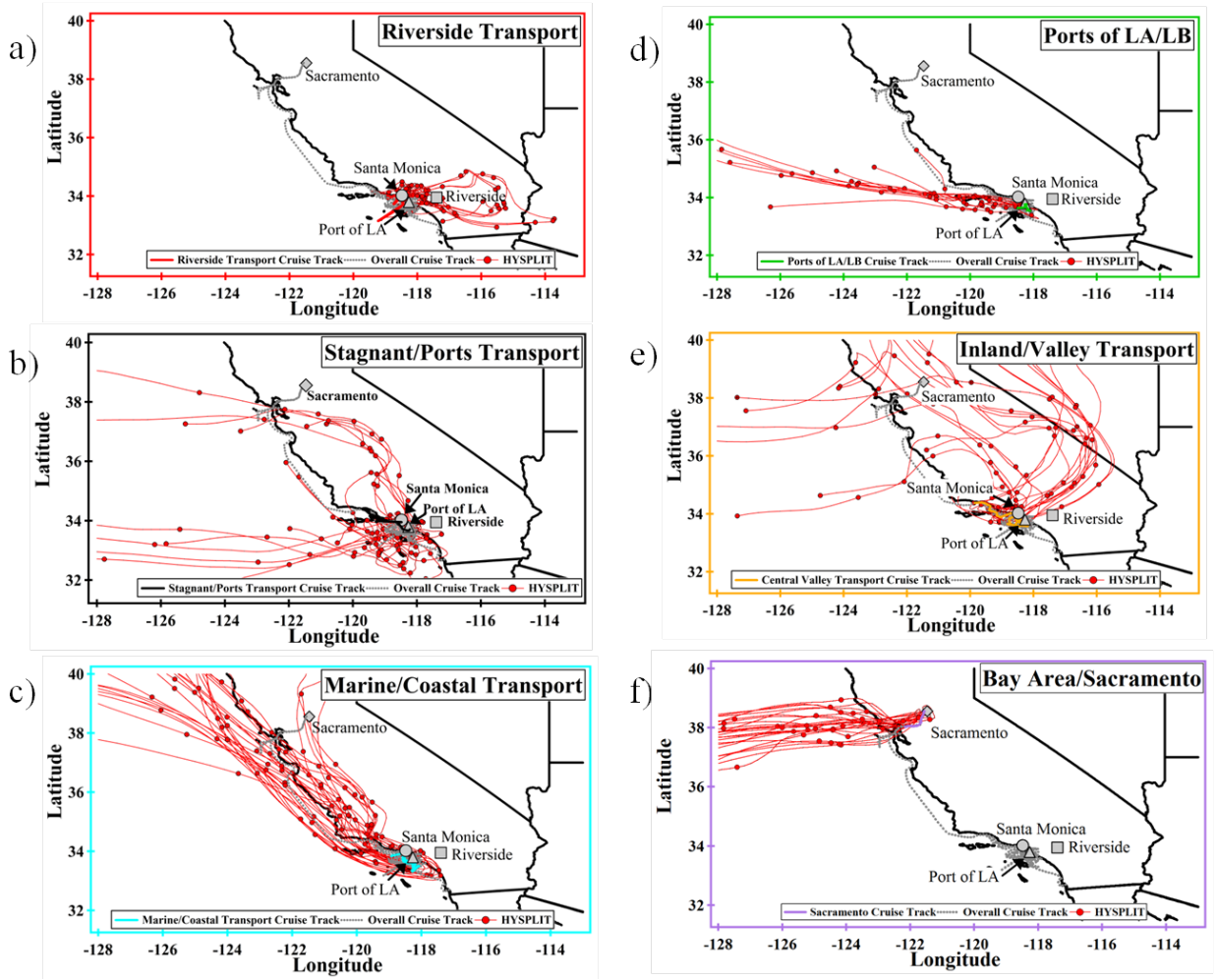

Figure 6: 48-hour HYSPLIT air mass back-trajectories at 500 m (red lines) shown during the R/V Atlantis cruise (grey dotted line) corresponding to: a) Period 1: Riverside Transport boxed in red, b) Period 2: Stagnant/Ports Transport boxed in black, c) Period 3: Marine/Coastal Transport boxed in cyan, d) Period 4: Ports of LA/LB Transport boxed in green, e) Period 5: Inland/Valley Transport boxed in orange, and f) Period 6: Bay Area/Sacramento boxed in purple. Red dots on the HYSPLIT trajectories denote 12 hour increments. The Port of Los Angeles (grey triangle), the Santa Monica area (grey dot), Riverside (grey square) and the Sacramento area (grey diamond) are also shown.

1.3.1.3.1.1 Period 1: Riverside Transport

During the Riverside Transport period, Hybrid Single-Particle Lagrangian Integrated Trajectory (HYSPLIT) analysis indicates that the sampled air masses were transported from the Riverside and Imperial Valley regions before traversing the port and Santa Monica regions (see Figure 6a). Thus, the Riverside Transport period is expected to be influenced by urban, port, and agricultural emissions. Particulate matter in Riverside typically is well-aged as indicated by high concentrations of secondary species such as nitrate, amines, ammonium, and secondary organics [*Hughes et al.*, 2000; *Hughes et al.*; *Liu et al.*, 2000; *Pastor et al.*, 2003; *Pratt et al.*, 2009a; *Pratt and Prather*, 2009; *Qin et al.*, 2012]. The ratio of toluene to benzene was not available during

this period; however, available NOx/NOy ratios indicated that the air masses during this period were photochemically aged. The average radon concentration was high (2500±760 mBq/m^3) indicating that continentally influenced air masses were sampled. The daily mean temperature was low (13.2±0.6 °C) while the daily mean RH was high (89±3%).

1.3.1.3.1.2 Period 2: Stagnant/Ports Transport

Sampled air masses stagnated around the coast, near the ports of LA/LB and Santa Monica region, during the Stagnant/Ports Transport period. Thus, port emissions (e.g., emissions from vehicles, ships, etc.) contributed more significantly to the aerosol burden during the Stagnant/Ports Transport than during the Riverside Transport period. Some air masses also originated from the inland Central Valley area toward the end of the Stagnant/Ports Transport period, potentially carrying agricultural emissions. The lowest average toluene to benzene ratio, 0.4, was observed during air masses originating from the Central Valley suggesting that air masses sampled during this period were photochemically aged. High daily mean RH (91±3% on average) and low daily mean temperatures (13.4±1.1 °C) were observed.

1.3.1.3.1.3 Period 3: Marine/Coastal Transport

During the Marine/Coastal Transport period, most air masses followed a north to south trajectory along the California coast. Wind speeds reached 14.5 m/s, which enhanced the production of fresh sea spray particles from bursting bubbles generated by breaking waves [*Blanchard and Woodcock, 1957*; *Monahan et al., 1983*; *O'Dowd and De Leeuw, 2007*]. Thus, the Marine/Coastal Transport period is characterized by ocean-derived aerosol composed of both fresh sea salt and biogenic organics. This period, however, is not necessarily representative of clean marine conditions based on the relatively high radon concentrations (1550±1080 mBq/m^3) and high average particle number counts (5721±2680 cm^{-3}) [*Fitzgerald, 1991*; *Hawkins et al., 2010*; *O'Dowd and De Leeuw, 2007*; *Twohy et al., 2005*]. Further evidence that the Marine/Coastal Transport period is not entirely a clean marine period also stems from the toluene to benzene ratio, which ranged from 0.03 during clean marine conditions to 3.74 when fresh urban emissions were encountered with an average of 0.85.

1.3.1.3.1.4 Period 4: Ports of LA/LB

The Ports of LA/LB period was characterized by relatively high SO_2(g) concentrations (3.4±5.2 ppbv on average with a maximum of 40 ppbv) compared to the previous three Periods when average SO_2 concentrations ranged from 0.06 to 0.45 ppbv. Furthermore, low wind speeds (2.4±1.2 m/s) and low radon concentrations (740±320 mBq/m^3) were also encountered. Toluene to benzene ratios were high with an average of 1.89 and a maximum of 6.1, indicating a fresh, photochemically-unprocessed, air mass. It is likely that local urban, port, and shipping emissions dominated the particle composition during this period with little influence from other continental or transported sources.

1.3.1.3.1.5 Period 5: Inland/Valley Transport

Figure 6e shows air masses traveling across the Central Valley and the desert before traversing the LA basin and Santa Barbara regions during the Inland/Valley Transport period. Higher radon and O_3 concentrations were measured during this time period compared to other time periods with averages of 3200±3000 mBq/m^3 and 44±11 ppbv, respectively. Toluene to benzene ratios had an average of 0.84 indicating that air masses sampled during this period were fairly well-aged. Similar to Riverside, aerosol from the Central Valley is typically characterized by high concentrations of secondary species, namely, secondary organic aerosol and ammonium nitrate due to contributions from dairy farms and other agricultural emissions in addition to urban emissions from sources such as vehicles [*Chen et al.*, 2007; *Chow et al.*; *Chow et al.*, 2006b; *Eatough et al.*, 2008]. Hence, particulate matter observed during this period is expected to show similar signs of particle aging as the Riverside Transport period.

1.3.1.3.1.6 Period 6: Bay Area/Sacramento

During the Bay Area/Sacramento period, air masses traveled over the San Francisco Bay area prior to arriving in the Sacramento region, which is within the Central Valley. Diurnal temperature and RH profiles were observed with night and day values ranging from 16 to 30 °C and 24 to 93%, respectively. High toluene to benzene ratios were observed with an average of 1.74, suggesting that the sampled air masses were relatively fresh, similar to the Ports of LA/LB period; however, unlike the Ports of LA/LB period, sampling during the Bay Area/Sacramento period occurred within the Central Valley and not within a major port region.

1.3.1.3.2 Observed Particle Types

1.3.1.3.2.1 Submicron Particle Composition

Particle composition varied based on sources and transport conditions (Figures 5 and 7). High number fractions of soot-containing particles (up to ~89% of submicron particles by number with an average of ~38±27%) were observed in Southern California, particularly during the Riverside Transport, Stagnant/Ports Transport, and Ports of LA/LB periods (Periods 1, 2, and 4) when port and urban (e.g., vehicles) emissions were dominant. The main exception to this trend in high soot-containing number fractions in Southern California occurred during the Marine/Coastal Transport period (Period 3) when submicron particle composition was dominated by sea-salt particles (~63±17% of submicron particles on average) due to transport of marine air. The dominance of soot-containing particles in Southern California is in agreement with aircraft ATOFMS measurements made during CalNex where Cahill et al. [2012] reported high soot-containing number fractions in the Southern California/LA Basin region.

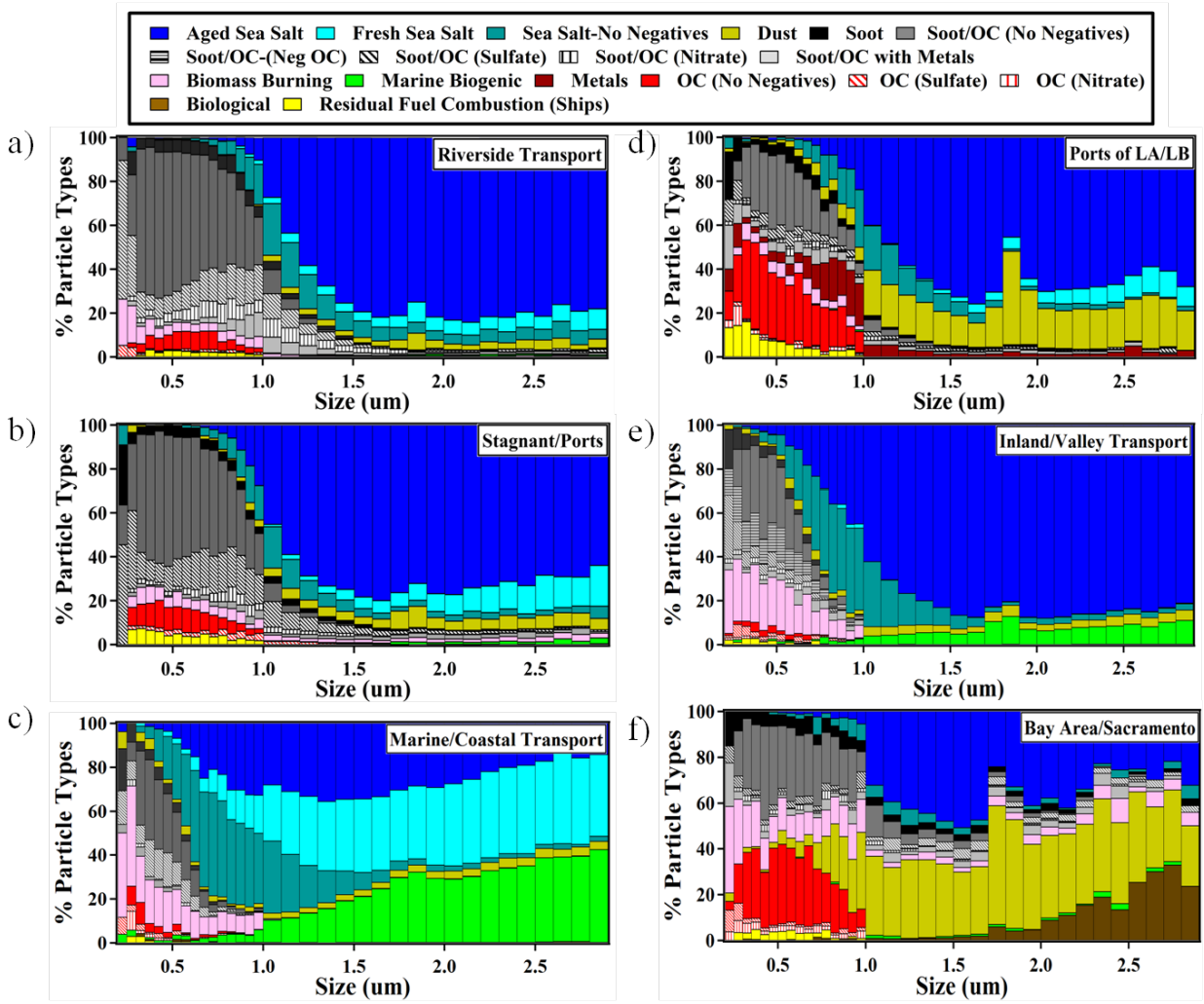

Figure 7: Fraction of particle types as a function of size observed during the six different time periods. Submicron particles (0.2-1.0 µm) are plotted in 0.05 µm bins while supermicron particles (1.0-3.0 µm) are plotted in 0.1 µm bins.

Particles from residual fuel combustion (e.g., emissions from ships and oil refineries) were also observed, primarily during the Stagnant/Ports Transport and Ports of LA/LB periods when port and shipping emissions strongly influenced particle composition. This residual fuel combustion particle type represented at most ~25% of the submicron particles and is characterized by ion peaks associated with transition metals found in residual fuel oil, notably vanadium ($^{51}V^{+}$, $^{67}VO^{+}$), nickel ($^{58,60}Ni^{+}$), and iron ($^{54,56}Fe^{+}$), in addition to organic carbon, sulfate ($^{97}HSO_4^{-}$) and, to a lesser extent, nitrate ($^{46}NO_2^{-}$, $^{62}NO_3^{-}$) (see Figure 8a for an example mass spectrum); these particles are herein referred to as vanadium-organic carbon (V-OC) particles [*Agrawal et al.*, 2008; *Ault et al.*, 2010; *Ault et al.*; *Corbett and Fischbeck*, 1997; *Healy et al.*, 2009; *Murphy et al.*, 2009]. During the Ports of LA/LB period, additional industrial particle types were observed, including metals concentrated in the submicron size mode, which most likely represent emissions from incineration [*Moffet et al.*, 2008] and are the subject of a different paper [*Weiss-Penzias et al.*, 2013]. Additionally, organic carbon (OC) represented a much higher fraction of

the detected submicron particles during the Ports of LA/LB period (~14±14% of the total submicron particles detected, on average) than previous periods likely due to elevated fossil fuel emissions in the Ports of LA and LB from vehicles, heavy-duty diesel trucks, and ships, which have been shown to contribute high mass concentrations of organic carbon to the aerosol burden [*Lack et al.*, 2009; *Murphy et al.*, 2009; *Russell et al.*, 2000; *Sodeman et al.*, 2005].

In contrast, soot-containing and V-OC particles made smaller contributions to the number concentration in southern California during Inland/Valley Transport conditions and in the northern California, especially the Sacramento region, during the Bay Area/Sacramento period (Periods 5 and 6). As shown in Figures 5 and 7, particles from biomass burning were elevated in the submicron mode during these two periods representing up to ~61% of submicron particles. Biomass-burning particles are characterized by an intense potassium peak ($^{39}K^+$) in addition to carbonaceous peaks (both elemental and organic), organic nitrogen peaks ($^{26}CN^-$, $^{42}CNO^-$), ion peaks associated with potassium salts ($^{113}K_2Cl^+$, $^{213}K_3SO_4^+$, etc.), and secondary species such as sulfate and/or nitrate (Figure 8b) [*Pratt et al.*, 2010; *Qin and Prather*, 2006; *Silva et al.*, 1999].

The key difference in particle composition observed in Northern California during the Bay Area/Sacramento period (Period 6) was the high percentage of submicron OC particles detected, constituting ~29±23% of submicron particles by number on average and up to ~78%. Unlike the OC detected during the Ports of LA/LB period, which originated from fossil fuel sources in the Ports of LA and LB, OC detected in Sacramento is likely the result of biogenic emissions due to the fact that biogenics were dominant during the first half of the Carbonaceous Aerosol Radiative Effects Study (CARES) in the Sacramento Valley [*Cahill et al.*, 2012]. Numerous new particle formation (NPF) events were observed across the Sacramento Valley during CalNex and the first part of CARES during this period [*Ahlm et al.*, 2012; *Setyan et al.*, 2012]. While the lower size limit of the nozzle-inlet ATOFMS (~0.2 μm) cannot be used to probe the composition of newly formed particles, ATOFMS measurements can provide insight into the composition of these particles as they grow to sizes detectable by the instrument [*Creamean et al.*, 2011]. Figure 9 shows particle number concentration as a function of diameter measured by a differential mobility particle sizer [*Bates et al.*, 2012]. Two distinct events are highlighted in black boxes when high number concentrations of small particles (~0.02 μm) were observed followed by rapid growth, which is indicative of NPF events [*Creamean et al.*, 2011; *Hegg and Baker*, 2009; *Kulmala*, 2003]. As shown in Figure 9, the percentage of OC particles was smallest when the NPF event was actually occurring. This is because the size of the newly formed particles is below the size detection limit of the instrument. The percentage of OC particles increased primarily after these NPF events occurred as the newly formed particles grew to sizes detectable by the instrument suggesting that organics contributed to this growth in agreement with previous studies [*Creamean et al.*, 2011; *Kulmala*, 2003; *Smith et al.*, 2008; *Zhang et al.*, 2004], and with recent measurements during CARES in the Sacramento Valley from an aerosol mass spectrometer [*Setyan et al.*, 2012]. The formation of new particles occurred under conditions of lower RH and intense solar radiation; these low RH conditions also favor the formation of high

molecular weight secondary organic aerosol from biogenic emissions that may have contributed to particle formation and/or growth [*Nguyen et al.*, 2011]. Growth of these particles into sizes detectable by the ATOFMS occurred as RH increased with many of the detected OC particles lacking negative ion spectra (85±16% on average) indicating that an appreciable amount of particulate water was associated with these particles [*Neubauer et al.*, 1997; *Neubauer et al.*, 1998].

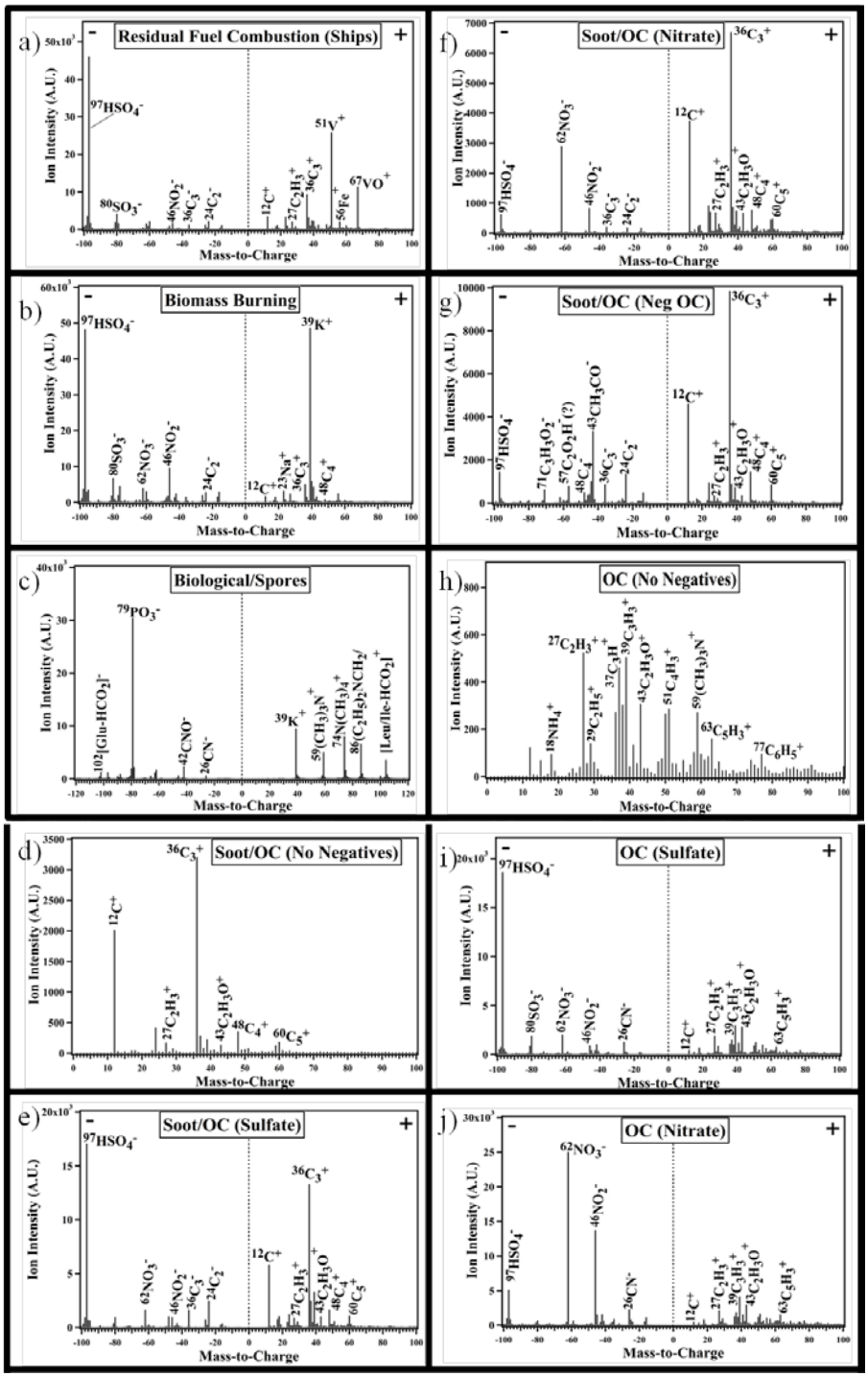

Figure 8: Representative mass spectra of a) Residual Fuel Combustion from ships, b) Biomass Burning, c) Biological/Spores, d) Soot/OC (No Negatives), e) Soot/OC (Sulfate), f) Soot/OC (Nitrate), g) Soot/OC (Neg OC), h) OC (No Negatives), i) OC (Sulfate), j) OC (Nitrate) particles are shown. For mass spectra containing both positive and negative ions, dashed lines separate negative ions (left side) and positive ions (right side).

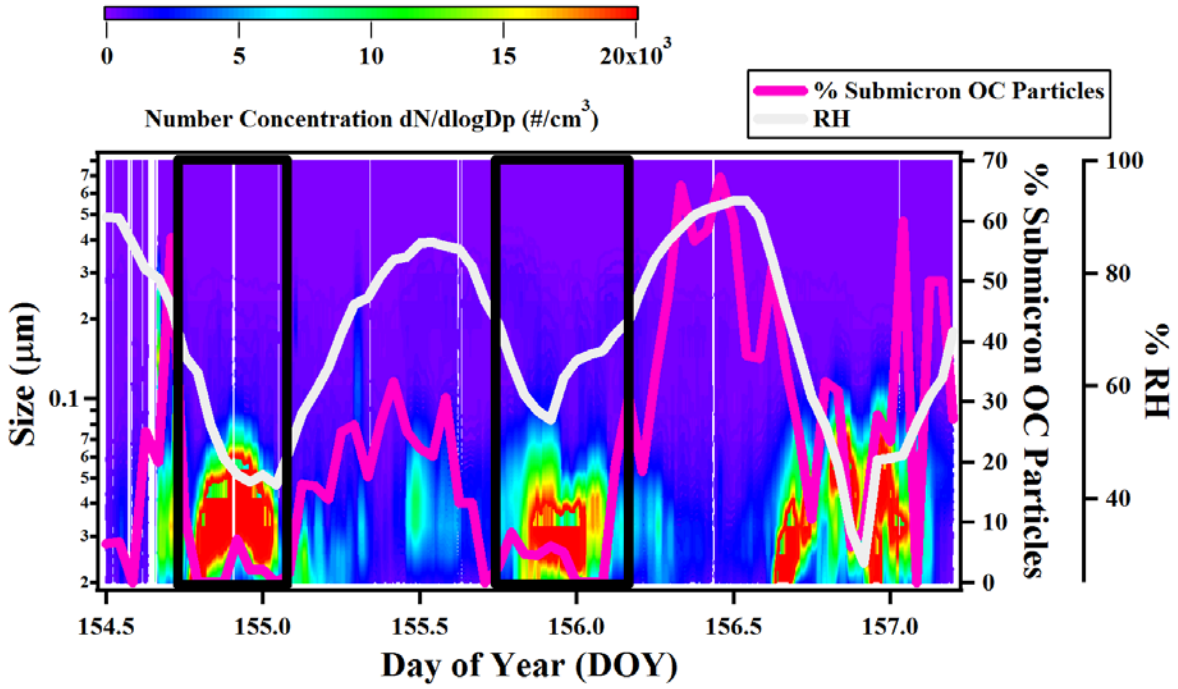

Figure 9: Size distributions of particle number concentrations as a function of size and DOY are shown on a log scale. The percentage of submicron OC particles detected by ATOFMS (pink line) and RH (grey line) are shown as a function of DOY. Time periods when new particle formation events were observed are shown in black boxes.

1.3.1.3.2.2 Supermicron Particle Chemistry

Aged sea salt dominated the supermicron particle composition during most periods, making up 50±27% of total supermicron particles on average, as shown in Figures 5 and 7. Aged sea-salt particles result from heterogeneous reactions with gas-phase nitrogen oxides (e.g., N_2O_5(g), HNO_3(g)), which lead to the displacement of chloride and the formation of particulate nitrate [*Behnke et al.*, 1991; *Chang et al.*, 2011; *Gard et al.*, 1998; *Vogt et al.*, 1996]. In addition to nitrate, methanesulfonic acid (MSA) and sulfate were also found on ~14% of aged sea-salt particles, on average, possibly contributing to the observed particulate chloride displacement [*Hopkins et al.*, 2008; *Laskin et al.*, 2012]. During the Marine/Coastal Transport period (Period 3), fresh sea salt and marine biogenic particle types dominated the supermicron particle composition making up 33±11% and 30±17% of supermicron particles, respectively. Marine biogenic particle types include Mg-type [*Gaston et al.*, 2011] and sulfur-type particles (C. J. Gaston et al., manuscript in preparation, 2013), which represent ocean-derived particle types associated with marine biological activity and/or dissolved organic material. The combined high wind speeds in addition to the elevated biological activity, as evidenced by the presence of red tide blooms along the Southern California coast (www.sccoos.org), explain the dominance of fresh sea salt and marine biogenic emissions during this period.

Marine particle types were negligible in the inland Sacramento region during the Bay Area/Sacramento period. Instead, dust particles were found to represent 39±23% of supermicron

particles, and biological particles were found to constitute up to ~64% of supermicron particles as shown in Figures 5 and 7f. Most of the biological particles detected by ATOFMS were determined to be spores containing dipicolinic acid, a compound that is easily detected using laser/desorption ionization at 266 nm radiation and serves as a unique matrix allowing for the detection of amino acids, which typically have low absorption cross sections at 266 nm [*Silva and Prather*, 2000; *Srivastava et al.*, 2005]. Consistent with previous measurements of spores using laser/desorption ionization at 266 nm, spores detected during CalNex contained $^{39}K^+$, $^{59}(CH_3)_3N^+$, $^{74}(CH_3)_4N^+$, *m/z* +86 due to either $(C_2H_5)_2NCH_2^+$ or the amino acids [leucine- HCO_2] and [isoleucine-HCO_2], *m/z* +104, which is yet to be identified, phosphate ($^{63}PO_2^-$, $^{79}PO_3^-$), organic nitrogen ($^{26}CN^-$, $^{42}CNO^-$), and *m/z* -123, which is most likely due to dipicolinic acid-HCO_2 (Figure 8c) [*Srivastava et al.*, 2005]. Spores have rarely been detected by ATOFMS in ambient environments and represent a very unique particle type most likely detected due to agricultural and biogenic emissions from the Sacramento area.

1.3.1.3.3 Variations in the Mixing State of Carbonaceous Particle Types

1.3.1.3.3.1 Soot Particle Mixing State

In addition to probing overall particle composition, observed differences in the mixing state of soot-dominated particles were also investigated (Figure 10a). These particles are characterized by intense elemental carbon ion peaks ($^{12}C^+$, $^{36}C_3^+$, $^{48}C4^+$, C_n^+). A small percentage of freshly emitted elemental carbon particles, herein referred to as "soot," contained intense elemental carbon peaks indicative of long-chain elemental carbon (e.g., elemental carbon ion peaks extending out to higher masses in both the positive and negative ion spectra) with only low-intensity peaks from secondary species such as sulfate and/or nitrate [*Cahill et al.*, 2012; *Moffet and Prather*, 2009]. Most of the soot-containing particles, however, contained intense elemental carbon peaks that did not extend out to higher masses and were internally mixed with low-intensity organic peaks ($^{27}C_2H_3^+$, $^{43}C_2H_3O^+$, etc.) in addition to other secondary species (e.g., nitrate and/or sulfate) in agreement with aircraft observations during CalNex [*Cahill et al.*, 2012; *Metcalf et al.*, 2012]. This second class of soot-containing particles is herein referred to as Aged Soot particles, consistent with Cahill et al. [2012], and is further subdivided into Aged Soot (No Negatives), Aged Soot (Sulfate), Aged Soot (Nitrate), and Aged Soot (Neg OC) particle classes. Overall, the majority of Aged Soot particles (~62±20% of soot-containing particles on average) lacked negative ion spectra and are classified as Aged Soot (No Negatives) (see Figures 8d and 9a), with sizes peaking in number concentration at ~0.5–0.6 μm and extending up into the supermicron size range (Figure 7). The lack of negative ion spectra and larger sizes suggests that these particles were hydrated (contained appreciable water) [*Moffet et al.*, 2008; *Neubauer et al.*, 1997; *Neubauer et al.*], possibly due to cloud or fog processing.

The most striking feature shown in Figure 10a is the high percentage of Aged Soot (sulfate) particles detected in Southern California (representing, on average, ~30±18% of detected submicron soot-containing particles during the Riverside Transport, Stagnant/Ports Transport, Marine/Coastal Transport, and Ports of LA/LB periods) that decreased significantly to ~11±10%

as the ship moved north along the California coast. Aged Soot (sulfate) particles are characterized by intense sulfate peaks ($^{80}SO_3^-$, $^{97}HSO_4^-$; Figure 8e) [*Moffet and Prather*, 2009]. This feature in the Aged Soot (sulfate) particles measured on the R/V Atlantis is in contrast to the aircraft measurements made by ATOFMS, which mainly observed internal mixtures of soot and nitrate as opposed to sulfate in Southern California [*Cahill et al.*, 2012] due to the accumulation of ammonium nitrate coatings [*Metcalf et al.*, 2012]. The most likely explanation is that soot-containing particles were measured in the western port regions of the LA basin onboard the R/V Atlantis where fresh shipping and port emissions prevailed as opposed to the more aged emissions sampled onboard the aircraft. Fresh emissions from industrial sources at the port and ocean-going vessels contain high levels of SO_2 leading to elevated levels of particulate sulfate [*Agrawal et al.*, 2008; *Ault et al.*, 2010; *Corbett and Fischbeck*, 1997; *Corbett and Koehler*, 2003]. During CalNex, Aged Soot (sulfate) particles were typically found to peak at ~0.55 μm on average, which is larger than expected for freshly emitted soot particles [*Moffet and Prather*, 2009]; this is likely due to condensation and aqueous phase processing of SO_2, which has been shown to contribute high quantities of sulfate to particles in this size range in the LA basin [*Hegg*, 1985; *Hering and Friedlander*, 1982; *Meng and Seinfeld*, 1994]. It should be noted that regulations were adopted in 2009 requiring ships to switch from high-sulfur to low-sulfur fuel within 24 nautical miles of the California coast [*CARB*, 2009]. In addition to fresh port and shipping emissions, another potential source of elevated sulfate on soot particles, particularly during Marine/Coastal Transport conditions (Period 3), is the presence of red tide blooms in Southern Californian waters during CalNex (www.sccoos.org) of Lingulodinium polyedrum, a marine organism that has been shown to contribute biogenic sulfur to aerosols [*Gaston et al.*, 2010]. Although ATOFMS cannot be used to distinguish biogenic and anthropogenic sulfate, MSA, an ocean-derived biogenic form of sulfur, can be detected and used to assess the possibility of biogenic contributions to detected sulfate levels [*Gaston et al.*, 2010]. In fact, ~38% of Aged Soot (sulfate) particles, on average during the Riverside, Stagnant/Ports, Marine, and Ports of LA/LB periods, were found to also contain MSA with the highest percentage (~62% of Aged Soot (sulfate) particles) occurring during the Marine/Coastal Transport period while the lowest percentage (~13% of Aged Soot (sulfate) particles) was observed during the Ports of LA/LB period. This suggests that at least some of the observed sulfate was from a biogenic source.

Agricultural emissions were also found to impact soot mixing state by contributing Aged Soot (nitrate) particles, particularly during the Riverside Transport and Bay Area/ Sacramento periods and toward the end of the Stagnant/Ports Transport period, when air masses were transported from the Central Valley. These particles had similar positive ion markers to the Aged Soot (sulfate) particles, but contained nitrate peaks ($^{46}NO_2^-$, $^{62}NO_3^-$) that were more intense than sulfate (see Figure 8f). This particle type has been shown to result from the acquisition of nitrate namely formed through photochemically-produced nitric acid (HNO_3(g)), which condenses onto particles causing them to grow; aqueous phase processing may also contribute to this growth and the acquisition of nitrate [*Moffet et al.*, 2008; *Moffet and Prather*, 2009]. This particle type

represented up to ~33% of soot-containing particles and was observed to peak at a larger size mode than the other soot-containing particle types at ~0.75 μm during the campaign (Figure 7).

In addition to Aged Soot (nitrate) particles, unique Aged Soot particles containing sulfate and intense ions at *m/z* -43, -57, and -71 (see Figure 8g) were detected during a period of agricultural influence (Inland/Valley Transport conditions). To the best of our knowledge, mixtures of soot and these ions have never been detected before by ATOFMS. Since organic peaks in Aged Soot particles typically appear as positive ions, this particle type has been labeled Aged Soot (Neg OC). It is most likely that this particle type is derived from a unique, fresh source near the sampling site, as these ion markers were not observed on other particle types. Further evidence for this speculation comes from the fact that this particle type peaks at a smaller size (~0.35 mm) than the other soot-containing types, as shown in Figure 7e, suggesting a local source. The unique organic markers likely correspond to $^{43}CH_3CO^-$, $^{57}C_2O_2H^-$, and $^{71}C_3H_3O_2^-$ [*McLafferty and Turecek*, 1993; *Silva et al.*, 1999; *Silva and Prather*, 2000] possibly due to contributions from levoglucason and/or methylglyoxal (*m/z* -71), glyoxal (*m/z* -57), and acetaldehyde (*m/z* -43) [*Silva et al.*, 1999]. These organic species could represent secondary organic aerosol (SOA) formed from the photolytic processing of organics in the aqueous phase [*Bateman et al.*, 2011]; this mechanism was suggested to contribute organic components with elevated atomic O:C ratios during CalNex [*Duong et al.*, 2011]. Additional field and laboratory measurements are required to confirm the identification of these ion peaks.

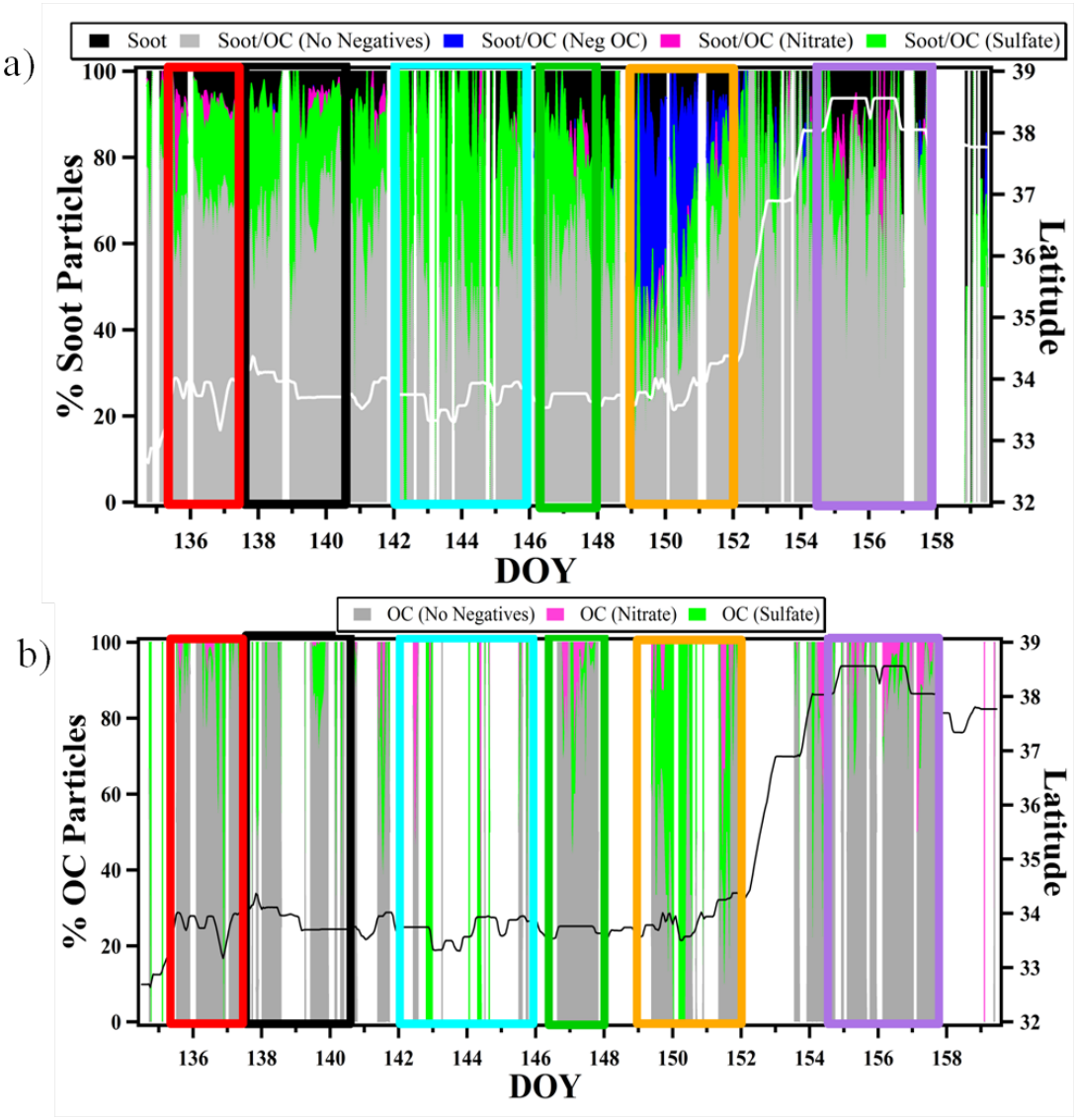

Figure 10: Hourly temporal variations in carbonaceous mixing-state. The top panel a) shows hourly temporal trends for different soot particle types: Soot (black), Soot/OC (No Negatives) (grey), Soot/OC (Sulfate) (green), Soot/OC (Nitrate) (pink), and Soot/OC (Neg OC) (blue) in addition to latitude (white line). The bottom panel b) shows hourly temporal variations for different organic particle types: OC (No Negatives) (grey), OC (Sulfate) (green), and OC (Nitrate) (pink) in addition to latitude (black line). White spaces denote periods when no OC particles were present. The six different time periods are shown with different colored boxes.

1.3.1.3.3.2 The Mixing State of Organic Particles

In addition to soot-containing particles, the mixing state of OC particles (e.g., non-soot-containing OC particles) was also investigated by examining temporal trends. These non-soot-containing OC particles are distinguished from the Aged Soot types described above in that these particles are not characterized by intense elemental carbon peaks at *m/z* +12, +24, +36, etc., but instead have *m/z* +27, +37, and/or +43 as the main positive ion peaks. Three types of OC particles were identified during CalNex: OC (no negatives), OC (sulfate), and OC (nitrate).

Temporal trends of the OC particle types are shown in Figure 10b. Most OC particles were found to lack negative ion spectra (~67±37% on average; see Figure 8h) and peaked in the 0.5–0.6 μm size range (Figure 7) suggesting that they contained appreciable particulate water similar to soot-containing particles. However, during Marine/Coastal and Inland/Valley Transport conditions (Periods 3 and 5), OC particles containing intense sulfate peaks (see Figure 8i) were more common, representing ~55±40% of organic particles on average, likely due to photochemically-produced sulfate possibly derived from biogenic emissions. In addition to sulfate, OC particles with intense nitrate peaks (see Figure 8j) were also observed, primarily at night during the Marine/Coastal Transport, Ports of LA/LB, Inland/Valley Transport, and Bay Area/Sacramento periods (Periods 3–6) and represented ~9±17% of organic particles, on average. Overall, OC (nitrate) particles peaked at a smaller particle size (~0.35 μm) suggesting that not all of the nitrate on these particles was photochemically-produced nitrate, which typically leads to larger particle sizes. Instead, these observations suggest possible contributions of organonitrates formed from reactions with gas-phase precursors and nitrate radical at night that then condense onto particles [*Ng et al.*, 2008]; organonitrates were also found to contribute to the organic aerosol burden during CalNex in Bakersfield, CA [*Rollins et al.*, 2012].

The OC types described above also frequently contained aromatic peaks ($^{51}C_4H_3^+$, $^{63}C_5H_3^+$, $^{77}C_6H_5^+$, etc.) [*Silva and Prather*, 2000], which have been associated with secondary processing of organic species in vehicle exhaust [*Shields et al.*, 2007; *Sodeman et al.*, 2005; *Spencer et al.*, 2006; *Toner et al.*, 2008] and humic substances formed from biomass burning [*Holecek et al.*, 2007; *Mayol-Bracero et al.*, 2002; *Qin and Prather*, 2006]. OC particles also contained ion peaks indicative of amines (e.g., $^{59}(CH_3)_3N^+$, $^{86}(C_2H_5)_2NCH_2^+$, $^{101}(C_2H_5)_3N^+$, $^{118}(C_2H_5)_3NOH^+$, etc.), which are semi-volatile species that can partition onto preexisting particles [*Angelino et al.*, 2001; *Pratt and Prather*, 2009; *Schade and Crutzen*, 1995], and oxidized organic markers (e.g., $^{43}C_2H_3O^+$) that indicate the presence of SOA (see Figure 8h) [*Qin et al.*, 2012]. Ternary plots were used to examine the prevalence of these compounds and to further elucidate the mixing state and sources of OC particles using the ion peaks $^{59}(CH_3)_3N^+$, $^{43}C_2H_3O^+$, and $^{77}C_6H_5^+$ as markers for amines, SOA/oxidized organics, and aromatics, respectively (see Figure 11).

Amines were found to dominate the OC mixing state during the first two periods, with 65±33% of OC particles containing intense amine markers during the Riverside Transport period and 48±44% during the Stagnant/Ports Transport period (Figure 11). Dairy farm emissions from the Chino and Central Valley regions, in addition to possible contributions from traffic emissions wherein ammonia and amines can be produced from catalytic converters [*Fraser and Cass*, 1998; *Sodeman et al.*, 2005], explain the dominance of amines during these two time periods [*Hughes et al.*, 2002; *Pastor et al.*, 2003; *Pratt and Prather*, 2009; *Qin et al.*, 2012; *Schade and Crutzen*, 1995; *Sorooshian et al.*, 2008b]. Furthermore, during these two periods, low temperatures and the highest average RH values were measured on the ship; similar meteorological conditions encountered during transport would also favor the detection of amines during these periods [*Angelino et al.*, 2001]. Furthermore, 18±23% of OC particles contained

intense amine markers during the Ports of LA/LB period even though inland transport conditions were not encountered suggesting that the ports could contribute an industrial source of amines, possibly from vehicular emissions, including heavy-duty diesel vehicles [*Bishop et al.*, 2012; *Fraser and Cass*, 1998; *Sodeman et al.*, 2005]. Amines could also have resulted from marine biogenic emissions [*Facchini et al.*, 2008a; *Sorooshian et al.*, 2009].

Oxidized organics were prevalent during Inland/Valley Transport conditions (Period 5; Figure 11e). The high O_3 concentrations and photochemically-aged nature of the sampled air masses suggest that the organics during the Inland/Valley Transport period resulted from secondary rather than primary sources [*Na et al.*, 2004; *Qin et al.*, 2012]. Oxidized organics at *m/z* +43 were also prevalent during the Stagnant/Ports Transport period, when photochemically-aged air masses were sampled, and dominant during Marine/Coastal Transport conditions (Period 3), likely due to secondary contributions. Another source of the oxidized organics during the Marine/Coastal Transport period could be organics from marine biogenic sources, such as lipopolysaccharides, that have higher oxygen content than organics from anthropogenic sources [*Facchini et al.*, 2008b; *Ovadnevaite et al.*, 2011; *Russell et al.*, 2011; *Russell et al.*, 2010].

SOA from aromatics was more prevalent during the Ports of LA/LB and Bay Area/Sacramento periods than during any other periods; however, oxidized organics were still the most prevalent type of organics during these two periods. The increased frequency of aromatic markers in the Ports of LA and LB is likely due to increased emissions from diesel combustion by trucks [*Kasper et al.*, 2007; *Maricq*, 2007; *Shields et al.*, 2007; *Spencer et al.*, 2006] in addition to emissions from ships [*Kasper et al.*, 2007; *Lack et al.*, 2009; *Murphy et al.*, 2009; *Russell et al.*, 2009]. Oxidized organics and amines in Sacramento are likely from agricultural and biogenic emissions [*Chow et al.*, 2006a; *Setyan et al.*, 2012; *Sorooshian et al.*, 2008b] while the observed SOA from aromatics are likely humic substances derived from biomass burning [*Holecek et al.*, 2007; *Mayol-Bracero et al.*, 2002].

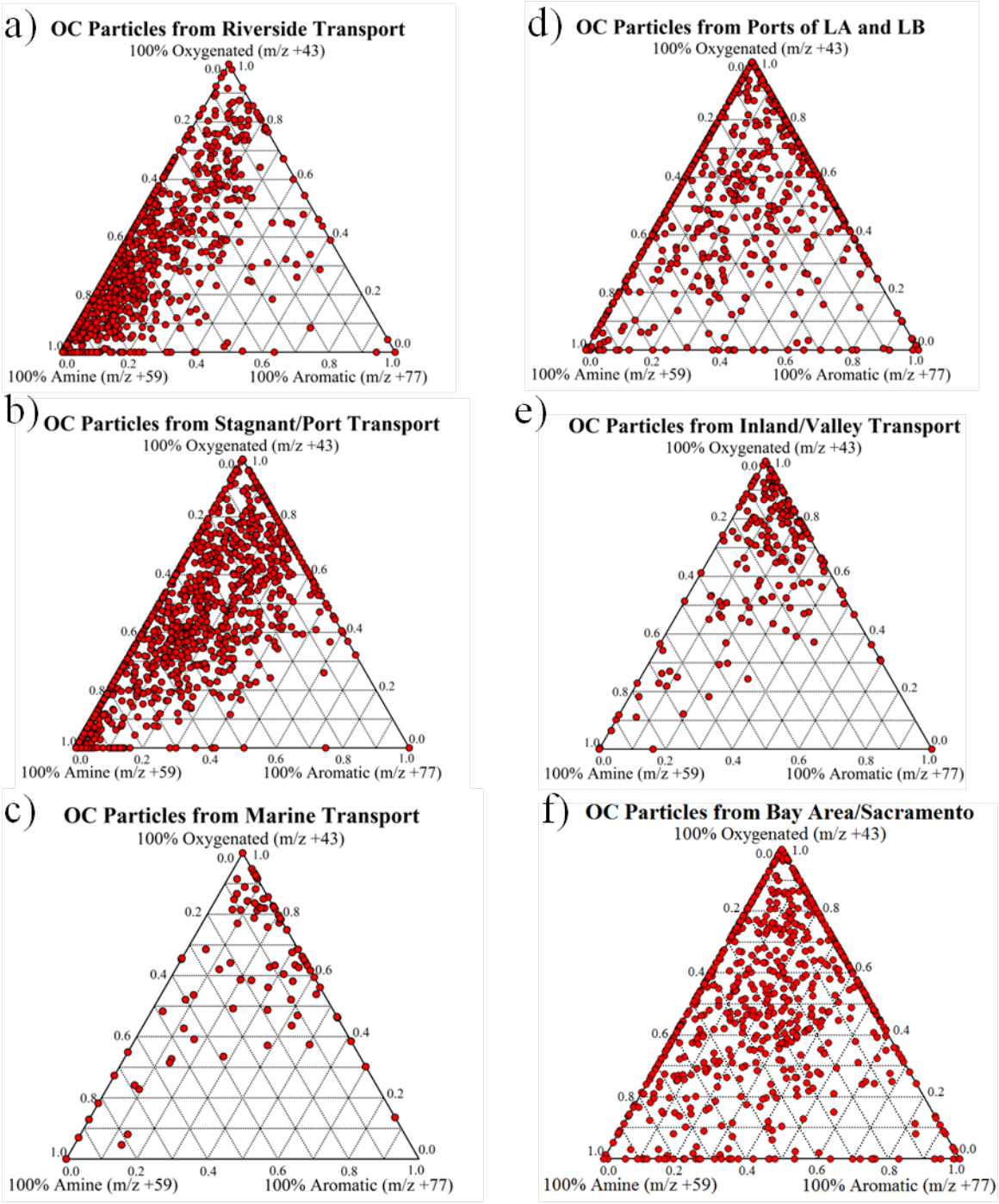

Figure 11: Ternary plots for individual OC particles observed for the six different time periods. The top corner of the ternary plots corresponds to OC particles containing only the oxygenated organic peak ($^{43}C_2H_3O^+$), the left bottom corner denotes OC particles containing only the amine peak ($^{59}(CH_3)_3N^+$), and the right bottom corner corresponds to OC particles containing only the aromatic peak ($^{77}C_6H_5^+$).

1.3.1.4 Conclusions and Implications for California

Overall, this study showed that the chemical properties of aerosol particles differed widely across California based on particle source and transport conditions. As evidenced by the particle chemistry and mixing state measured onboard the R/V Atlantis, Southern California was impacted by fresh shipping and vehicular emissions from cars and diesel trucks in addition to marine biogenic emissions. Soot-containing particles were the most prevalent submicron particles in southern California and were typically mixed with sulfate while aromatic markers were found to contribute to organics due to residual fuel, distillate fuel, and gasoline combustion. These fresh emissions were episodically mixed with inland, agricultural emissions leading to the presence of secondary species such as amines. It is important to note that the particles measured in southern California contained elevated levels of sulfate because these measurements focused on fresh emissions from the Ports of LA and LB; if these measurements were made farther inland of the ports, enhancements in nitrate due to particle aging and contributions of ammonium nitrate, as seen by other measurements, would have been observed instead [*Cahill et al.*, 2012; *Metcalf et al.*, 2012].

In contrast, northern California was impacted by biogenic emissions from the forested Sierra Nevada foothills and agricultural emissions as evidenced by the prevalence of organic carbon [*Cahill et al.*, 2012; *Setyan et al.*, 2012]. Oxidized organic compounds were frequently associated with particles during Inland/Valley transport conditions and, in Sacramento, are likely due to contributions from SOA while aromatic markers observed in Sacramento are likely due to contributions from biomass burning.

Overall, we found that the mixing state of particles in California varies significantly on a regional scale due to diverse local sources. Furthermore, the mixing state of particles from these local emissions can be significantly altered based on differences in meteorological conditions and air mass histories, which will most likely result in regional differences in the health, optical, and cloud-nucleating properties for the aerosol populations observed across California. This should be taken into account when determining which emissions sources to regulate in order to mitigate the adverse effects of aerosols on both human health and climate change.

1.3.2 The Mixing State of Carbonaceous Aerosol Particles In Northern And Southern California Measured During CARES and Calnex 2010

1.3.2.1 Methods and Materials

1.3.2.1.1 Aircraft Aerosol Time-of-Flight Mass Spectrometer

A description of the A-ATOFMS is given in detail elsewhere [*Pratt et al.*, 2009b]. In brief, the A-ATOFMS measures the vacuum aerodynamic diameter (d_{va}) and chemical composition of single particles in real time for particles between ~100 – 1000 nm, with peak transmission between 200 – 700 nm. After passing a Polonium (Po^{210}) neutralizer and pressure controlled inlet [*Bahreini et al.*, 2008], particles are focused through an aerodynamic lens [*Liu et al.*, 1995a; *Liu et al.*, 1995b], where they are accelerated to their aerodynamic terminal velocity. The particles then pass through two continuous wave 532 nm lasers (JDSU) spaced 6.0 cm apart. The time difference between the scattering signals is used to calculate the velocity and size (d_{va}) of the particle. The velocity is used to queue the firing of a 266 nm Nd:YAG laser (Quantel), operating at 0.5-1.5 mJ, for desorption and ionization of the particle. Dual polarity mass spectra are acquired after ions pass through a time-of-flight mass spectrometer (Tofwerk). The particle source is determined using positive spectra, while negative spectra provide information on the secondary species and chemical processing that the particle has undergone [*Guazzotti et al.*, 2001; *Noble and Prather*, 1996; *Prather et al.*, 2008].

The Twin Otter aircraft (CalNex) inlet transmitted ~100% of particles up to 3500 nm [*Hegg et al.*, 2005], and the Gulfstream-1 (CARES) transmitted near unity up to 5000 nm [*Zaveri et al.*, 2012]. The Twin Otter inlet is sub-isokinetic while the Gulfstream-1 inlet is isokinetic (leading to the lower size cutoff compared to the Gulfstream-1). However, the transmission of both inlets is near unity within the A-ATOFMS size range (100-1000nm). In both aircraft sampling lines were reasonably similar, ~2 m long and unheated, so no further corrections are warranted.

Single-particle mass spectra were imported into Matlab (The MathWorks, Inc.) using the YAADA software toolkit (www.yaada.com). An adaptive resonance theory-based clustering algorithm (ART-2a, vigilance factor of 0.80, learning rate of 0.5, 20 iterations, and regroup vigilance factor of 0.85) was used to group spectra into clusters based on similar mass spectral characteristics [*Allen*, 2002; *Rebotier and Prather*, 2007; *Song et al.*, 1999]. Data from each campaign were grouped and then analyzed separately using ART-2a. Greater than 95% of ART-2a analyzed particles were grouped into clusters, which were further combined manually into 11 general particle types based on characteristic ion markers. Mass spectral peaks were identified according to the most probable ions at a given mass-to-charge (*m/z*) ratio. Particle source classifications were established based upon characteristic peaks identified in previous studies; however, these labels do not reflect all of the species present in a particle type (i.e., the presence of secondary species, such as sulfate or nitrate). Calculated standard errors of number fractions were small, <1%, and hence are not included in this discussion.

High sensitivity of the A-ATOFMS detectors occasionally led to the acquisition of gas phase species ionized by a laser pulse. These signals were occasionally counted as particles, and were removed from analysis by retroactively raising the peak area threshold above the gas phase baseline. During CalNex, sampling inlet pressures were changed for flights after 10 May 2010; hence, the transmission efficiency of the aerodynamic lens was altered. Therefore, a direct

comparison of particle number between early fights and later fights is not possible. However, fractional compositions of particles can still be compared as there was no noticeable change in size distribution with the differing inlet pressure, just overall transmission, as indicated by a high correlation of size distributions before and after inlet pressure change ($R^2 = 0.97$).

1.3.2.1.2 CalNex - Southern California

Measurements were taken onboard Twin Otter operated by the Center for Interdisciplinary Remotely-Piloted Aircraft Studies (CIRPAS). Flight operations were based out of Ontario, CA through the Guardian Jet Center, a part of the Los Angeles (LA)/Ontario International Airport. There were nine flights during the study period of 5 May 2010 – 18 May 2010, with each flight lasting ~4 hours with a usual start time of ~11 AM local time (PDT). All flight tracks are shown in Figure 12 and flight dates can be found in Table 3. Flights focused on the LA basin, often making multiple circuits over the same area. Results from the CalNex campaign are hereafter referred to as southern California. Particle concentrations and sizes from 100 – 3000 nm were measured by a Passive Cavity Aerosol Spectrometer Probe (PCASP), and two Condensation Nuclei Counters (CPC, TSI models 3010 and 3025), detecting particles down to 10 and 3 nm, respectively. Both instruments maximum size exceeds the maximum of the aircraft inlet (3500 nm). The A-ATOFMS collected data for 8 out of 9 flights, measuring the chemical composition and size of 75,969 particles during this study.

Campaign	Flight Name[1] (yyyymmdd)	Temperature (°C)	RH (%)	UF-CPC (#/ccm)*10^4	CPC (#/ccm)*10^3	PCASP/UHSAS[2] (#/ccm)*10^3
CalNex	20100504a	20.8 ± 2.6	39 ± 12	1.5 ± 1.0	11.6 ± 5.0	1.5 ± 0.4
	20100505a	18.8 ± 2.4	51 ± 33	1.0 ± 0.5	N/A	5.8 ± 5.1
	20100506a	17.0 ± 1.9	58 ± 54	1.2 ± 0.6	10.6 ± 4.5	1.4 ± 0.4
	20100507a	21.6 ± 2.3	35 ± 22	1.4 ± 0.6	11.4 ± 4.3	3.3 ± 3.9
	20100510a	13.7 ± 1.3	61 ± 37	1.3 ± 0.7	11.0 ± 4.9	0.7 ± 0.3
	20100512a	18.8 ± 3.2	35 ± 15	1.4 ± 0.8	11.2 ± 5.3	2.9 ± 3.8
	20100513a	21.3 ± 3.9	31 ± 14	1.1 ± 0.7	8.2 ± 4.1	1.0 ± 0.6
	20100514a	16.6 ± 2.3	64 ± 10	1.5 ± 0.8	12.1 ± 5.2	1.3 ± 0.4
	20100515a	19.3 ± 3.2	56 ± 29	1.2 ± 0.5	10.8 ± 4.0	1.6 ± 0.4
	All Flights	18.6 ± 3.6	48 ± 31	1.3 ± 0.7	10.9 ± 4.8	2.2 ± 2.9
CARES	20100603a	20.2 ± 4.0	60 ± 7	2.2 ± 1.9	18.1 ± 12.5	N/A
	20100606a	23.5 ± 2.1	55 ± 5	2.2 ± 1.8	18.0 ± 11.4	N/A
	20100606b	24.4 ± 6.7	41 ± 9	1.3 ± 1.0	10.8 ± 6.4	N/A
	20100608a	20.1 ± 2.0	56 ± 10	2.0 ± 2.0	1.0 ± 0.8	N/A
	20100608b	20.5 ± 4.6	40 ± 14	1.3 ± 1.3	0.9 ± 0.7	N/A
	20100610a	17.4 ± 3.8	38 ± 8	1.7 ± 1.0	1.0 ± 0.3	1.1 ± 0.6
	20100612a	20.9 ± 2.7	28 ± 2	1.2 ± 1.8	0.5 ± 0.7	0.9 ± 0.2
	20100612b	25.1 ± 2.5	25 ± 4	1.4 ± 1.0	0.7 ± 0.3	1.5 ± 0.8
	20100614a	23.8 ± 2.9	32 ± 9	2.8 ± 2.4	1.3 ± 1.0	2.1 ± 1.9
	20100615a	17.3 ± 1.9	55 ± 12	2.2 ± 1.9	1.1 ± 1.5	1.6 ± 1.9
	20100615b	20.7 ± 5.5	42 ± 9	1.5 ± 0.9	1.1 ± 0.6	2.6 ± 0.8
	20100618a	21.5 ± 5.7	25 ± 12	2.2 ± 1.6	1.1 ± 0.8	2.3 ± 1.9
	20100619a	18.5 ± 3.6	39 ± 9	2.0 ± 1.0	1.5 ± 0.7	1.9 ± 1.0
	20100621a	18.8 ± 1.7	43 ± 7	1.9 ± 2.2	1.1 ± 1.2	1.9 ± 1.1
	20100621b	25.2 ± 6.6	21 ± 7	1.1 ± 0.9	0.8 ± 0.5	1.8 ± 1.1
	20100623a	19.6 ± 4.0	40 ± 10	0.8 ± 1.2	0.6 ± 1.0	3.2 ± 1.0
	20100623b	25.0 ± 6.8	30 ± 8	1.3 ± 0.7	0.9 ± 0.5	3.9 ± 1.8
	20100624a	19.1 ± 2.1	44 ± 15	2.1 ± 2.1	1.0 ± 1.0	1.2 ± 0.8
	20100624b	22.1 ± 3.8	37 ± 8	2.1 ± 1.6	2.4 ± 3.1	2.3 ± 1.0
	20100627a	25.6 ± 2.1	41 ± 10	0.6 ± 0.9	0.5 ± 0.6	3.4 ± 3.1
	20100628a	28.2 ± 2.6	38 ± 7	1.0 ± 1.0	0.8 ± 0.8	3.9 ± 1.9
	20100628b	35.5 ± 5.7	25 ± 4	0.8 ± 0.5	0.6 ± 0.3	3.5 ± 1.6
	All Flights	22.4 ± 5.7	39 ± 14	1.6 ± 1.6	2.7 ± 6.1	2.2 ± 1.7
	NoCal-1	21.0 ± 4.7	41 ± 14	1.9 ± 1.6	3.9 ± 7.6	1.8 ± 1.4
	NoCal-2	24.3 ± 6.5	36 ± 1	1.3 ± 1.5	1.0 ± 1.3	2.7 ± 1.9

[1] Flight names labeled "a" occurred in the morning, while those labeled with a "b" were in the afternoon

[2] PCASP was used during CalNex while the UHSAS was used during CARES

Table 3: Mean (± std dev) meteorological data and particle concentrations over all of CalNex, CARES, NoCal-1, and NoCal-2.

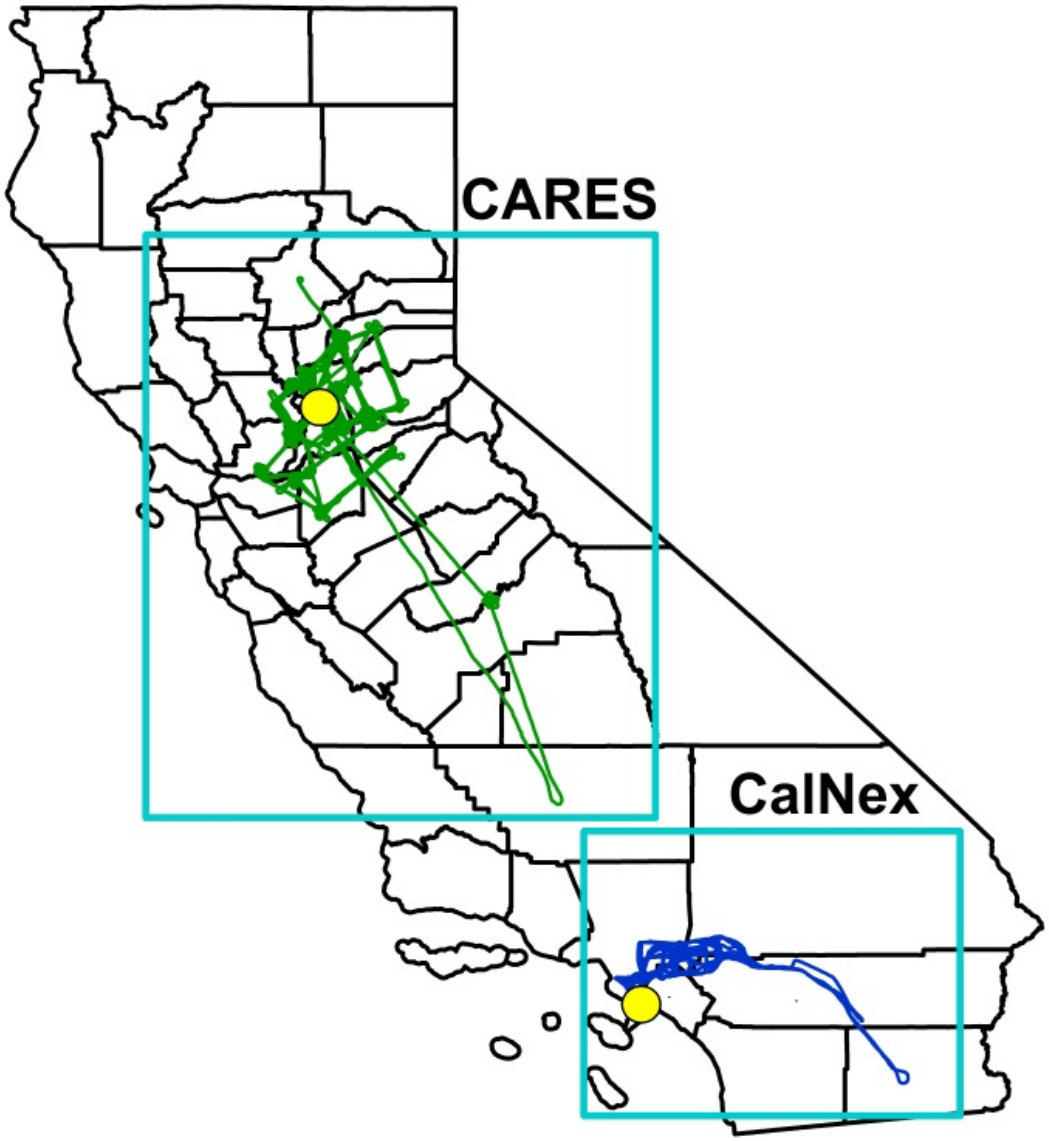

Figure 12: Operational areas for CARES and CalNex. All flight paths are overlaid on each other. Yellow dots represent Sacramento (CARES) and Los Angeles (CalNex).

1.3.2.1.3 CARES – Northern California

Flights were operated out of the McClellan Airfield in Sacramento, CA from June 2 – 28, 2010 onboard the Department of Energy Gulfstream-1. This study focused on the surrounding urban Sacramento area and Sierra Nevada foothills. Thus, results from this campaign are interchangeably referred to as northern California. Usually each sampling day consisted of a flight in the morning, ~8AM local, and in the afternoon, ~2 PM local, with most flights lasting

~4 hours. Flight dates are given in Table 3, while the flight paths for all 22 flights during the study are shown in Figure 12. More details on the campaign and instrumentation aboard the aircraft can be found elsewhere [*Zaveri et al.*, 2012]. Gas-phase concentrations of SO_2 and NO_X, as well as other species, were measured in flight. Total condensation nuclei (CN) concentrations were measured using the same CPC models used in the CalNex campaign (TSI models 3010 and 3025). Number concentration and size for particles with sizes from 55-1000 nm were detected using an Ultra-High Sensitivity Aerosol Spectrometer (UHSAS) probe (Droplet Measurement Technologies). For direct comparisons of gas-phase species and particle concentrations between CalNex and CARES, representative average concentrations were calculated using data from the California Air Resources Board (CARB, http://www.arb.ca.gov) ground based measurements from North Main Street in LA and from Del Paso Manor in Sacramento to represent CalNex and CARES, respectively. The A-ATOFMS was on-line for 20 of 22 total flights, chemically analyzing 60,230 particles.

A noticeable shift in particle composition, particulate mass, and meteorology occurred during CARES after June 21 (Figure 15). The sources and processes contributing to these two periods were quite different. To examine these differences in detail, the CARES study was separated into two periods, Northern California-1 (NoCal-1) and Northern California-2 (NoCal-2), representing fights from June 2 – 19, 2010 and June 21 – 28, 2010, respectively. These two periods are discussed in more detail a later section**.**

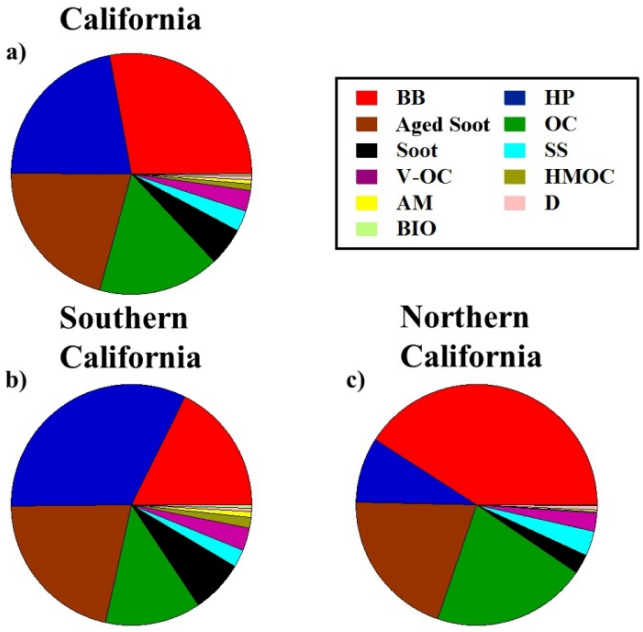

Figure 13: Number fractions of A-ATOFMS particle sources, determined by the most dominant ions in A-ATOFMS mass spectra, for California (a), southern California (b), and northern California (c).

1.3.2.2 Results and Discussion

1.3.2.2.1 Particle sources throughout California

As shown in Figure 13a, predominant particle sources by number fraction in the boundary/residual layers of both campaigns were identified as biomass burning (BB), highly processed (HP), soot mixed with OC (Aged Soot), OC, and soot, which represented 28, 22, 21, 16, and 5% of total particle counts measured by the A-ATOFMS in both studies, respectively. BB originated from agricultural and residential burning, which is most prevalent in the rural regions of northern California. These spectra are characterized by an intense potassium peak at mass/charge (*m/z*) $^{39}K^+$ (Figure 14a) in addition to less intense OC and soot peaks at *m/z* $^{12}C^+$, $^{24}C_2^+$, $^{27}C_2H_3^+/CHN^+$, $^{29}C_2H_5^+$, $^{36}C_3^+$, and $^{43}C_2H_3O^+/CHNO^+$ [*Bi et al., 2011*; *Guazzotti et al., 2001*; *Hudson et al., 2004*; *Silva et al., 1999*]. HP particles are particles for which only negative ion spectra were acquired. Because the core, which is shown in the positive ion spectra, was not obtained, the source of these particles cannot be identified; however, they are hypothesized to be carbonaceous particles that have undergone extensive processing based on the high sulfate and nitrate content. Additionally this type was only seen after takeoff in both studies. The size distributions of these particles are nearly identical to those of Aged Soot particles ($R^2 = 0.98$) and to a lesser extent BB and OC particles ($R^2 = 0.93$ and 0.89, respectively) and lend support to the hypothesis that they are most likely heavily-coated soot particles. Thus, these particles will be included as carbonaceous aerosol in subsequent discussions.

Negative ion spectra were absent in 13% of particles in California. This has previously been attributed to significant amounts of water present on the particle which inhibits the formation of negative ions [*Neubauer et al., 1997*; *Neubauer et al., 1998*]. However, due to the low average relative humidity (RH) during the studies, 49±30% and 39±14%, for CalNex and CARES respectively, and typical deliquescent RH thresholds of >60% [*Neubauer et al., 1998*], it is unlikely that there was significant water present on the particles to justify the lack of negative spectra. Similar conclusions were deduced from modeling of the CARES study [*Fast et al., 2012*]. Further, spectra with only positive ions were less frequent during CalNex (4%) than CARES (24%) despite the higher RH during CalNex. Temporal comparisons of positive only spectra with RH do not indicate any correlation between the two. Further, significantly higher fractions of particles contain negative ion spectra during NoCal-1, 94%, compared to NoCal-2, 62%. This is despite the higher RH of 41±15% compared to 36±12% for NoCal-1 and NoCal-2, respectively. It is hypothesized that for these studies the acquisition of negative ion spectra was dependent on the presence of secondary species, like sulfate or nitrate, rather than the amount of water present.

Aged Soot, formed primarily through fossil fuel combustion and subsequent coagulation with or condensation of semi-volatile organic species, has intense elemental carbon C_n^+ peaks ($^{12}C^+$, $^{24}C_2^+$, $^{48}C_3^+$) with weaker OC peaks, *m/z* $^{27}C_2H_3^+$, $^{29}C_2H_5^+$, $^{37}C_3H^+$, $^{39}C_3H_3^+/K^+$, $^{43}C_2H_3O^+$ [*Moffet and Prather, 2009*; *Spencer and Prather, 2006*] (Figure 14b). Peaks at *m/z* $^{27}C_2H_3^+/CHN^+$, $^{29}C_2H_5^+$, $^{37}C_3H^+$, $^{39}C_3H_3^+/K^+$, and $^{43}C_2H_3O^+/CHNO^+$ are indicative of OC species from vehicle and biogenic emissions (Figure 14c). Peaks at *m/z* $^{50}C_4H_2/C_3N^+$, $^{59}C_3H_9N^+$ and peaks at *m/z* $^{12}C^+$, $^{24}C_2^+$, $^{48}C_3^+$, similar to soot, were occasionally also seen on OC particles but at significantly lower relative intensities [*Spencer and Prather, 2006*]. Figure 14d shows soot spectra which consist of almost entirely elemental carbon C_n^+ peaks out to the high mass range (i.e., *m/z* $^{12}C^+$,

$^{24}C_2^+$ … $^{180}C_{15}^+$, and C_n^- peaks from *m/z* $^{12}C^-$, $^{24}C_2^-$ … $^{72}C_6^-$ in negative spectra). As this particle type doesn't typically contain secondary species, it is thought to be relatively fresh. Other carbonaceous and non-carbonaceous particle types, like vanadium mixed with OC (V-OC) [*Ault et al., 2009*], high mass OC (HMOC) [*Silva and Prather, 2000*], amine (AM) [*Angelino et al., 2001*; *Pratt and Prather, 2010*; *Sorooshian et al., 2008b*], biological (BIO) [*Fergenson et al., 2004*; *Pratt and Prather, 2010*; *Russell, 2009*], dust (D) [*Pratt and Prather, 2010*; *Silva and Prather, 2000*], and sea salt (SS) [*Gard et al., 1998*], each represented <3% of the total aerosol measured by the A-ATOFMS (2.78, 0.86, 0.56, 0.30, 0.50, 2.80%, respectively). Vanadium mixed with OC (V-OC) that was emitted from the combustion of ship fuels composed ~3% of particles measured by the A-ATOFMS [*Ault et al., 2009*]. This particle type has intense peaks at $^{51}V^+$ and $^{67}VO^+$ as well as OC peaks at *m/z* $^{27}C_2H_3^+/CHN^+$, $^{29}C_2H_5^+$, $^{37}C_3H^+$, $^{39}C_3H_3^+/K^+$, and $^{43}C_2H_3O^+/CHNO^+$ [*Ault et al., 2009*]. HMOC consists of OC peaks at *m/z* $^{27}C_2H_3^+/CHN^+$, $^{37}C_3H^+$, $^{39}C_3H_3^+/K^+$ as well as many intense peaks >100 *m/z*. These types likely represent polycyclic aromatic hydrocarbons or other oligomers formed through cooking processes [*Silva and Prather, 2000*]. Occasionally this particle type contained peaks similar to organosulfates (OS) that may lead to an overestimation of OS number fractions, especially during CalNex where HMOC was more prevalent (1.42% compared to 0.16% for CalNex and CARES, respectively). However the number fractions of HMOC are significantly smaller than the observed number fraction of OS (28 and 35% for CalNex and CARES, respectively); hence, overestimation of OS number fractions is likely small. Amines are OC particles that contain an intense peak at *m/z* $^{56}C_2HNO^+$, $^{59}C_3H_9N^+$, $^{86}(C_2H_5)_2NCH_2^+$, and/or $^{118}(C_2H_5)_3NOH^+$ and originate from agricultural processes, animal husbandry, or photochemical processing [*Angelino et al., 2001*; *Pratt and Prather, 2010*; *Sorooshian et al., 2008b*]. Biological particles contain intense $^{40}Ca^+$, $^{56}CaO^+$, and $^{96}Ca_2O^+$ peaks along with OC ($^{27}C_2H_3^+/CHN^+$, $^{37}C_3H^+$, $^{39}C_3H_3^+/K^+$), soot ($^{12}C^+$, $^{24}C_2^+$, $^{48}C_3^+$), and phosphate ($^{79}PO_3^-$) peaks [*Fergenson et al., 2004*; *Pratt and Prather, 2010*; *Russell, 2009*].

Dusts contained a wide variety of metals (Na, K, Ti, Ca, and Fe), as well as phosphate ($^{79}PO_3^-$) and silicate ($^{44}SiO^-$, $^{60}SiO_2^-$, and $^{103}Si_2O_3^-$). Sea salt is characterized by an intense sodium peak ($^{23}Na^+$) and chlorine peaks ($^{35}Cl^-$ and $^{37}Cl^-$) as well as clusters of the two ($^{81}Na_2Cl^+$) [*Gard et al., 1998*; *Pratt and Prather, 2010*; *Silva and Prather, 2000*]. Often SS was aged significantly, containing significant nitrate, sulfate, and OC peaks. Most particle types did not have a strong dependence on size (Figure 16) with the one exception of SS particles, which had a clear dependence towards larger (> 600 nm) sizes.

Negative ion spectra were absent in 13% of particles for both studies, with the majority of these occurring during the CARES (24%) rather than the CalNex campaign (4%). This has previously been attributed to significant amounts of water present on the particle, which inhibits the formation of negative ions [*Neubauer et al., 1997*; *Neubauer et al., 1998*]. However, due to the low average relative humidity during the studies, 49±30% and 39±14%, for CalNex and CARES respectively, and typical deliquescent RH thresholds of >60% [*Neubauer et al., 1998*], it is unlikely that there was significant water present on the particles to justify the lack of negative spectra. Similar conclusions were deduced from modeling of the CARES study [*Fast et al., 2012*]. Further, spectra with only positive ions were less frequent during CalNex (4%) than during CARES (24%) despite the higher RH during CalNex. Temporal comparisons of positive only spectra with RH do not indicate any correlation between the two. Further, significantly higher fractions of particles contain negative ion spectra during NoCal-1, 94%, compared to

NoCal-2, 62%. This is despite the higher RH of 41±15% compared to 36±12% for NoCal-1 and NoCal-2, respectively. It is hypothesized that, for these studies, the acquisition of negative ion spectra was dependent on the presence of secondary species, like sulfate or nitrate, rather than the amount of water present.

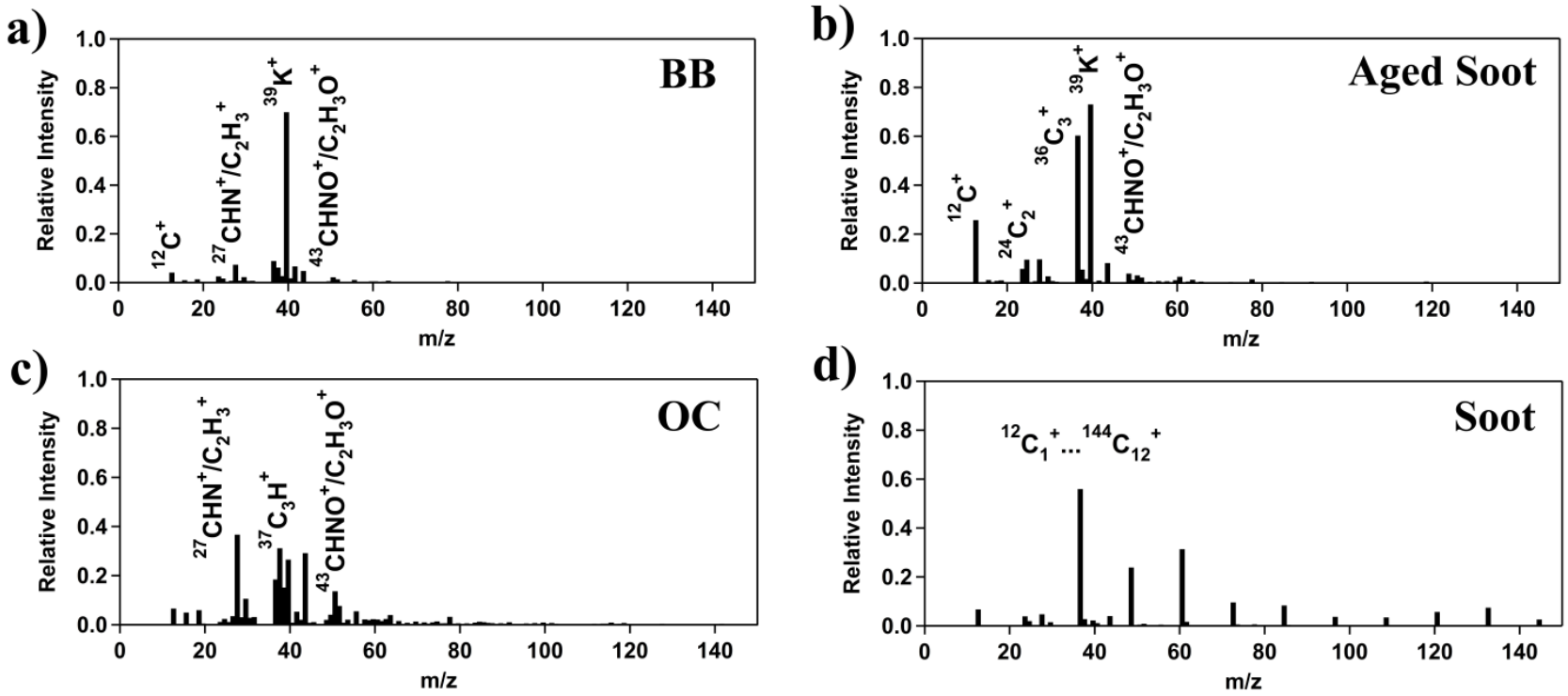

Figure 14: A-ATOFMS particle types for the main carbonaceous species: a) biomass burning, b) soot mixed with organic carbon (Aged Soot), c) organic carbon (OC), and d) soot. A wide array of negative ions, indicative of secondary species, was observed for these particle sources (hence are not show here), but common negative ions are discussed in the text and can be found in Figure 18.

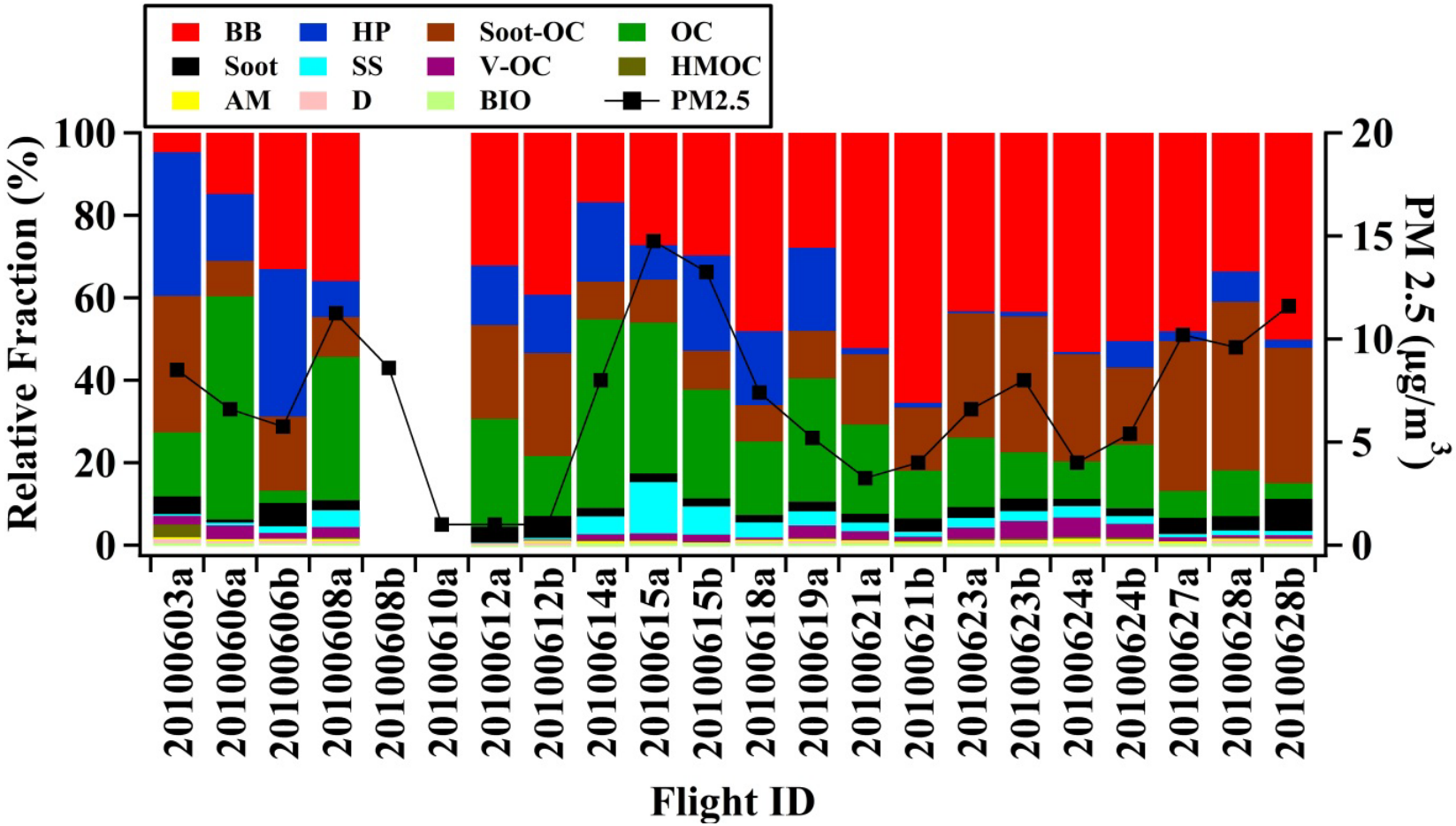

Figure 15: A-ATOFMS relative fractions of particle types and average PM2.5 mass concentrations for each flight during the CARES study. Flight labels indicate the date of the flight and if it was in the morning (a) or afternoon (b). A change in chemistry and a general increase in PM2.5 mass were observed after 6/19/10.

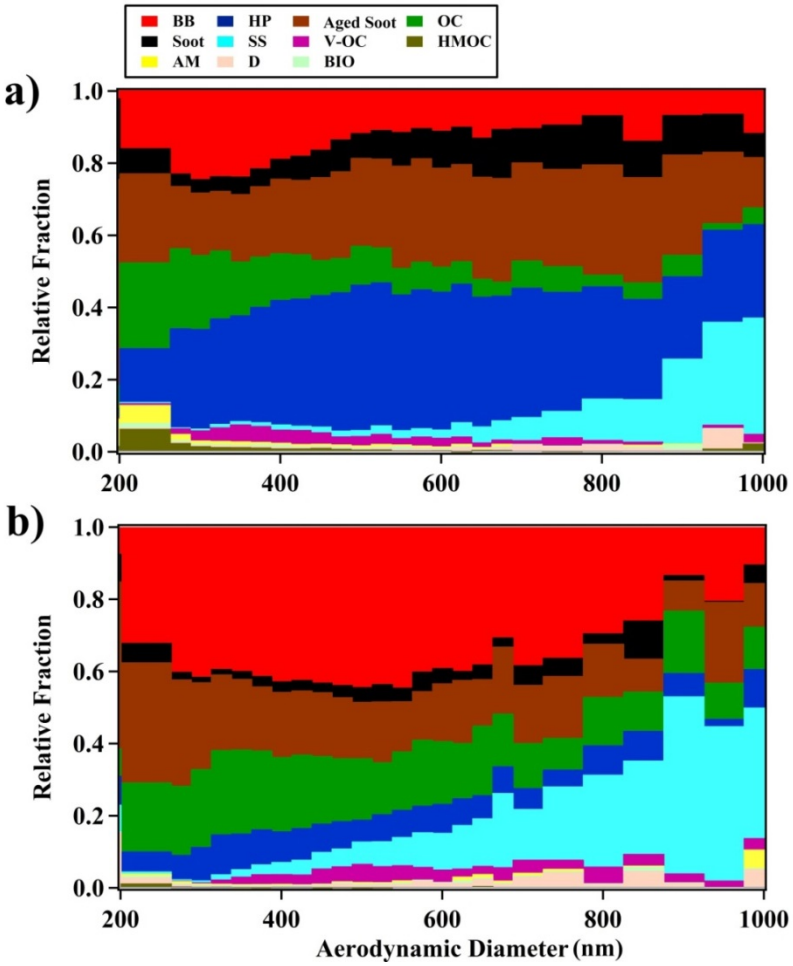

Figure 16: Size resolved mixing state for (a) southern and (b) northern California.

1.3.2.2.2 Particulate secondary species in California

For particles with the same base chemical signature (i.e., biomass, soot, OC, etc.), relative peak areas (RPA) qualitatively reflect the amount of a species on a particle in relation to other species [*Bhave et al., 2002*; *Gross et al., 2000*; *Prather et al., 2008*]. Previous studies in California have shown that the presence of ammonium nitrate [*Langridge et al., 2012*; *Sorooshian et al., 2008b*] and ammonium sulfate [*Qin et al., 2012*] can influence single particle mixing state. During this study, partitioning of methanesulfonic acid (MSA) and OS to particles was likely to occur in the vicinity of marine and heavily forested areas where MSA and OS, respectively, originate [*Gaston et al., 2010*; *Hatch et al., 2011*]. To examine the mixing state of particles with biogenic, marine, and anthropogenic species, single particle mixing state was examined by identifying peaks of ammonium ($^{18}NH_4^+$), sulfate ($^{97}HSO_4^-$, $^{195}H_2SO_4HSO_4^-$), nitrate ($^{46}NO_2^-$, $^{62}NO_3^-$, $^{125}H(NO_3)_2^-$) [*Silva and Prather, 2000*], MSA ($^{95}CH_3SO_3^-$) [*Gaston et al., 2010*], and/or OS (derived from glycolic acid (*m/z* -155), 2-methylglyceric acid (*m/z* -199), and isoprene epoxydiol (*m/z* -215)) [*Hatch et al., 2011*]. Other secondary species were investigated, but no significant trends were seen. A particle is considered to contain these species if the RPA for *m/z* ratios indicative of those species exceeds 0.5% of the mass spectrum. For example, a particle contains sulfate if the RPA at *m/z* -97 or -195 is greater than 0.5% of the ions in the entire mass spectrum.

Most particles in California were found to be internally mixed with secondary species, with nearly 88% of particles by number containing sulfate, nitrate, MSA, OS, or ammonium individually or internally mixed together. Commonly, particles contained sulfate (82%) or nitrate (82%), and 76% of particles had both, but, as discussed below, the magnitude of these species varied greatly between southern and northern California.

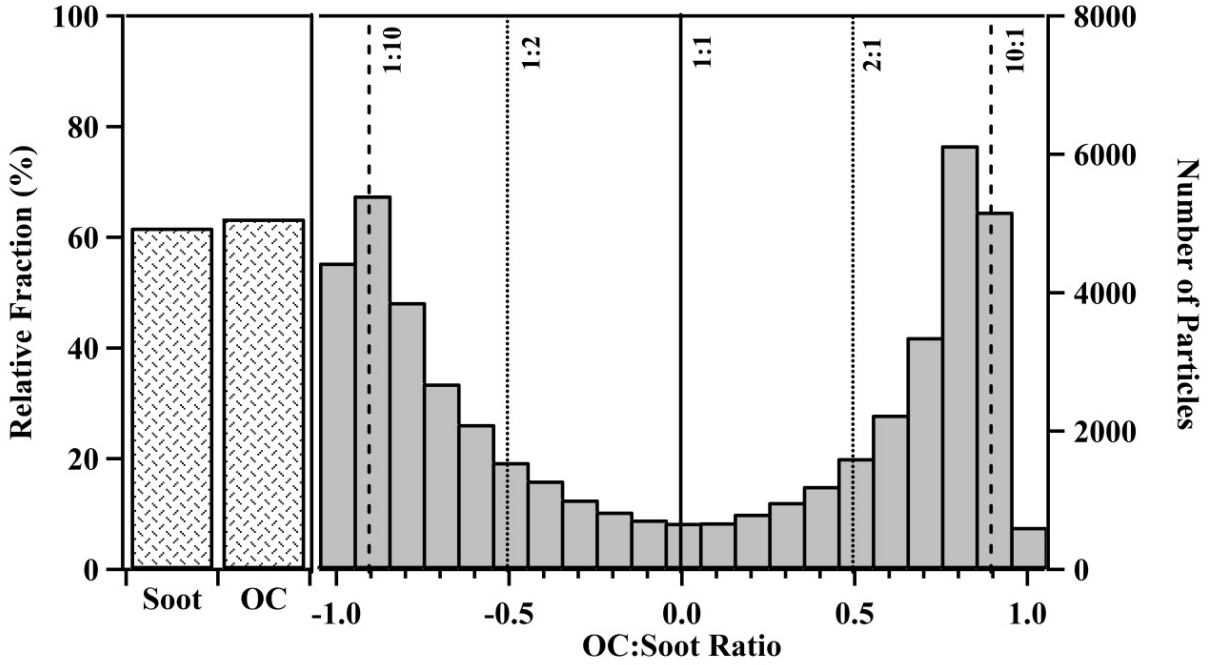

Figure 17: Fraction of particles containing soot and OC with RPA > 0.5% in southern California (left panel). Single particle OC:soot peak ion ratio distributions are shown in the right panel. Values < 0 indicate more soot than OC on single particles and values > 0 indicate more OC than soot. Ratios representing 1:1, 2:1, and 10:1 are shown by solid, dotted, and dashed lines, respectively.

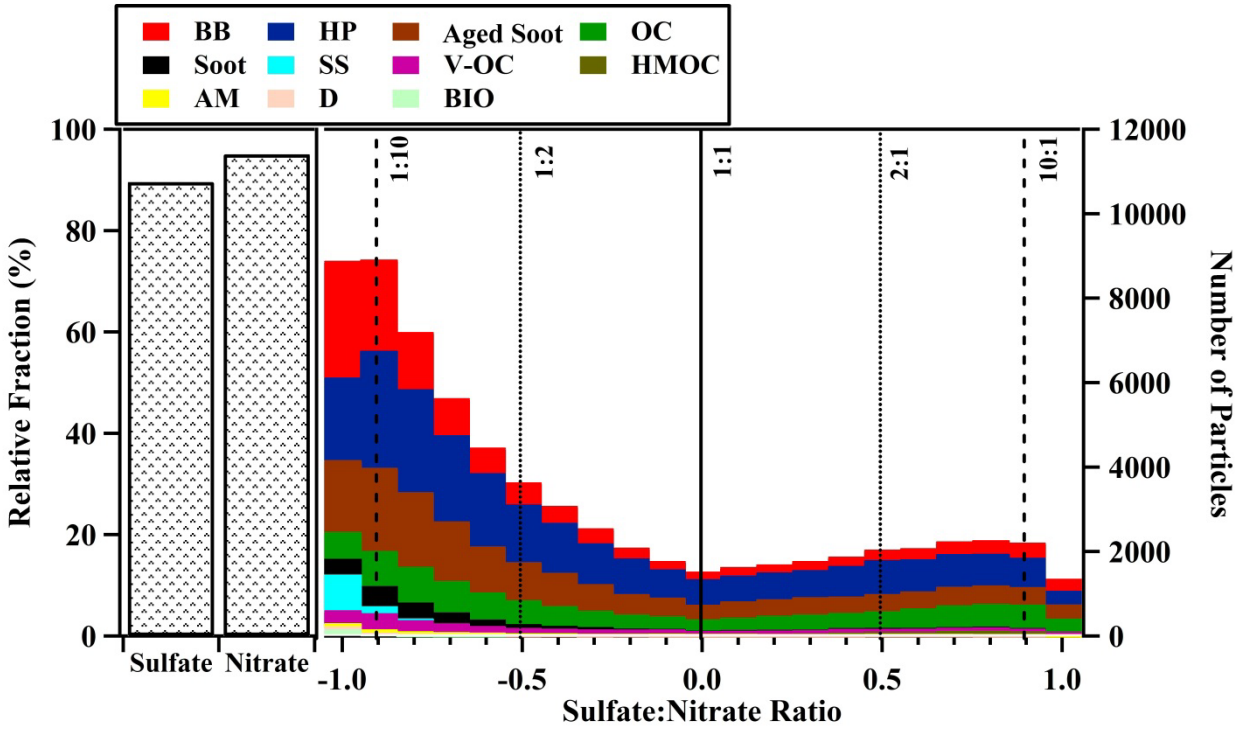

Figure 18: Fraction of particles containing sulfate and nitrate with RPA > 0.5% in southern California (left panel). Sulfate:nitrate ion ratio distributions are shown in the right panel. Values < 0 indicate more nitrate than sulfate and values > 0 indicate more sulfate than nitrate. Ratios representing 1:1, 2:1, and 10:1 are shown by solid, dotted, and dashed lines, respectively.

1.3.2.2.3 Southern California aerosol mixing state

In the LA basin, which is frequently capped by a temperature inversion, a prevalent sea breeze typically transports air to the east toward the outflow pathways of the basin. Most Twin Otter flights in southern California were carried out at low altitudes, <700 m, sampling within the boundary layer. The number fractions of the main carbonaceous aerosol types from southern California differed greatly from those in California as a whole, as shown in Figure 13b. Particles were generally highly-aged, as seen by the high fraction of HP aerosols in the region (33%). Particles are often entrained within the basin, where they can undergo significant atmospheric processing [*Schultz and Warner, 1982*; *Ulrickson and Mass, 1990*]. Aged Soot, BB, OC, and soot were the other main particle types present, comprising 21, 18, 13, and 7% of A-ATOFMS total particle counts in southern California. V-OC, AM, HMOC, and BIO represented 3.0, 0.8, 1.4, and 0.5% of total particles, respectively. Excluding HP particles, nearly 96% of submicron particles measured by the A-ATOFMS in southern California contained carbonaceous material. Though some variability was seen from flight to flight during CalNex, number fractions for the main particle types did not generally deviate greatly from the number fractions reported above.

Representative soot ($^{36}C_3^+$, $^{48}C_4^+$, $^{60}C_5^+$) and OC ($^{27}C_2H_3^+$, $^{29}C_2H_5^+$, $^{37}C_3H^+$, $^{43}C_2H_3O^+$) ions > 0.5% of the mass spectrum were present in 62% and 63% of total particles, respectively (Figure 17, left panel) [*Spencer and Prather, 2006*]. Normally soot is emitted at sizes below the detection limit of the instrument (100 nm). The fact that particles with intense soot peaks were seen indicates that soot particles had grown into the A-ATOFMS size range. Secondary species,

such as nitrate, sulfate, and OC, contribute to this growth, but the extent each component plays in particle growth is unknown. OC RPA cannot be compared directly to sulfate and nitrate RPA as their ion formation mechanisms are different. However, OC and soot RPAs can be compared to determine the relative amount of OC mass on a particle. If the magnitude of OC peaks is low, then other species must have contributed to the growth of soot into larger sizes. To elucidate the magnitude of soot with OC in the same particle, a peak ion ratio of OC:soot was calculated by dividing the total RPA for each species by the other. These ratios form a distribution of values that represents all of the variance in magnitude of these species on particles ranging from pure OC to pure soot. Since these ratios are calculated for a single particle, they are not dependent on laser fluence or matrix effects, assuming that the entire particle is completely ablated and that matrix effects suppress the selected ions equally [*Morrical et al.*, 1998; *Wenzel and Prather*, 2004]. It should be noted that OC particles could contain a soot core that was not ablated fully, which would affect these calculations, and that HP particles were not included in this analysis since they did not contain positive ions [*Morrical et al.*, 1998; *Pratt and Prather*, 2009; *Steele et al.*, 2003].

The OC:soot ion ratio distribution for particles in southern California is shown in Figure 17, right panel. For visual clarity, the OC:soot ratio has been normalized so that ratios < 1 will approach -1 as it proceeds to -∞ (i.e., soot without OC) using the formula ($Ratio_{normalized}$ = Ratio - 1), and a ratio > 1 will approach 1 as the ratio proceeds to +∞ (i.e., OC without soot) using the formula ($Ratio_{normalized}$ = 1 – {1/Ratio}). It should be emphasized that as ratios approach -1 or 1, they are exponentially increasing, while nearing zero the RPA of each species is essentially the same. This results in a broader range of ratios for bins near -1 or 1, while near 0 bins include a smaller range of ratios. As expected, a distribution of OC:soot ratios exists, demonstrating the variability in mixing state observed in southern California. As shown in Figure 17, right panel, a nearly equal number of particles have ratios above and below 0, although pure soot has nearly seven times as many particles as pure OC. On days when OC dominates the mass spectra, influences from BB were significant, which is expected since BB is composed of nearly 62% OC by mass for smoldering fires [*Reid et al.*, 2005]. Soot likely originated from fossil fuel vehicle emissions in the LA basin [*Ying and Kleeman*, 2006].

Most particles in southern California had been processed to some degree, as indicated by ~96% of particles producing negative ion spectra with secondary species. Similarly, Metcalf et al. [2012] found that most soot particles were present with coatings of varying thicknesses during the CalNex study. Nitrate appeared on 95% of particles by number, and 90% of particles contained sulfate peaks (Figure 18, left panel). Ratios of sulfate:nitrate RPAs, calculated in the same manner as OC:soot ratios, for every particle (including HP) are shown in Figure 18, right panel. Most particles contain more nitrate than sulfate, but still a significant number of particles contain more sulfate than nitrate. This largely corroborates findings reported from other measurements during CalNex [*Langridge et al.*, 2012; *Metcalf et al.*, 2012]. To see if there is preferential partitioning of nitrate or sulfate to any particular source, the ion ratio distribution in Figure 18, right panel was split into particle sources. Most particle sources have very similar ion ratio distributions that cover a wide range of sulfate:nitrate values, indicating that nitrate and sulfate partitioned to particles regardless of the original source/core. SS and V-OC are the only exception, as both of these types are present with ion ratio distributions exclusively favoring nitrate. Nitrate is known to heterogeneously replace chloride on SS particles as they age, which may explain the preference of nitrate to SS observed in peak ratios [*Gard et al.*, 1998]. Ault et

al. [2010] measured V-OC particles near to the emission source and hypothesized that vanadium acted as a catalyst to produce sulfate from SO_2. In the present work, particles were measured farther from the source and are processed to a higher degree such that nitrate might have replaced sulfate on those particles. This analysis demonstrates that ion ratio distributions may be used to identify different processing mechanisms when preferential partitioning of species to distinct types is observed.

Large nitrate fractions can be attributed to high NO_x concentrations over Los Angeles, an average of 32 ppb for the study period (CARB, 2009). In addition, ammonium nitrate originates from animal husbandries surrounding the Los Angeles area near Chino, which have been shown to be a large source of ammonia in the region [*Kleeman and Cass*, 1998; *Singh et al.*, 2002; *Sorooshian et al.*, 2008b; *Ying and Kleeman*, 2006]. Ammonium was found to be present in 37% of total particles, so the high nitrate seen in CalNex could in part be due to the presence of ammonium nitrate. Nearly 98% of particles internally mixed with sulfate were also mixed with nitrate, whereas only 93% of particles internally mixed with nitrate were mixed with sulfate in southern California. MSA was present on 52% of total particles in southern California, indicating that sulfate originating from marine sources was prevalent in the region, as expected due to the close proximity of LA to the ocean (~30 km) [*Ying and Kleeman*, 2006]. A small fraction of particles contained organosulfate peaks (28%), likely due to smaller biogenic influence in the LA basin.

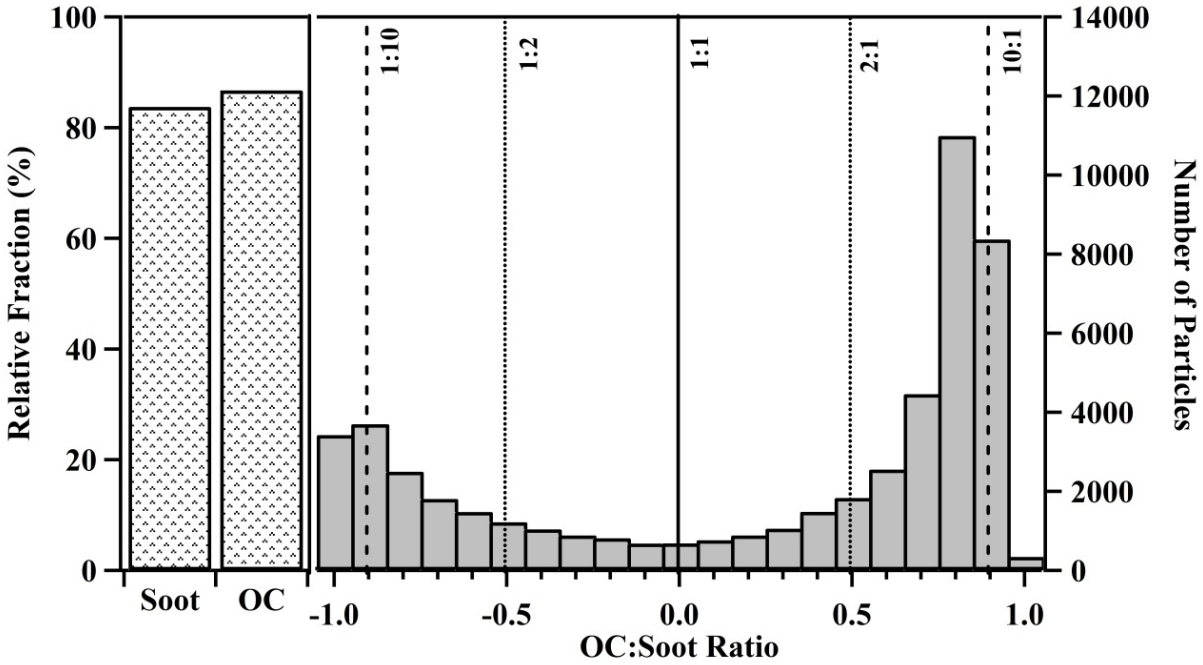

Figure 19: Fraction of particles containing soot and OC with RPA > 0.5% in northern California (left panel). OC:soot ion ratio distributions are shown in the right panel. Values < 0 indicate more soot than OC and values > 0 indicate more OC than soot. Ratios representing 1:1, 2:1, and 10:1 are shown by solid, dotted, and dashed lines, respectively.

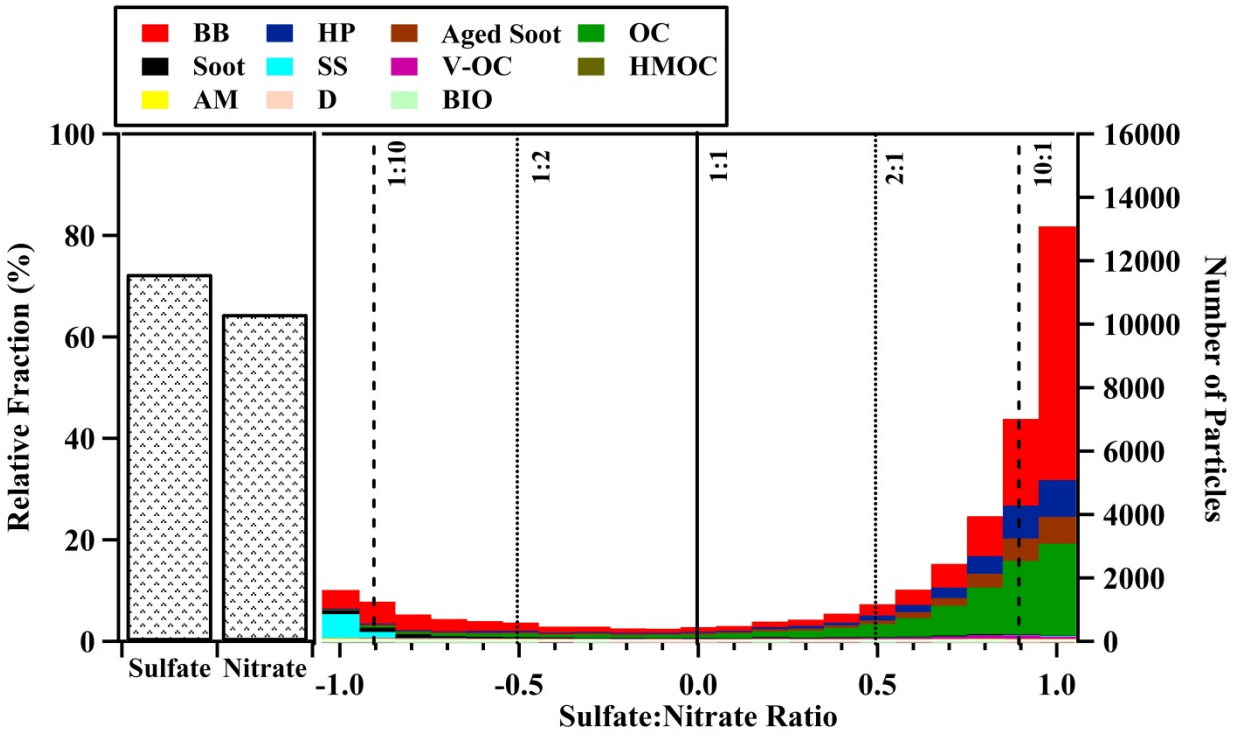

Figure 20: Fraction of particles containing sulfate and nitrate with RPA > 0.5% in northern California (left panel). Sulfate:nitrate ion ratio distributions are shown in the right panel. Values < 0 indicate more nitrate than sulfate and values > 0 indicate more sulfate than nitrate. Ratios representing 1:1, 2:1, and 10:1 are shown by solid, dotted, and dashed lines, respectively.

1.3.2.2.4 Northern California aerosol mixing state

The Sacramento region is characterized by consistent southwesterly flow that carries air into the Sierra Nevada foothills during the day and recirculates the air back towards Sacramento at night, forming a residual layer of aged air the next day [*Fast et al.*, 2012; *Zaremba and Carroll*, 1999]. Most flights sampled at low altitudes, <700 m, in either the boundary layer or residual layer. Number fractions of particles in northern California are shown in Figure 13c. Unlike in southern California, BB represented a more significant fraction of particles (41% by number), due to increased residential and agricultural burning in the rural regions in northern California. HP particles did not represent as large a fraction in northern California, comprising only 9% of particles versus 33% in Southern California. Furthermore, only 76% of particles contained negative ion spectra, suggesting that particles in northern California had not undergone as much processing as in southern California. Often the lack of negative ion spectra is attributed to the presence of water [*Neubauer et al.*, 1997; *Neubauer et al.*, 1998], however relative humidity was lower on average during the CARES study (39±14%) compared to CalNex (49±30%); hence, the potential impact of water on suppressing negative ion spectra should be less relative to CalNex.

As was observed in southern California, OC and Aged Soot comprised a significant fraction of total aerosol in northern California, 21% and 20%, respectively. Pure soot was present at lower

number fractions (3%) than in southern California (7%), though a better representation of soot and OC content can be found through peak areas and peak area ratios. Significant soot and OC peaks were found in 84% and 87% of total particles, respectively (Figure 19, left panel). The single particle ion ratio distribution of OC:soot (Figure 19, right panel), which are directly comparable between studies, indicates that OC was more significant in northern California as compared to southern California, with nearly 64% of ratios >1 (having more OC than soot). This fraction is significantly higher than that in southern California (48%) and is likely due to the heavily-forested Sierra Nevada foothills lying to the northeast of Sacramento, which act as a source of biogenically-derived OC particles.

In contrast to southern California, most particles in northern California were primarily mixed with sulfate rather than with nitrate. Sulfate peaks were internally mixed with 72% of particles in northern California (Figure 20, left panel). Of those particles containing sulfate, 59% contained nitrate, though sulfate markers were usually many times more prominent than nitrate markers on the same particle. Few particles contained only nitrate (~3%), while 13% of particles comprised only sulfate. Figure 20, right panel shows the sulfate:nitrate ion ratio distribution for particles containing sulfate or nitrate in northern California. 80% of particles contained more sulfate than nitrate and ~51% of those particles had a ratio >10:1. Similar to southern California, ratios covered a wide range of values, though in northern California ion ratio distributions did not indicate preferential partitioning of sulfate or nitrate to any particle type, with the exception of SS which was present with high ratios of nitrate, as in southern California. The decreased prevalence of nitrate in northern California can be attributed to lower NO_X emissions in northern California as compared to southern California, with 1-hour averages of 4 and 32 ppb, respectively, based on measurements at ground sites in Sacramento and LA (CARB, 2009). Ammonium was present in amounts similar to those in southern California, representing nearly 42% of total particles, suggesting the presence of ammonium sulfate. Recently published findings from AMS measurements at the T1 rural ground site during CARES, near the Sierra Nevada foothills, determined that much of particulate sulfate was indeed present as ammonium sulfate [*Setyan et al.*, 2012].

One can gain insight into the source of sulfur species by examining the presence of MSA (originating from marine air) and OS (originating from biogenic aerosol) on single particles. While OS and MSA peaks were detected on 35% and 50% of particles, respectively, sulfate was present on 72% of particles, and usually exhibited higher peak intensities. Fast et al. [2012] hypothesized that a significant fraction of SO_2 present in the CARES region originates from the oil refineries in the Carquinez Strait, near San Francisco, as no substantial sources of SO_2 exist in the Sacramento area. While anthropogenic SO_2 from this source is likely responsible for the high sulfate present on single particles, some days were observed to have high fractions of particles containing OS and MSA, indicating significant contributions from natural sources. For example, on June 14, nearly 70% of the particles contained OS, and on June 3, 72% of particles contained MSA. These elevated fractions occurred toward the beginning of the study and, as will be discussed in the following section, particle composition exhibited significant temporal variability during the CARES study. It should be noted that the current CARB inventory of sulfur from natural sources is zero, while the data here suggests some fraction due to natural sources. Additional studies focused just on the potential sources of OS (forest) and MSA (ocean derived) could shed more insight into these natural sources of sulfate.

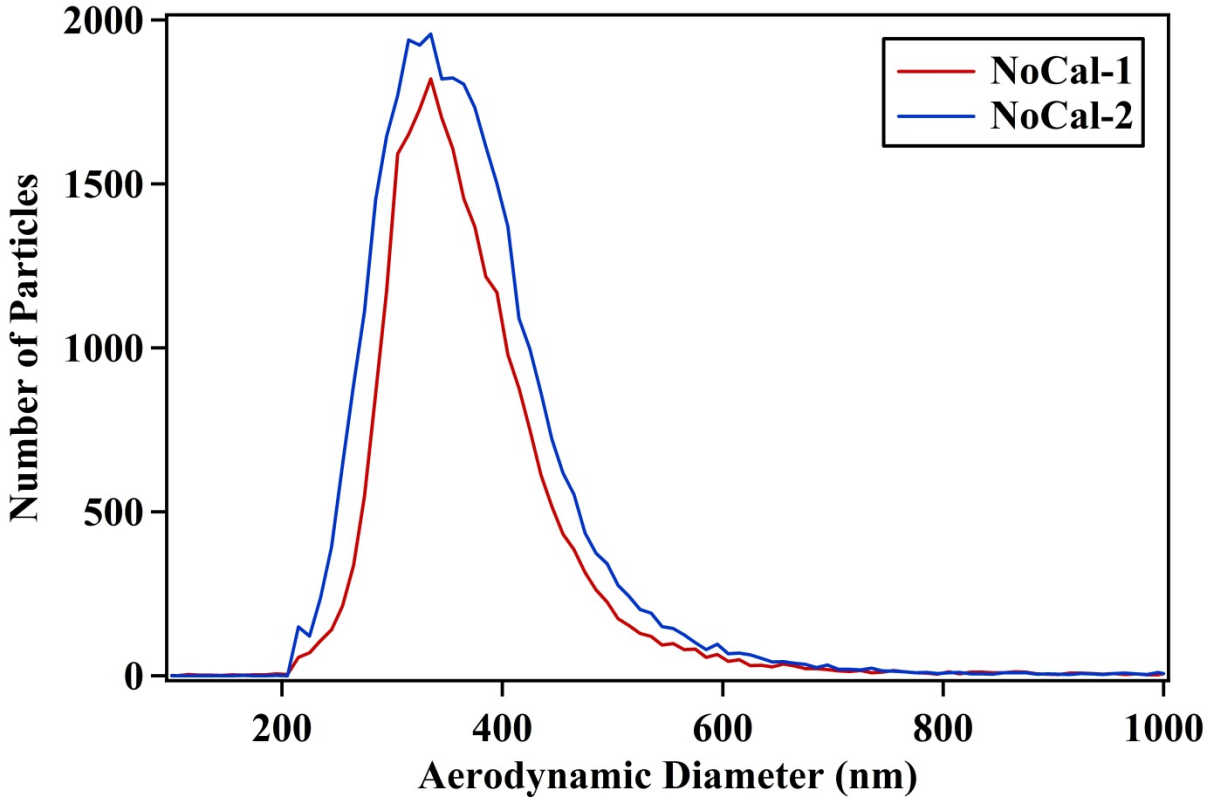

Figure 21: Size distributions measured by A-ATOFMS during NoCal-1 (red) and NoCal-2 (blue).

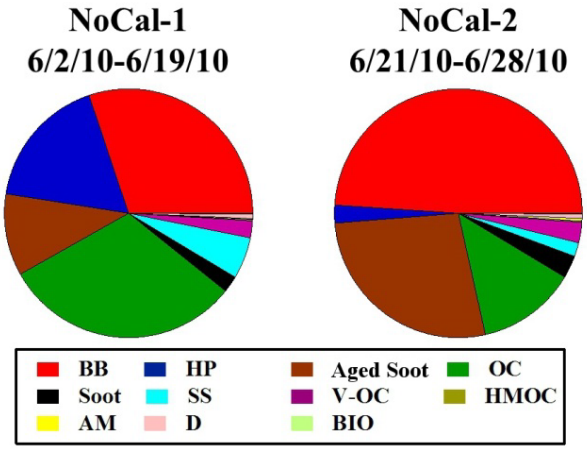

Figure 22: Number fractions of A-ATOFMS particle types for two periods in the CARES campaign, NoCal-1 and NoCal-2.

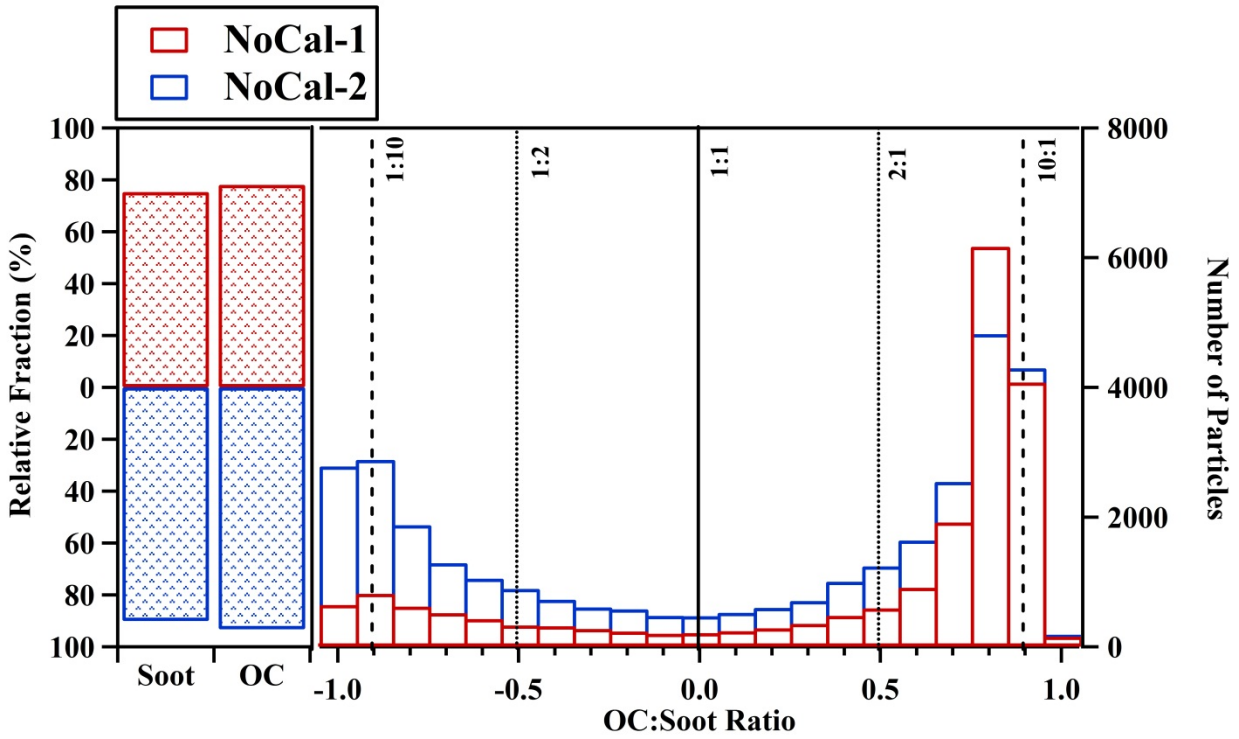

Figure 23: Fraction of particles containing soot and OC with RPA > 0.5% in NoCal-1 (red) and NoCal-2 (blue) (left panel). OC:soot ion ratio distribution are shown in the right panel. Values < 0 indicate more soot than OC and values > 0 indicate more OC than soot. Ratios representing 1:1, 2:1, and 10:1 are shown by solid, dotted, and dashed lines, respectively.

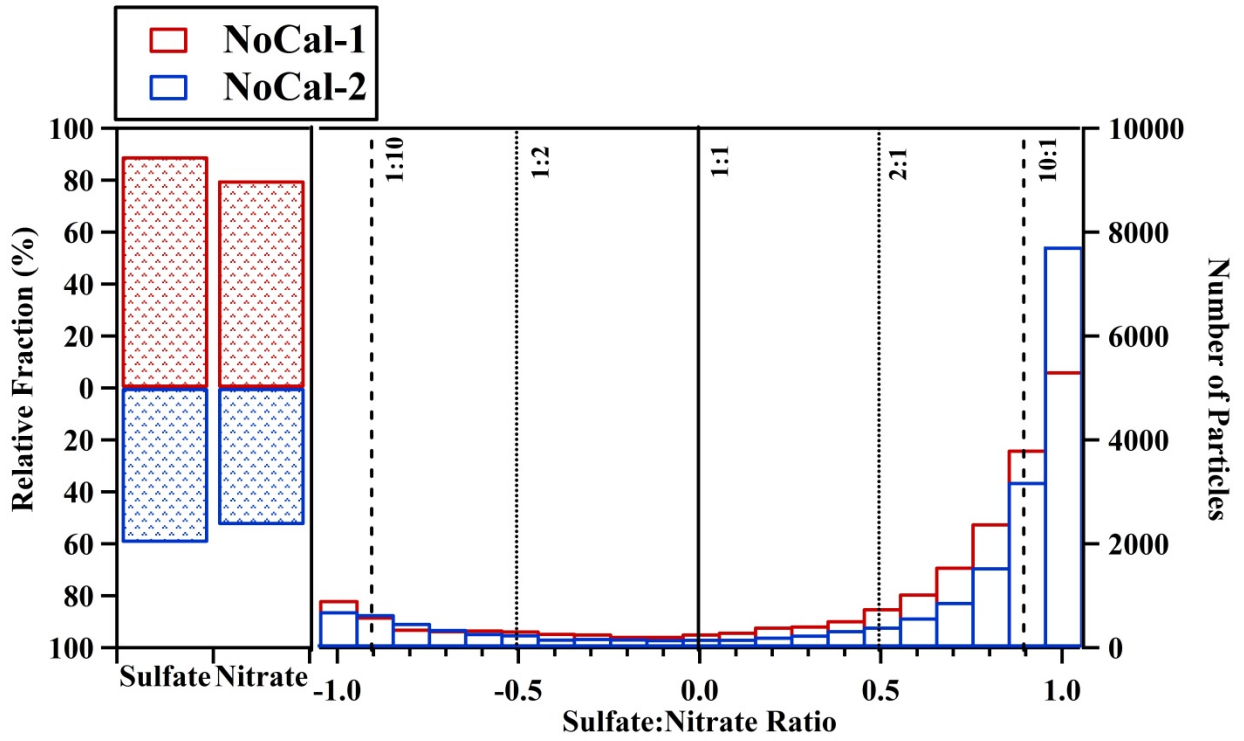

Figure 24: Fraction of particles containing sulfate and nitrate with RPA > 0.5% in NoCal-1 (red) and NoCal-2 (blue, left panel). Sulfate:nitrate peak ratios are shown in the right panel. Values < 0 indicate more soot than nitrate and values > 0 indicate more sulfate than soot. Ratios representing 1:1, 2:1, and 10:1 are shown by solid, dotted, and dashed lines, respectively.

1.3.2.2.5 Temporal differences in northern California aerosol: NoCal-1 and NoCal-2

As mentioned previously, the particle sources during CalNex were quite stable over the duration of the study. However, a noticeable shift in particle composition, particulate mass, and meteorology occurred during CARES after June 21 (Figure 15 and Table 3). The sources and processes contributing to these two periods were quite different. To examine these differences in detail, the CARES study was separated into two periods, Northern California-1 (NoCal-1) and Northern California-2 (NoCal-2), representing fights from June 2 – 19, 2010 and June 21 – 28, 2010, respectively. Particle number concentrations, RH, and temperature can be found in Table 3. NoCal-1 was relatively clean compared to NoCal-2, which was influenced more by local sources as evidenced by an increase of particulate matter < 2.5 µm (PM2.5) by 12% measured at the CARB Del Paso Manor site, from 5.7 to 8.0 µg/m^3 for NoCal-1 and NoCal-2, respectively. Mean gas-phase concentrations of SO_2 and NO_X measured in flight increased as well from NoCal-1 to NoCal-2 by 23% (1.7 vs. 2.1 ppb) and 25% (1.3 vs. 1.6 ppb), respectively. Similarly, Fast et al. described increased O_3 and weaker winds during the same approximate period as NoCal-2 [*Fast et al.*, 2012]. Mean UF-CPC particle concentrations decreased by ~32%, while larger particles measured by the UHSAS, which are detected more efficiently by the A-ATOFMS, increased in number by 56%. Correspondingly, A-ATOFMS average particle counts per flight increased between the first and second half of CARES by 71%. ATOFMS size distributions also broadened from NoCal-1 to NoCal-2 (Figure 21).

As shown in Figure 15, the relative fractions of particle types for each flight during CARES change after 19 June 2010, which coincides with an increase in average PM2.5 mass. NoCal-2 exhibited significantly higher fractions of Aged Soot and BB than in NoCal-1 (Figure 22), an increase of 17 and 19% by number, respectively, and a corresponding decrease in the fraction of OC, suggesting less biogenic influence in the region. Interestingly, the particulate chemistry in NoCal-2 and southern California was remarkably similar, with the exception of the relative magnitudes of sulfate and nitrate on particles. Since it is unlikely that a new source of soot emerged from Sacramento during NoCal-2, the increased detection of soot-containing particles resulted from the growth of preexisting soot particles through condensation of organic vapors and SO_2, manifested as more Aged Soot mixed with sulfate in A-ATOFMS data. The number fractions of particles containing peaks of soot, 75% and 90%, and OC, 78% and 93%, for NoCal-1 and NoCal-2 respectively, were similar in magnitude during both periods but increased in NoCal-2 (Figure 23, left panel). However, a comparison of the OC:soot ion ratio distributions from NoCal-1 to NoCal-2 indicates a shift in the OC:soot ion ratio distribution towards a nearly identical distribution as that observed in southern California (Figure 17, right panel), where nearly half of the ion ratio distribution favored soot (Figure 23, right panel). In contrast, the OC:soot ion ratio distribution for NoCal-1 (Figure 23, right panel) was dominated by OC. Higher UF-CPC concentrations during NoCal-1 indicate that soot particles were present over the urban Sacramento region during this first period, but at sizes below the A-ATOFMS detection limit (<100 nm). During NoCal-1, OC content can primarily be attributed to biogenically-derived OC from the surrounding forested regions, whereas during NoCal-2 OC primarily existed as a coating on a soot core similar to observations in southern California. With higher NO_X emissions, soot particles in LA exhibit higher number fractions mixed with nitrate observed by the A-ATOFMS. Similarly to LA, higher SO_2 and NO_X concentrations during NoCal-2 led to the faster growth of soot, and an increase in the fraction of ratios favoring soot measured by the A-ATOFMS.

Sulfate:nitrate ion ratio distributions were relatively unchanged between NoCal-1 and NoCal-2 (Figure 24). However, the fractions of MSA and OS on total particles decreased significantly from NoCal-1 to NoCal-2, from 66% to 38% and 49% to 24% for MSA and OS, respectively. One concludes that particulate sulfate was heavily influenced by natural sources during NoCal-1 while anthropogenic sources dominated during NoCal-2.

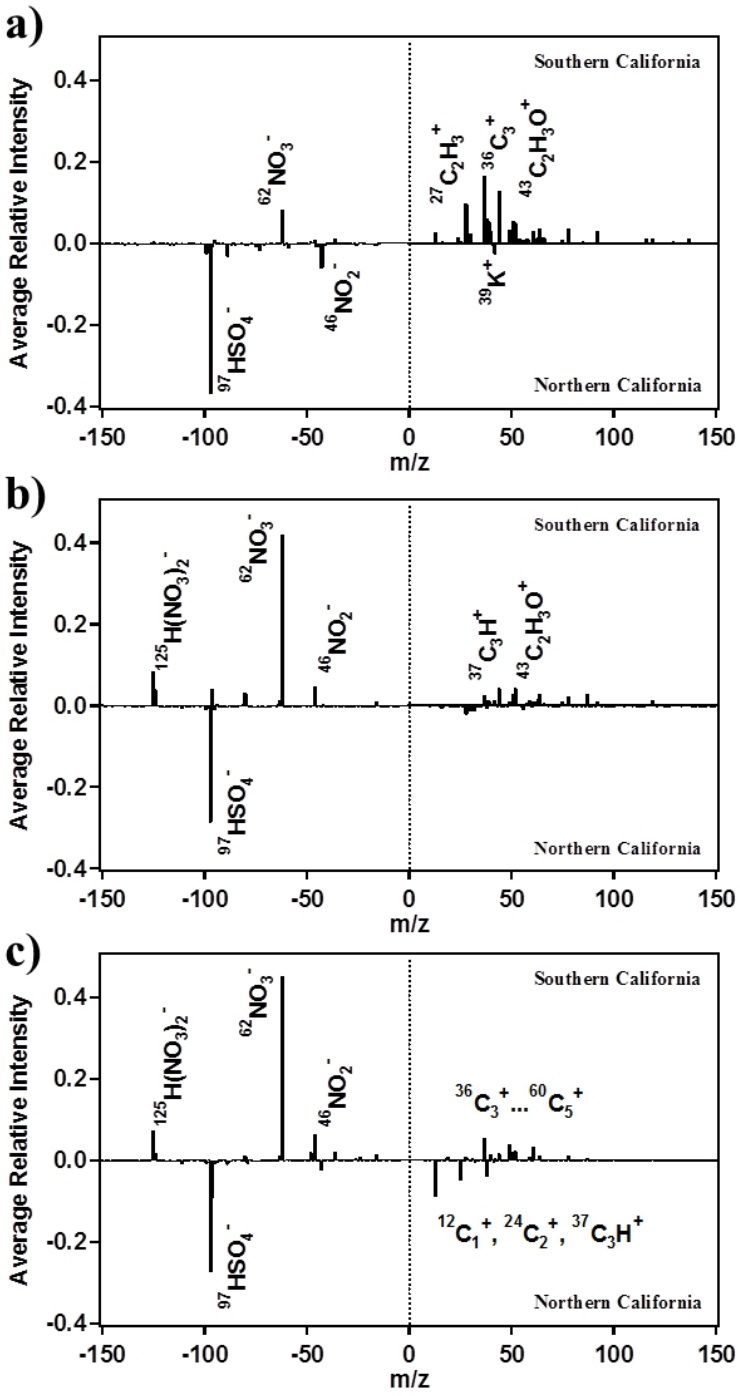

Figure 25: Spectral difference plots of a) BB, b) OC, and c) Aged Soot particles from southern (top) and northern (bottom) California. Secondary species show the greatest difference between the two regions.

1.3.2.2.6 Comparison between northern and southern California aerosol mixing state

The most striking difference between mixing states in northern and southern California is the greater magnitude of single particles mixed with sulfate in the north and nitrate in the south. Figure 25 shows the difference in RPA from averaged BB, OC, and Aged Soot mass spectra obtained in southern (top) and northern (bottom) California. Positive intensities indicate peaks that were more prevalent in southern California while negative intensities indicate prevalence in northern California. All three particle types clearly indicate more intense sulfate peaks in the north and more intense nitrate peaks in the south. Both Langridge et al. [2012] and Metcalf et al. [2012] found significant contributions of nitrate and OC to the aerosol in LA as well. In contrast, previous ground-based measurements in the LA and Port of Long Beach areas found higher fractions of sulfate on particles [*Pastor et al.*, 2003; *Qin et al.*, 2012; *Whiteaker et al.*, 2002], and recent findings during the CalNex ship campaign [*Gaston et al.*, 2012] observed a higher abundance of sulfate in southern California than northern California, though the latter is likely more indicative of port regions which are known to have large sources of sulfate from ship emissions [*Ault et al.*, 2009].

The contributions of soot and OC to single particle mixing state were found to vary greatly depending upon the region, with soot having a larger influence in the south and OC being more prevalent in the north, as shown by measured OC:soot ion ratio distribution. The largest difference in the nature of particles between southern California and NoCal-1 occurred when the influence of biogenic OC was the greatest in the north. During this period, the number fraction of OC particles was nearly 18% higher in the north than in the south. Both NoCal-2 and southern California aerosol exhibited similar chemistry, with most particles containing a soot core with OC, sulfate, and nitrate coatings, though the large difference in magnitude between sulfate and nitrate peaks in each region is a persistent feature. Distributions of OC:soot ratios during NoCal-2 and southern California (Figure 17 and 23) correlate very well, $R^2 = 0.92$, as compared to NoCal-1 and southern California, $R^2 = 0.56$, highlighting the similarity between NoCal-2 and southern California.

1.3.2.3 Conclusion

Two aircraft field campaigns, CalNex and CARES, provide insight into the distribution and mixing state of carbonaceous aerosols in California during the late spring and early summer of 2010. Most submicron particles (~97%) in California contain carbonaceous material, and nearly 88% of all particles show signs of atmospheric aging. Particles are internally mixed with secondary species, including sulfate, nitrate, MSA, OS, and ammonium. Most strikingly, nitrate is more prevalent on particles in southern California, whereas this is the case for sulfate in northern California. This suggests that different sources are impacting particles in the two regions.

OC:soot ion ratio distributions in southern California show that most particles are soot-dominated with an OC coating, whereas OC-dominated particles from biogenic sources are more prevalent in northern California. Single-particle measurements also show that many particles contain both OC and soot, which will lead to increased radiative absorption and scattering [*Moffet and Prather*, 2009; *Schnaiter et al.*, 2005; *Schwarz et al.*, 2008]. A shift in chemistry was observed during the latter half of the CARES campaign, from OC-dominant to soot-dominant, as particles in northern California became very similar in composition to particles in southern California. In addition, total PM2.5 reflected this change in particle composition, as

PM2.5 concentrations increased significantly in the latter half of the study. This suggests similar particle mixing states are present during periods of relatively higher PM2.5 levels in California. Thus, regionally specific mixing states, as well as temporal changes in mixing state, will need to be taken into account for accurate regional aerosol-climate modeling.

1.3.3 Relating Aerosol Absorption Due To Soot, Organic Carbon, and Dust To Emission Sources Determined From In-Situ Chemical Measurements

1.3.3.1 Materials and Methods

Russell et al. [2010] used the Absorption Ångström Exponent (AAE) as an indicator of aerosol chemical composition and they showed a clustering by absorbing aerosol types on an AAE vs. EAE (Extinction Ångström Exponent) scatter plot. In this study, we apply a similar methodology, based on a previous study by Bahadur et al. [2012], dividing the AAE vs. SAE (Scattering Ångström Exponent) space, called the Ångström matrix, into different regions that are associated with different absorbing aerosol types.

1.3.3.1.1 Remote sensing measurements

Most previous studies showing a connection between absorbing aerosol types and optical properties were based on remote sensing measurements at locations with a strong dominant aerosol source type (e.g., deserts, urban polluted areas, regions prone to wildfires).

AERONET [*Holben et al.*, 1998] is an optical ground-based aerosol monitoring network that provides globally distributed observations of aerosol spectral optical depths (AOD), and other properties derived by inversion such as aerosol size distributions and single scattering albedo (SSA). AERONET follows a protocol for the quality assured data (Level 2.0). AERONET Level 2.0 data are cloud-screened and only measurements with an AOD at 440 nm greater than 0.4 are used, for which the uncertainty of the AOD is between 0.01 and 0.02, depending on the wavelength [*Holben et al.*, 1998], and this uncertainty results in a variation of 0.03 to 0.04 in the Ångstrom exponent [*Schuster et al.*, 2006] and of 0.03 to 0.07 in the SSA [*Dubovik et al.*, 2002].

In this study, we used AERONET measurements from 33 stations around the world with a dominant absorbing species (Table 4). In addition, we used measurements from a total of ten operational AERONET stations in California. The stations are divided by region, into Northern California for the stations with latitude above 36ºN and Southern California for the stations below 36ºN. Southern California is characterized by densely populated cities, such as Los Angeles or San Diego where the main source is anthropogenic. On the other hand, northern California is, in general, a less-populated region with the Central Valley characterized by extensive agricultural activity. Data are also divided by seasons. Due to the limited availability of Level 2.0 AERONET data, seasons were grouped using winter and spring in one season and summer and autumn in another season. Table 5 presents the name, location, available period of time in years, and number of valid Level 2.0 measurements for the 10 California AERONET stations. The stations are also shown on the map in Figure 26.

In order to calculate the AAE and SAE, the Single Scattering Albedo (SSA) derived by inversion in AERONET is used to calculate the Absorption and Scattering components of the aerosol optical depth (AOD). This way, AAOD = AOD*(1-SSA) and SAOD = AOD*SSA are calculated. Then, AAE and SAE are calculated using Eq. (1) and Eq. (2) respectively:

$$AAE = -\frac{\log\left(AAOD(\lambda_1)/AAOD(\lambda_2)\right)}{log\left(\lambda_1/\lambda_2\right)} \quad (1)$$

$$SAE = -\frac{log\left(SAOD(\lambda_1)/SAOD(\lambda_2)\right)}{log\left(\lambda_1/\lambda_2\right)} \quad (2)$$

where the wavelengths, λ_1 and λ_2, are 440 and 675 nm, respectively [*Bahadur et al.*, 2012].

The spectral dependence of the absorption coefficient, AAE in Eq. (1), can be related to the dominant absorbing aerosol type for a mixture of aerosols. Black carbon typically follows an inverse wavelength (λ^{-1}) spectral dependence, yielding an AAE of 1 [*Bergstrom et al.*, 2002], while organic carbon in biomass smoke aerosols and mineral dust contribute to light absorption in the ultraviolet and blue spectral regions yielding an AAE greater than 1 [*Kirchstetter et al.*, 2004], with a magnitude depending on the range of wavelengths used for its calculation. Gyawali et al., [2009] and Lack and Cappa [2010] found that values of AAE > 1 are also possible on particles with BC cores and a non-absorbing coating. On the other hand, the spectral dependence of the scattering coefficient, the SAE as shown in Eq. (2), depends primarily on the dominant size mode for a mixture of aerosols, ranging from 4 to 0 where larger numbers associate with small particles (i.e., fine mode) and smaller numbers suggest the dominance of large particles (i.e., coarse mode) [*Bergstrom et al.*, 2007].

Thus, in a very intuitive way, the AAE vs. SAE space partitions into regions that correlate to combinations of a dominance of fine and coarse modes, and a dominance of particles that follow the λ^{-1} trend for absorption, and those with absorption enhancement at the shorter wavelengths. The principal advantage of this dual size-chemistry partitioning is that, in the ideal case, it separates the three aerosol absorbing species – EC, OC, and mineral dust. First, measurements representing dust separate along the SAE axis, as dust is primarily found in the coarse mode as compared to carbonaceous aerosols that are primarily in the fine and ultra-fine mode close to emission sources. Second, EC is an efficient absorber at all wavelengths compared to OC which absorbs strongly only at short wavelengths, separating these species along the AAE axis. In addition to these ideal cases, we can relate the remainder of the phase space to aerosols with predicted combinations of SAE (representing size) and AAE (representing chemistry), and their mixtures. This partition is based on a simplified division published by Bahadur et al. [2012]. In the supplemental material of Bahadur et al. [2012], a threshold value of AAE=1.5 was found to demarcate the dust-dominated region fairly well, containing 72% of all measurements in dust-dominated regions, but only 17% of measurements in fossil fuel-dominated regions. Therefore, the condition of AAE>1.5 has been retained to delineate the aerosols that have an enhanced absorption at shorter wavelengths (i.e., dust and OC) with smaller values of AAE considered to have an influence of EC leading to more complex mixtures. Similarly, SAE of 1.5 was found to reasonably delineate the fine mode aerosols (EC and OC) with smaller values of SAE considered

to have an influence of larger particles (such as dust or other non-absorbing species), again leading into the mixture containing regions of the phase space. In this new partition, the inclusion of mixtures requires the addition of new phase boundaries. Thus, the phase boundaries for large particles and "EC-dominated" particles were set to 1.0.

Figure 27 illustrates the division of the Ångström matrix with labels that represent the three absorbing aerosol species and their mixtures. The lower-left quadrant has been labeled as "coated large particles" indicating that it contains a species with AAE<1 but larger in size. Lack and Cappa [2010] showed that black carbon particles with a sulfate coating might present those optical properties, and polluted dust with strong absorbers might also present the same spectral response. Figure 27 also shows data from the 33 AERONET stations, color-coded by dominant type. Table 4 lists the stations, locations, and dominant aerosol species at each site.

Measurements from dust-dominant stations (orange squares) fall mainly into the dust dominant area (upper left quadrant); however, some measurements fall into the phase space representing polluted dust, mixed aerosols, or the coarse coated type. On the other hand, there is a larger overlap between absorbing particles from fossil fuel (cyan triangles) and biomass burning sources (red circles) since all combustion produces both EC and OC, and there are no pure EC or OC present in field measurements. However, the fossil fuel category presents more variability in size than the biomass burning category due to the origin of the measurements. Whereas biomass burning-dominant stations are mainly areas prone to wildfires, the stations marked as fossil fuel-dominant correspond to urban areas that are expected to contain a large amount of primary carbonaceous aerosols, but likely also contain larger aerosol particles (either lofted dust, or non-absorbing aerosols), and likely also contain aged secondary aerosols due to high NO_X and ozone conditions.

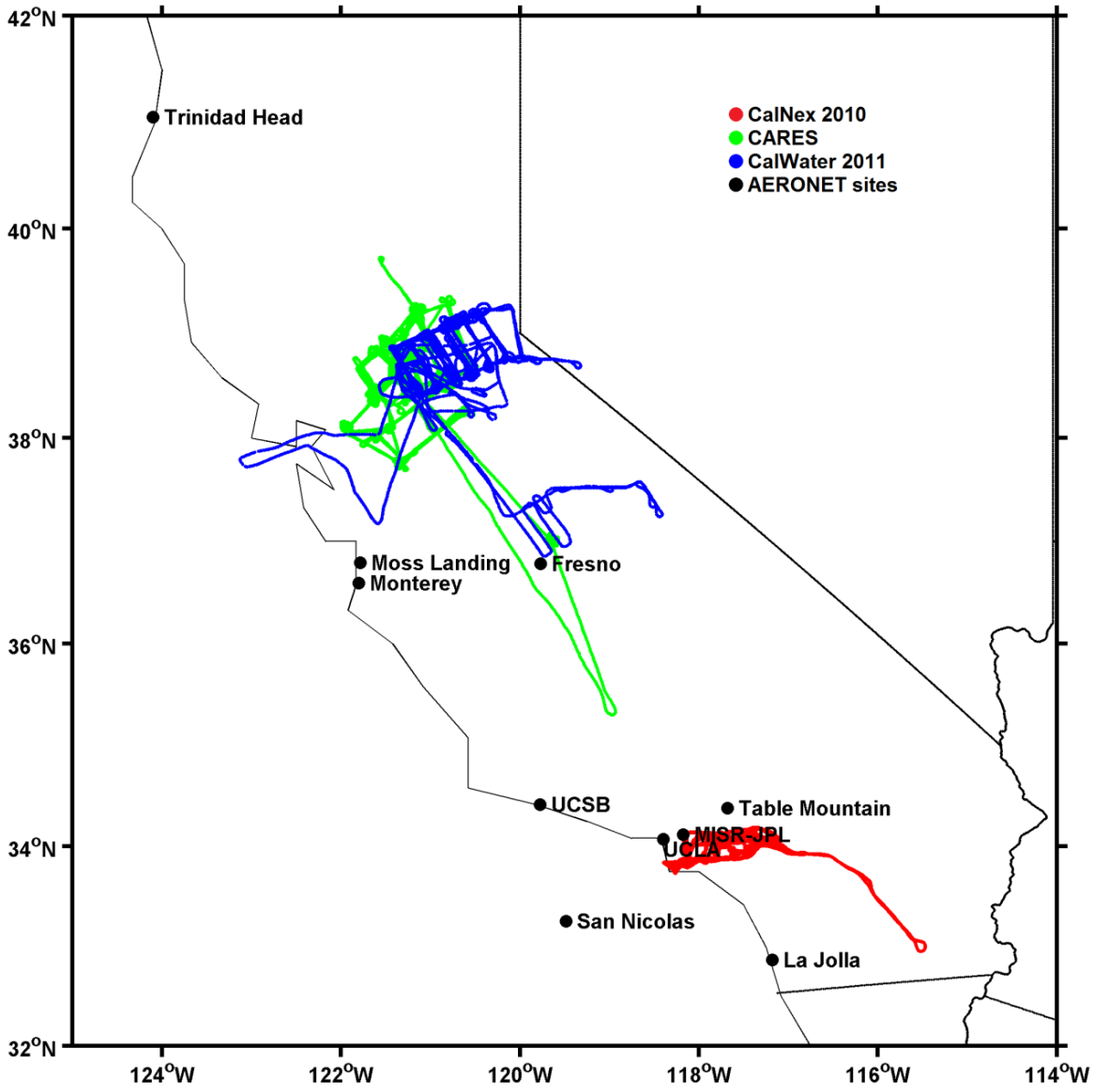

Figure 26: Map of California with the flight paths of the aircraft campaigns and the location of the AERONET stations.

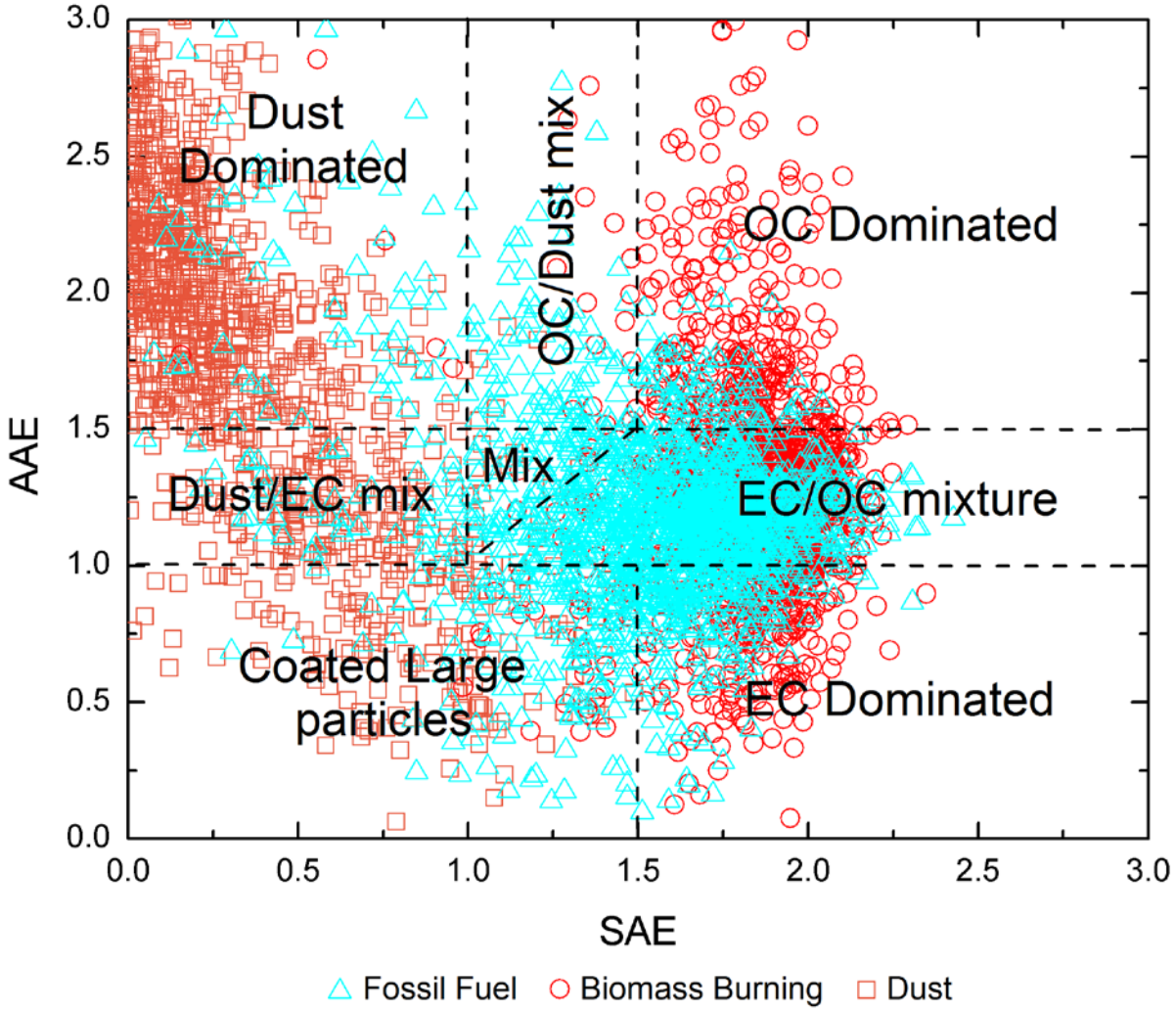

Figure 27: Division of the Absorption Ångström Exponent vs. Scattering Ångström Exponent space, the Ångström matrix, overlapped with the AERONET measurements from stations with a dominant sources (fossil fuel in cyan triangles, biomass burning in red circles or dust in orange squares).

AERONET station	Latitude (°) N	Longitude (°) W	Main source
Billerica	42.53	71.27	Fossil Fuel
CCNY	40.82	73.95	Fossil Fuel
Dayton	39.77	84.11	Fossil Fuel
Fresno	36.78	119.77	Fossil Fuel
GSFC	38.99	76.84	Fossil Fuel
Halifax	44.64	63.59	Fossil Fuel
Hamburg	53.57	-9.97	Fossil Fuel
Hong Kong	22.21	-114.26	Fossil Fuel
IFT Leipzig	51.35	-12.43	Fossil Fuel
Mainz	49.99	-8.3	Fossil Fuel
Maryland Sci. Cen.	39.28	76.62	Fossil Fuel
New Delhi	28.63	-77.17	Fossil Fuel
Palaiseau	48.7	-2.21	Fossil Fuel
Philadelphia	40.04	75	Fossil Fuel
Rome Tor Vergata	41.84	-12.65	Fossil Fuel
Sandy Hook	40.45	73.99	Fossil Fuel
UCLA	34.07	118.45	Fossil Fuel
Abracos Hill	10.76	62.35	Biomass Burning
Alta Floresta	-9.87	56.1	Biomass Burning
Belterra	-2.65	54.95	Biomass Burning
Campo Grande	-20.45	54.62	Biomass Burning
CELAP-BA	-34.57	58.5	Biomass

Table 4: List of the AERONET stations around the world with dominant sources used for the creation of the Ångström matrix.

AERONET station	Latitude (°) N	Longitude (°) W	Data Availability	Data points with SSA retrieval
Fresno	36.782	119.773	2002-2011	208
La Jolla	32.870	117.250	1994-2011	15
MISR-JPL	34.119	118.174	1996-2009	28
Monterey	36.593	121.855	1998-2011	6
Moss Landing	36.793	121.788	2004-2006	2
San Nicolas	33.257	119.487	1997-2007	14
Table Mountain	34.380	117.680	1998-2011	3
Trinidad Head	41.054	124.151	2005-2011	13
UCLA	34.070	118.450	2000-2009	55
UCSB	34.415	119.845	1994-2011	10

Table 5: Location and data availability of the AERONET stations in California.

1.3.3.1.2 In-situ aircraft measurements

In-situ data were collected by aircraft during three atmospheric measurement campaigns performed in California. CalNex 2010 was a joint field study coordinated by the California Air Resources Board (CARB) and, the National Oceanic and Atmospheric Administration (NOAA) and the California Energy Commission (CEC), with a primary goal to study atmospheric processes over California and the eastern Pacific coastal region. Measurements used in this work were taken onboard the Center for Interdisciplinary Remotely-Piloted Aircraft Studies (CIRPAS) Twin Otter, flying mainly in the Los Angeles basin during May 2010. CARES (Carbonaceous Aerosols and Radiative Effects Study), was a field study designed to increase scientific knowledge about evolution of black carbon and secondary organic aerosols from both urban/manmade and biogenic sources. Data used from this campaign were measured onboard the DOE Gulfstream–1 (G–1), based in Sacramento during June 2010. The CalWater 2011 field campaign was designed to better assess the effects of aerosols on precipitation in the Sierra Nevada during the winter season. Data used from this campaign were collected onboard the DOE G–1, based in Sacramento between February and March 2011. Figure 26 shows the flight paths for the three campaigns.

The different aircraft contained instrumentation for the retrieval of the optical properties of aerosols (i.e., absorption and scattering coefficients) and for the measurement of the chemical

composition of aerosol particles. The Absorption coefficient, σ_a, was derived using a Particle Soot Absorption Photometer (PSAP) operating at 462, 523 and 648 nm and sampling from an iso-kinetic inlet. The Scattering coefficient, σ_s, was measured using a nephelometer at 450, 550 and 700 nm during CARES and CalWater, also sampling from an iso-kinetic inlet, and derived from a Passive Cavity Aerosol Spectrometer Probe (PCASP) size distribution, in the range of 0.1 to 3 µm, applying Mie theory (using a refractive index of 1.5) during CalNex. PSAP data were corrected for scattering aerosol and spot size based on Bond et al. [1999] and Ogren [2010] using the nephelometer data for CARES and CalWater data, and the calculated scattering for CalNex. The uncertainty associated with σ_a is about 20% [*Bond et al.*, 1999]. Nephelometer data were corrected based on Anderson and Ogren [1998]. The uncertainty associated with σ_s is about 5%.

As discussed by Schmid et al. [2006] the Twin Otter samples aerosol from an iso-kinetic inlet whose passing efficiency was tested in airborne and wind tunnel experiments by Hegg et al. [2005]. They found no appreciable loss in efficiency for particles smaller than 3.5 µm aerodynamic diameter at the Twin Otter sampling velocity of 50 ms^{-1}. For larger particles, the efficiency decreases rapidly but levels off at an efficiency of slightly better than 0.6 for particles 5.5 - 9 µm (the latter being the upper diameter of their characterization). The G-1 iso-kinetic inlet used in CARES and CalWater has not yet undergone the same testing. Manufacturer specifications call for passing efficiency near unity dropping to 50% at 5 µm diameter at the G-1 research speed of 100 ms^{-1}. This claim has been substantiated with comparisons with ground-based nephelometers during fly-bys in CARES [*Zaveri et al.*, 2012].

Measurements of the chemical composition of individual particles during the three aircraft campaigns were performed using the aircraft aerosol time-of-flight mass spectrometer (A-ATOFMS) [*Pratt et al.*, 2009b]. The A-ATOFMS measures, in real time, the size and chemical composition of individual particles ranging in size from 100 to 2500 nm during CalWater and from 80 to 1000 nm during CalNex and CARES.

Using the in-situ optical properties and chemical composition measured during the three aircraft sampling campaigns, we can establish a link between the optical properties, in this case the AAE and the SAE, and the measured chemical composition of the aerosol particles.

AAE and SAE were calculated applying Eq. (1) and (2) respectively using σ_a instead of the column-integrated value (AAOD) and σ_s instead of the SAOD. Wavelengths used as λ_1 and λ_2 were 462 and 648 nm for the PSAP and 450 and 700 for the nephelometer because those are closer to the AERONET wavelength used in section 1.3.3.1.1.

For the chemical composition of the particles from the A-ATOFMS, spectra from individual particles (i.e., their chemical signature) are grouped into chemically similar clusters using the ART-2-a algorithm [*Song et al.*, 1999]. The initial clusters are then manually grouped into a small set of clusters based on the identification of the mass spectral peaks that correspond to the most probable ions for a given mass-to-charge ratio (*m/z*) based on previous lab and field studies. These clusters are then classified into different absorbing particle types: primary fossil fuel, secondary fossil fuel, primary biomass burning, secondary biomass burning and dust, excluding other non-absorbing particle types. Figure 28 shows a representative mass spectrum for each aerosol type where the mass-to-charge ratio (*m/z*) is on the x-axis, and the intensity of the ion peaks is on the y-axis (in arbitrary units).

Briefly, primary fossil fuel particles are characterized by the presence of carbon cluster ion peaks: C_n^+ and C_n^-, representative of the elemental carbon (EC), and spectra that also contain weak intensities at *m/z* $^{27}(C_2H_3^+)$, $^{37}(C_3H^+)$ and $^{39}(C_3H_3^+)$. Secondary fossil fuel particles contain signals at *m/z* $^{27}(C_2H_3^+/CHN^+)$, $^{37}(C_3H^+)$, $^{39}(C_3H_3^+)$ and $^{43}(C_2H_3O^+)$ in the positive spectra and mainly nitrate and sulfate ion peaks in the negative ion mass spectra: *m/z* $^{-62}(NO_3^-)$ and $^{-97}(HSO_4^-)$, respectively [*Moffet and Prather*, 2009; *Silva and Prather*, 2000; *Spencer and Prather*, 2006]. Biomass burning particles are characterized by an intense potassium peak at *m/z* $^{39}(K^+)$ with less intense carbonaceous markers (e.g., *m/z* $^{12}(C+)$, $^{27}(C_2H_3^+)$, $^{36}(C_3^+)$, $^{37}(C_3H^+)$ [*Hudson et al.*, 2004; *Silva et al.*, 1999]. The difference between primary and secondary biomass burning is established by looking at the negative spectra that presents carbon clusters in the case of primary biomass burning or mainly nitrate/sulfates in the case of secondary biomass burning. Finally, dust is characterized by inorganic ion peaks (e.g. *m/z* $^{27}(Al^+)$, $^{39}(K^+)$, and/or $^{40}(Ca^+)$, and the presence of silicates: $^{-60}(SiO_2^-)$ and $^{-76}(SiO_3^-)$ [*Silva and Prather*, 2000].

In order to validate the Ångström matrix, we matched the spectral optical properties and the aerosol absorbing types measured by the A-ATOFMS during the flights. For each flight, we calculated the 5-minute average of the AAE and SAE. On the other hand, for the same 5-minute periods, we calculated the fraction of the different aerosol absorbing types detected with the A-ATOFMS. We only considered periods with a dominant aerosol absorbing type (i.e., 75% of the particles detected by the A-ATOFMS are from one type). Thus, we screen the data using the 5-minute average values that correspond with a dominant aerosol absorbing type detected by the A-ATOFMS. This way we have, on one hand, the spectral optical properties (AAE and SAE) and we can obtain an estimation of the type of absorber using the Ångström matrix and, on the other hand, the actual aerosol chemical composition determined by the A-ATOFMS that correspond to those optical properties.

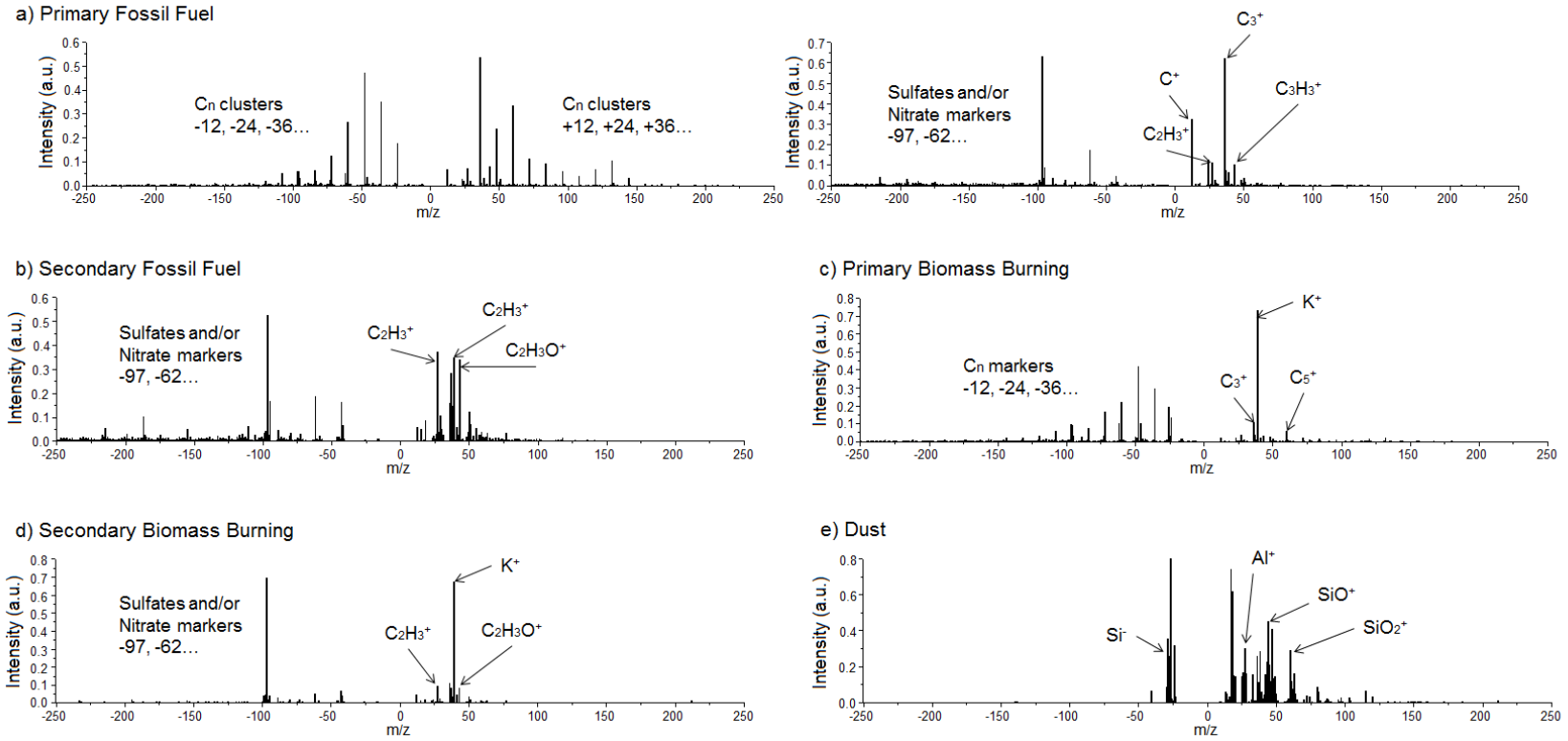

Figure 28: Representative A-ATOFMS spectra for different aerosol sources a) Primary fossil fuel, b) Secondary fossil fuel, c) Primary biomass burning, d) Secondary biomass burning, and e) dust.

		Ångström Matrix							
		EC dom.	EC/OC mix	OC dom.	OC/Dust mix	Dust dom.	Dust/EC mix	Coated	Mixed
A-ATOFMS	Prim. Fossil Fuel	1.20	27.71	31.33	21.69	1.20	0	10.84	6.02
	Sec. Fossil Fuel	0	0	10.47	27.91	8.14	39.53	9.30	4.65
	Prim. Biomass	0	0	25	25	0	0	0	50
	Sec. Biomass	0	3.70	18.52	40.74	14.81	0	18.52	3.70
	Dust	14.29	7.14	28.57	7.14	7.14	0	14.29	21.43

Table 6: Contingency matrix constructed from the aircraft measurements representing the percentage of aerosol sources from the A-ATOMFS classified into the different Ångström matrix classes.

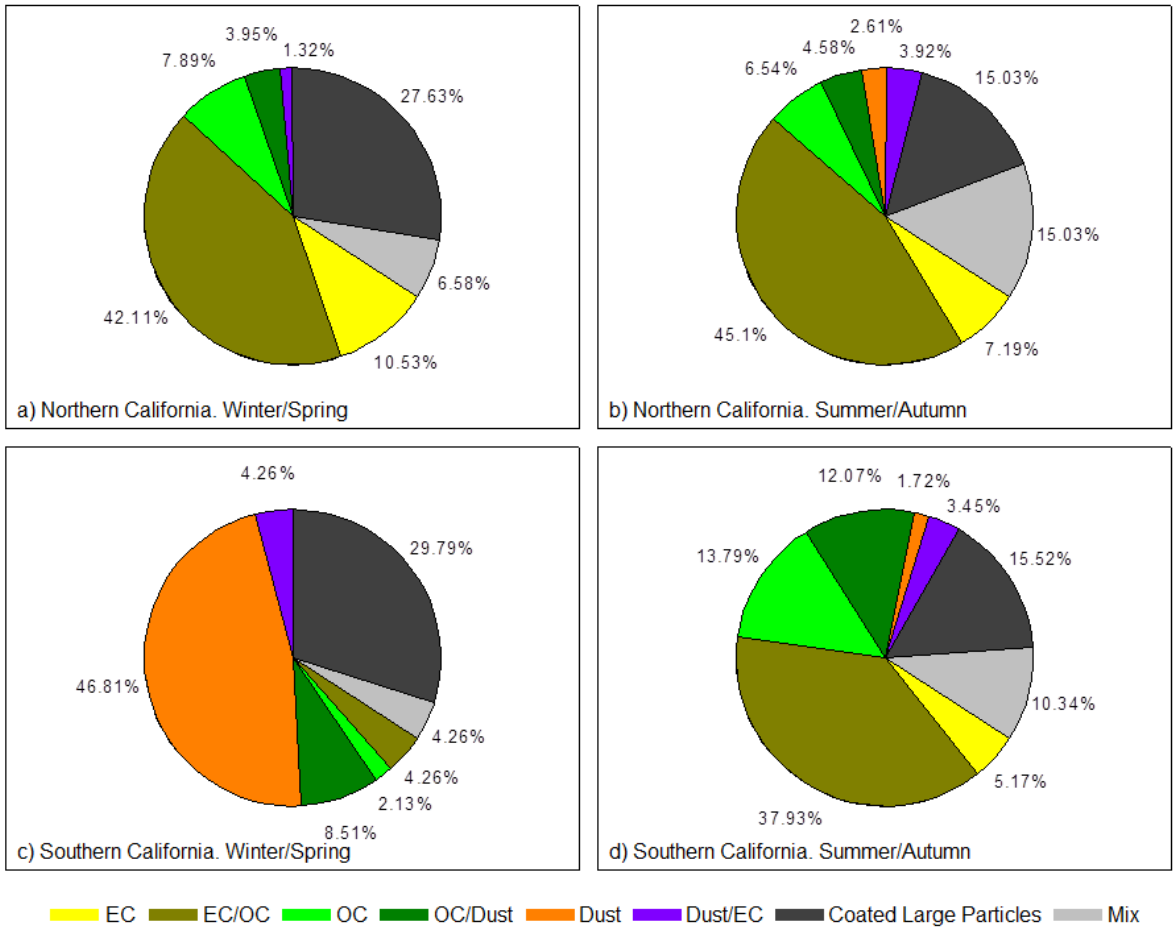

Figure 29: Estimated number fraction of the different aerosol absorbing types by the Angstrom matrix using aerosol properties from AERONET stations in California separated by region and season: a) Northern California – winter/spring, b) Northern California – summer/autumn, c) Southern California – winter/spring, and d) Southern California – summer/autumn.

1.3.3.2 Results

To gain a better understanding on how the optical properties of aerosols relate to chemical composition, we use aerosol data from California as an initial test case, where the Ångström matrix can be compared to a large wealth of field data. Applying the Ångström matrix to all the available Level 2.0 AERONET data, we obtain an estimate for the percentage of absorbers in different regions of California by means of optical properties. Figure 29 shows the fraction for the different regions and seasons in pie charts. Panel a) shows the fraction for Northern California during winter/spring; panel, b) shows the fraction for northern California during summer/autumn, while panels c) and d) show the fraction for southern California during winter/spring and summer/autumn, respectively. Due to the number of retrievals for each site (Table 5), the northern California is strongly biases by Fresno site, and southern California by

the Los Angeles basin measurements. Both seasons in northern California show a similar fraction of aerosol absorbing types and they are dominated by a mixture of EC and OC aerosol that comprise over 40% of all measurements. The difference lies in the coated large particles and mix types. For southern California, the summer/autumn season is dominated by a mixture, or EC and OC aerosol (almost 40%) as well as OC and OC mixed with dust type. The winter/spring season is dominated by dust (over 45%) and coated large particles (almost 30%).

On the other hand, a summary of the overall aerosol absorbing types detected with the A-ATOFMS during the three campaigns is shown in Figure 30. Each pie chart represents the number fraction of absorbing types detected during CalNex on the left panel, CARES in the middle, and CalWater on the right panel, calculated using all the available particles detected during the campaign flights. Also each campaign, because of the location and dates, can be associated with a region and season. CalNex corresponds with southern California during the summer, or more concretely, with the Los Angeles basin area, CARES with northern California also during the summer, and CalWater with northern California during the winter. We need to take into account that we are using different instruments and methodologies. On one hand, AERONET data represent a long term data set and Figure 29 represents the fraction of occurrences falling into one or another region in the Ångström matrix and, on the other hand, A-ATOFMS data shown in Figure 30 represents the fraction of particles detected at a specific location and time. Furthermore, for northern California, the AERONET retrievals are biased by the Fresno measurements and the aircraft measurements are mainly over the Sacramento area. Both seasons in northern California present similar aerosol absorbing type fraction with dominance of secondary fossil fuel aerosol and biomass burning particles. Also, more dust is detected during the winter. In southern California, the primary fossil fuel particles (35%) and secondary fossil fuel (47%) dominate in the summer.

In the validation process, the AAE and SAE values, calculated from the in-situ aircraft data, that match the dominant aerosol type criteria presented in section 1.3.3.1.1 are presented in Figure 31, on an AAE vs. SAE scatter plot with color representing the dominant aerosol type determined by the A-ATOFMS. Panels a), b), and c) correspond to each different field campaign (CalNex, CARES, and CalWater, respectively). Because the AAE is related to the chemical composition of aerosol, panel d) in Figure 31 shows a frequency histogram of the AAE associated to the aerosol types detected by A-ATOFMS showing that primary fossil fuel particles have a mean value of AAE = 1.1±0.6, which is close to the expected 1.0 for black carbon [*Bergstrom et al.*, 2002]. Secondary fossil fuel particles can be associated with an AAE = 1.5±0.3, which is in agreement with what was found by Gyawali et al. [2009] and Lack and Cappa [2010] for BC cores with non-absorbing coatings, and biomass burning to AAE = 1.8±0.4 [*Kirchstetter et al.*, 2004]. The AAE was smaller on average during CalNex than during CARES, consistent with the type of dominant aerosol detected, mainly primary fossil fuel during CalNex (i.e., elemental carbon) in contrast with the secondary fossil fuel particles that dominated during CARES. The number of samples from the CalWater campaign is small, as the flights focused on clouds and not many data samples were acquired from cloud-free air. The SAE exhibited less variability during CalNex than during CARES, but we need to take into account that the scattering coefficient measurements were taken differently for those campaigns and the range of particle sizes is different. Also, the data filtering might be introducing a bias, since we are using data corresponding to periods with a dominant aerosol source.

Finally, we apply the Ångström matrix to the in-situ optical properties, obtaining an estimate of the aerosol chemical composition using optical properties that can be compared with the actual aerosol chemical composition determined by the A-ATOFMS. Table 6 shows a contingency table where the rows are the chemical composition detected with the A-ATOFMS and columns are the different estimated aerosol types from the Ångström matrix. Values presented are percentages of measurements classified in one type or another and they sum 100 across rows. Primary fossil fuel particles (i.e., elemental carbon) were classified mainly as organic carbon or a mixture of organic carbon and elemental carbon or dust. Secondary fossil fuel particles (i.e., secondary organic aerosols) fall mainly into the dust/EC mix (almost 40%) indicating that those were particles with absorption properties similar to organic carbon, but larger in size, probably due to non-absorbing coating on the carbonaceous core. On the other hand, primary biomass burning sources were classified as organic carbon, organic mixed with dust, or well-mixed types. Secondary biomass burning sources are classified, almost 60% of the time, into the organic carbon or organic carbon mixed with dust categories. Finally, dust sources were only significant during CalWater. However, the Ångström matrix does not classify them correctly as the dust-dominated type mainly because the number of dust measurements is small.

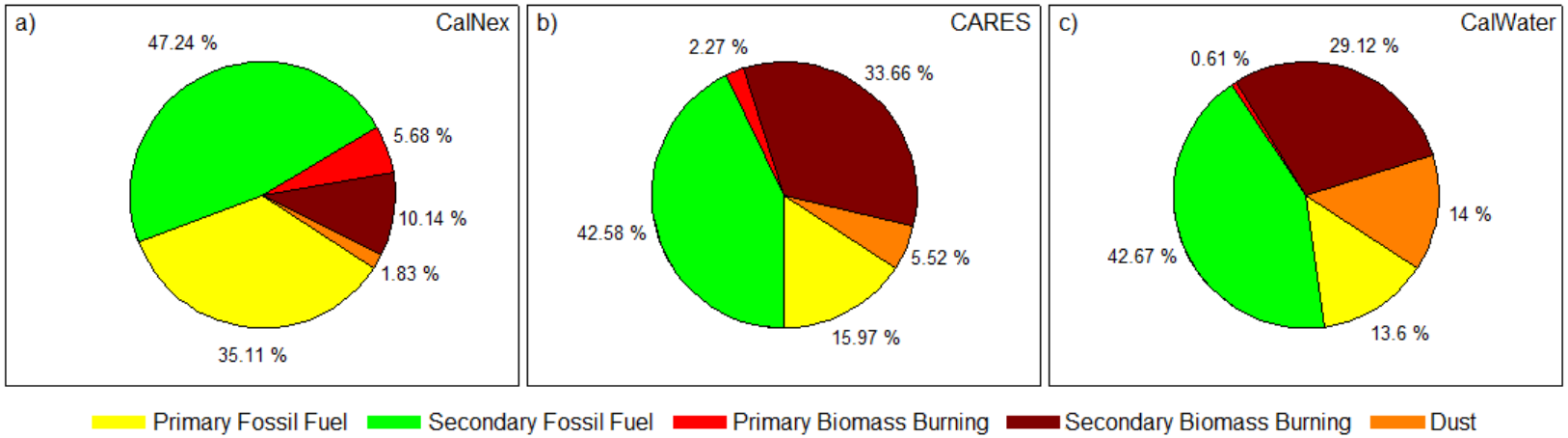

Figure 30: Overall aerosol sources detected with the A-ATOFMS in the three aircraft campaigns: a) CalNex, b) CARES, and c) CalWater.

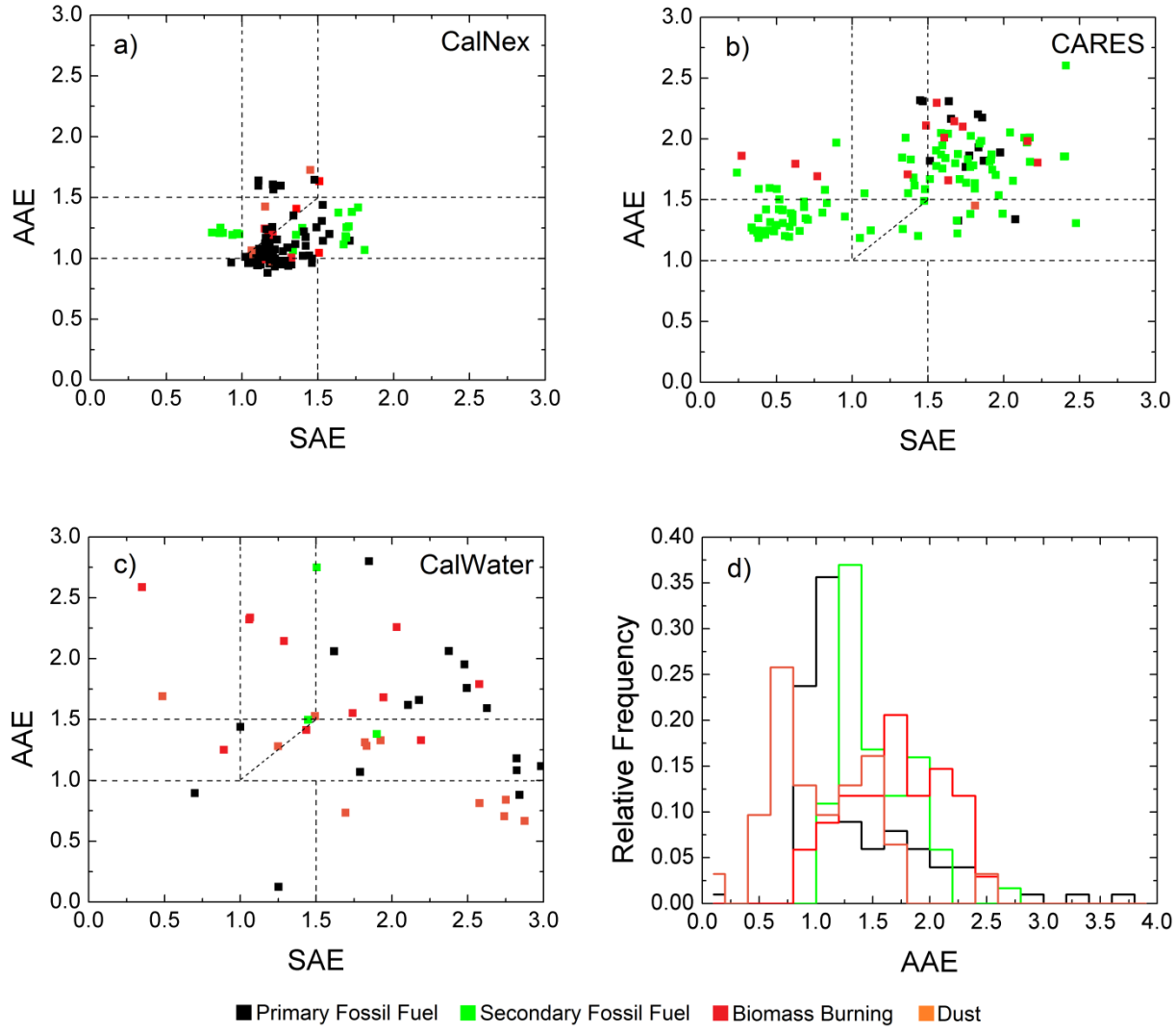

Figure 31: Absorption Ångström Exponent vs. Scattering Ångström Exponent scatter plot of in-situ aircraft measurements for a) CalNex, b) CARES, and c) CalWater where the color code represents the dominant aerosol source detected with the A-ATOFMS for each measurement. Panel d) is a frequency histogram of the Absorption Ångström Exponent for each aerosol source.

1.3.3.3 Discussion

The estimates of aerosol types applying the Ångström matrix to the California AERONET stations (Fig. 26) show similar aerosol contributions in both seasons in northern California. Over 40% of the contribution is due to a mixture of EC and OC, about 10% due to EC, and 11% due to OC or OC/dust mixture. For southern California, during the summer/autumn season almost 40% of the aerosol contribution corresponds to a mixture of EC and OC, 27% corresponds to OC or OC/dust types and 5% corresponds to EC. The winter/spring season is dominated by dust (over 45%) and coated large particles (almost 30%) and no EC type is present.

The EC/OC mixture type seems to dominate in the Ångström matrix classification and indicates the difficulty of separating the sources from column-integrated measurements. More fossil fuel sources (primary and secondary) were expected in southern California since it is a more populated, urban area and, in our particular case, the AERONET data are biased by the Los Angeles basin sites. The chemical composition detected during the aircraft campaigns for southern California (Fig. 27) shows about 35% of aerosol contribution being due to primary fossil fuel sources, 47% due to secondary fossil fuel sources, and about 15% due to biomass burning sources. Figure 31d shows that the chemistry component of the Ångström matrix (the AAE) has a mean value of 1.1 for primary fossil fuel sources, 1.5 for secondary fossil fuel sources and 1.8 for biomass burning. All those sources would fall into the EC/OC mixture type or the OC type, with some overlapping on the different sources, and leaving the EC type misclassified. On the other hand, northern California was expected to have more biomass burning sources with respect to the south because of the less populated and more rural environment (in particular the AERONET data are bias by the Fresno site in the Central Valley). The aircraft data in northern California (Fig. 27b and 27c) indicates about 40% of the contribution due to secondary fossil fuel sources and about 30% due to biomass burning sources with a small contribution due to primary fossil fuel sources (about 7 to 10%). Again, the overlapping of the optical properties results in the EC/OC mixture type dominating the classification scheme.

Pure dust was only a significant source for southern California during winter/spring. This is most likely a misclassification. The dust type measurements were concentrated in the UCLA and MISR-JPL AERONET stations, both in the Los Angeles metropolitan area, and dust is not expected to make such large contributions in urban areas, where fossil fuel sources are expected to dominate. This suggests that those dust cases were instead larger hygroscopic organic carbon particles that had undergone aqueous phase processing. The aerosol species producing strong absorption at short wavelengths and primarily in the coarse mode are most likely humic-like substances (HULIS) species formed by fog or cloud processing. These aerosols have been detected in California in previous studies (e.g. [*Qin et al.*, 2012; *Qin and Prather*, 2006]) and represent organic carbon particles, but are larger than 1μm due to their water content, therefore they might have spectral properties similar to dust, i.e. they are large particles and absorb more radiation at shorter wavelengths (AAE>1) which can fall in the dust dominant or dust/EC mixture types in the Ångström matrix. On the other hand, the in-situ chemical composition from the aircraft campaigns indicates the larger contribution due to dust from northern California during the winter as compare to the summer (14% vs. 6%). During the CalWater flights, dust particles were detected mainly at higher altitudes in layers, while during CARES, flights were focused at much lower altitudes. Long range transported dust crossing the Pacific has been detected at higher altitudes during the winter in northern California and it is thought to have an impact on the precipitation in California [*Ault et al.*, 2011; *Creamean et al.*, 2013].

Most of the AERONET stations used in California are coastal (Fig. 23), and the dominance of sea salt could be important. However, Smirnov et al. [2011; 2002] studied optical properties in maritime environment and found that the AOD has a mean value of 0.07 with standard deviation of 0.03 to 0.05. This means that, in a clean maritime environment dominated by sea salt, the AOD is far below the limit for AERONET Level 2.0 data. Values above the limit (the values included in this study) must be dominated by anthropogenic aerosol or dust. The limitation imposed by AERONET for the Level 2.0 data (AOD greater than 0.4) indicates that

anthropogenic aerosols or dust are dominating species in the mixture. Since the SAE is an intensive property that gives an idea of the dominant size mode, this must reflect the dominance of the anthropogenic aerosol or the dust. Moreover, we did not observe a significant bias in the spectral optical properties from inland and coastal AERONET sites. Other non-absorbing species that might be important such as nitrate or sulfate have been found internally mixed with carbonaceous aerosols in other studies in California (e.g. [*Cahill et al.*, 2012; *Pratt and Prather*, 2009]) rather than as single nitrate or sulfate particles.

The differences in sources associated with absorption in the various regions of California, as shown in Figure 30, could be biased by the objectives of the flights during each of the campaigns. During CalNex, the flights were comprised of mainly low-level passes within the boundary layer in the Los Angeles area, very close to the sources of pollution. On the other hand, CARES also had flights with passes over the Sierra foothills (away from urban sources in the Sacramento area), and intercepting plumes from fires when they were present. CalWater focused on clouds and most of the flights were either over the Sierra foothills or over the coastal area.

The overall in-situ AAE data agree with the detected chemical composition. By looking at Figure 31, we can see that the chemical component of the Ångström matrix, the AAE, is smaller on average during CalNex than during CARES, consistent with the type of dominant aerosol detected, more primary fossil fuel during CalNex, in contrast with the secondary fossil fuel and biomass that dominate during CARES. The number of samples for CalWater is small, as the flights focused on clouds. Also, Figure 31d shows that the AAE has a mean value of 1.1±0.6 for primary fossil fuel sources, secondary fossil fuel sources can be associated with an AAE = 1.5±0.3, and biomass burning to an AAE = 1.8±0.4. These values agree with the results shown by other authors for BC (AAE = 1) [*Bergstrom et al.*, 2002], and OC (AAE > 1) [*Kirchstetter et al.*, 2004] and for secondary aerosols (AAE>1) [*Gyawali et al.*, 2009; *Lack and Cappa*, 2010]. More dust data are needed to establish good statistics for this source. On the other hand, the size component of the Ångström matrix, the SAE, shows less variability during CalNex than during CARES, but we need to take into account that the SAE was calculated differently. In addition, the data shown are filtered using the A-ATOFMS, and the different particle size- cuts used in the different campaigns directly affects the ability to sample the largest aerosol.

Finally, the application of the Ångström matrix to the in-situ aircraft measurements and the comparison with the chemical composition of the aerosol (Table 6) shows some of the limitations of the Ångström matrix. Particles detected as a primary fossil fuel source (i.e., elemental carbon) were classified mainly as organic carbon or a mixture of organic carbon and elemental carbon or dust. Taking into account that the classification is based on considering that 75% of the particles detected by the A-ATOFMS are of that type, the optical properties might contain particles from other types, the same way the external mixing of aerosol on a column integrated value like the AOD, or its absorption and scattering components, would yield to a higher AAE value and, therefore misclassifies the EC type (primary fossil fuel source). This reinforces the conclusions extracted from the comparison of the overall chemical composition for the different regions and seasons in California. Particles detected as secondary fossil fuel (i.e., secondary organic aerosols) fall mainly into the dust/EC mix (almost 40%) indicating that those were particles with absorption properties similar to organic carbon (AAE > 1), but larger in size, probably due to the internal mixture with non-absorbing aerosols. This could be biased by the

size detection limit of the sampling inlets onboard the aircraft and the A-ATOFMS. Primary biomass burning measurements were limited: 5.7, 2.3 and 0.6% of the overall particles detected in CalNex, CARES and CalWater, respectively (Fig. 5), but when detected as dominant, the Ångström matrix classified them as organic carbon or organic mixed with dust (50%), or well-mixed types (the other 50%). The amount of data from this source is very limited and more values are necessary for accurate statistics. Secondary biomass burning dominant sources are the ones that the Ångström matrix classifies the best, with almost 60% falling into the organic carbon or organic carbon mixed with dust. Finally, the dust source is only significant during CalWater (14% of total) but more data are necessary for accurate statistics.

1.3.3.4 Conclusions

Numerous studies have estimated aerosol chemical composition from spectral optical measurements using ground-based remote sensing measurements (e.g., AERONET or satellites). These networks or satellite platforms provide optical properties on a global scale, which are needed for the assessment of the contribution of aerosols to the radiative forcing and climate. Including information on the chemical composition of aerosols from discrete cases, specifically the absorbing particles sources, can help to identify the sources that contribute to the forcing globally.

In this study, we presented a methodology to estimate absorbing aerosols speciation from spectral optical measurements, and explored its limitations using in-situ optical measurements and chemical composition. Our estimates are based on the division of the Absorption Ångström Exponent vs. Scattering Ångström Exponent space and it is applied to ten AERONET stations in California. In order to validate this approach, in-situ optical properties from three aircraft campaigns that took place in California between 2010 and 2011 with single particle chemical composition measurements were analyzed. To explore the range of sources, the AERONET data and in-situ aircraft data were divided into regions (northern and southern California) and seasons (winter/spring and summer/autumn).

In-situ chemical composition results reveal a higher contribution from fossil fuel sources in southern California in contrast with more biomass burning sources in northern California. The estimation of aerosol types with spectral optical properties shows a dominance of mixed types. Pure EC is underestimated because it is often being classified as a mixture of EC and OC. This is expected from column-integrated aerosol optical properties, and the overlapping of sources and optical properties is also revealed in the in-situ measurements. Also, non-absorbing species internally mixed with carbonaceous species might lead to mixture types with relatively larger sizes. Comparison of detailed chemical measurements and spectral properties reveals that secondary organic aerosols processed in the aqueous phase might be a significant contributor in urban areas with a predominance of smog events, such as the Los Angeles basin.

On the other hand, applying the technique to estimate the chemical composition with spectral optical measurements, the Ångström matrix, to in-situ optical measurements including the actual chemical composition also show the limitations in the optical separation of the sources. Primary sources are difficult to classify, because the column-integrated measurements result in particles being classified as a mixture. Secondary species are well-classified but the separation between fossil fuel and biomass burning sources has limitations because of the overlapping optical

properties. In general, OC is better identified as a biomass burning source than a secondary fossil fuel source.

In conclusion, the availability of long-term global optical properties provides an opportunity for longer term estimates of aerosol types over a larger spatial scale. However co-located studies for some overlapping period of time with actual chemical composition measurements are necessary in order to constrain the applicability of the technique to specific regions. This will be necessary if we want to develop this tool into a general approach for accurately addressing the contribution of different aerosol sources to regional and global radiative forcing.

1.3.4 Characterization of Single Particle Chemistry Over The Entire LA Basin Using Aircraft Measurements During Calnex

1.3.4.1 Materials and Methods

The methods and particle types used for this section were identical to those discussed in section 1.3.2. Please refer to this section for more information.

1.3.4.2 Results and Discussion

1.3.4.2.1 Size Resolved Chemistry

Particles sampled by the ATOFMS were classified as particular types, described in detail by Cahill et al. The particle types used herein were biomass burning (BB), organic carbon (OC), soot or elemental carbon, soot mixed with OC (Soot-OC), highly processed (HP), vanadium mixed with OC (V-OC), sea salt (SS), and amines (AM). Minor particle types seen during CalNex, such as dust, were grouped together into Other. For overall number fractions of the different particle types please refer to Cahill et al [2012]. Briefly the most common particle types observed were carbonaceous in origin, namely BB, Soot, and Soot-OC. HP particles are also hypothesized to be carbonaceous in origin.

Figure 32 shows the size resolved chemistry measured during the CalNex study. At small particle sizes (< 200 nm) Soot and Soot-OC represent nearly 60% of all particles. This is consistent with fresh combustion emissions. As size increases to >800 nm, SS represents the highest fraction of particles. Typically, SS concentrations peak in the supermicron size range. At the mode of the size distribution, ~300 nm, biomass burning is at its highest fraction. The high number fractions were primarily due to local fires during CalNex.

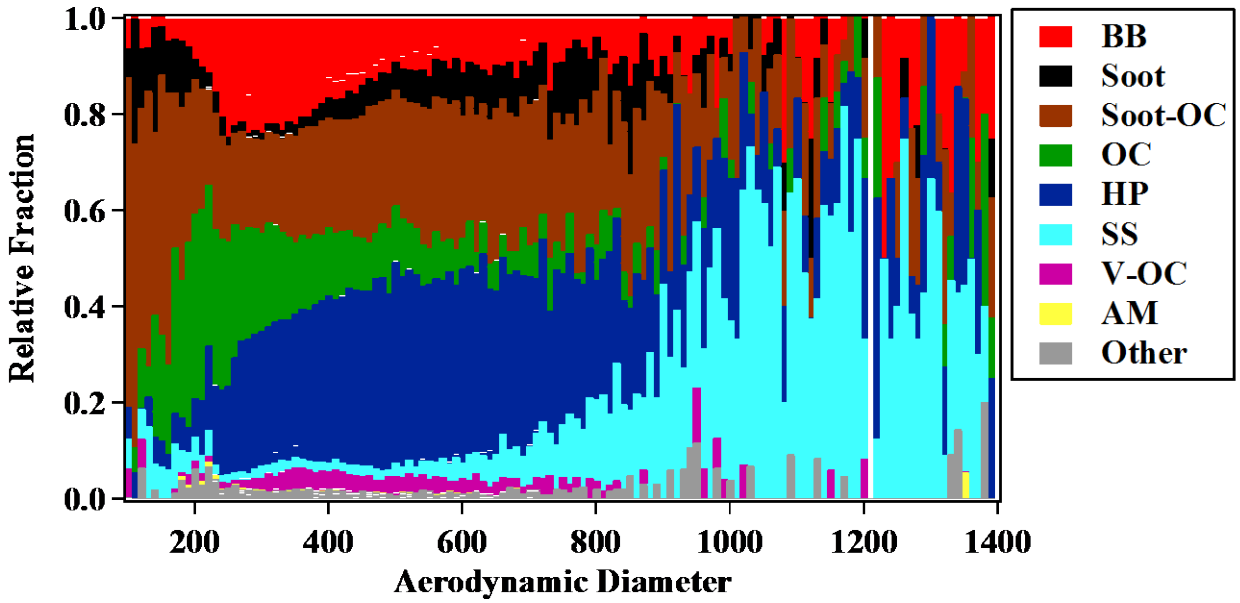

Figure 32: Size resolved chemistry during the CalNex study.

1.3.4.2.2 Regional variations

One of the goals of CalNex was to determine the various sources of soot in the LA Basin. Air flow within the basin generally travels eastward toward two outflow regions, known as the Banning and Cajon outflows. As particles are transported to these outflow regions they will undergo significant atmospheric processing or 'aging' which alters the chemical mixing state of the particle [*Riemer et al.*, 2010; *Rudich*, 2003; *Zaveri et al.*, 2010]. Understanding how single particle mixing state changes over time is incredibly important for accurate radiative forcing calculations [*Moffet and Prather*, 2009; *Schnaiter et al.*, 2005; *Schwarz et al.*, 2008]. Recent publications of CalNex data have targeted several different regions for more detailed analysis [*Metcalf et al.*, 2012]. This can provide insights into the changes in chemistry throughout the basin. A-ATOFMS data has been separated into different regions shown in Figure 33. Layered on top of these regions are flight paths for which the A-ATOFMS was on board the CIRPAS Twin Otter. East and west sections of the basin were separated to compare to the entire basin as a whole. Additionally, the chemistry below and above 700 m, the typical height of the boundary layer during CalNex, were compared as well.

ATOMFS particle fractions for each region are shown in Figure 34. The Long Beach region exhibited the highest fraction of soot aerosol, 24%, of the regions sampled, which had an average of 9%. This is expected as this region is highly impacted by port emissions and thus should exhibit a higher presence of combustion-generated aerosol. Aerosol in Pasadena, located to the northeast of Long Beach, had low fractions of soot aerosol relative to Long Beach. Instead the predominant fraction was the highly processed particle type, i.e. particles that had significant amounts of sulfate and nitrate. This is consistent with previous findings of particulate aging during transport within the region. Unfortunately, ATOFMS data on the outflow regions (Banning Pass, Banning Outflow, and Imperial Valley) is only available for one flight during the CalNex study. During this flight, a local fire along the flight path overwhelmed all signals besides biomass burning in the outflow regions. Therefore, we are unable to comment on the continued aging of aerosol as they travel out of the LA Basin. There were relatively minor differences between East and West sections of the LA Basin (Figure 34). The only difference in fractions was due to increased soot in the West Basin and, as already discussed, this can be traced back to Long Beach and port emissions.

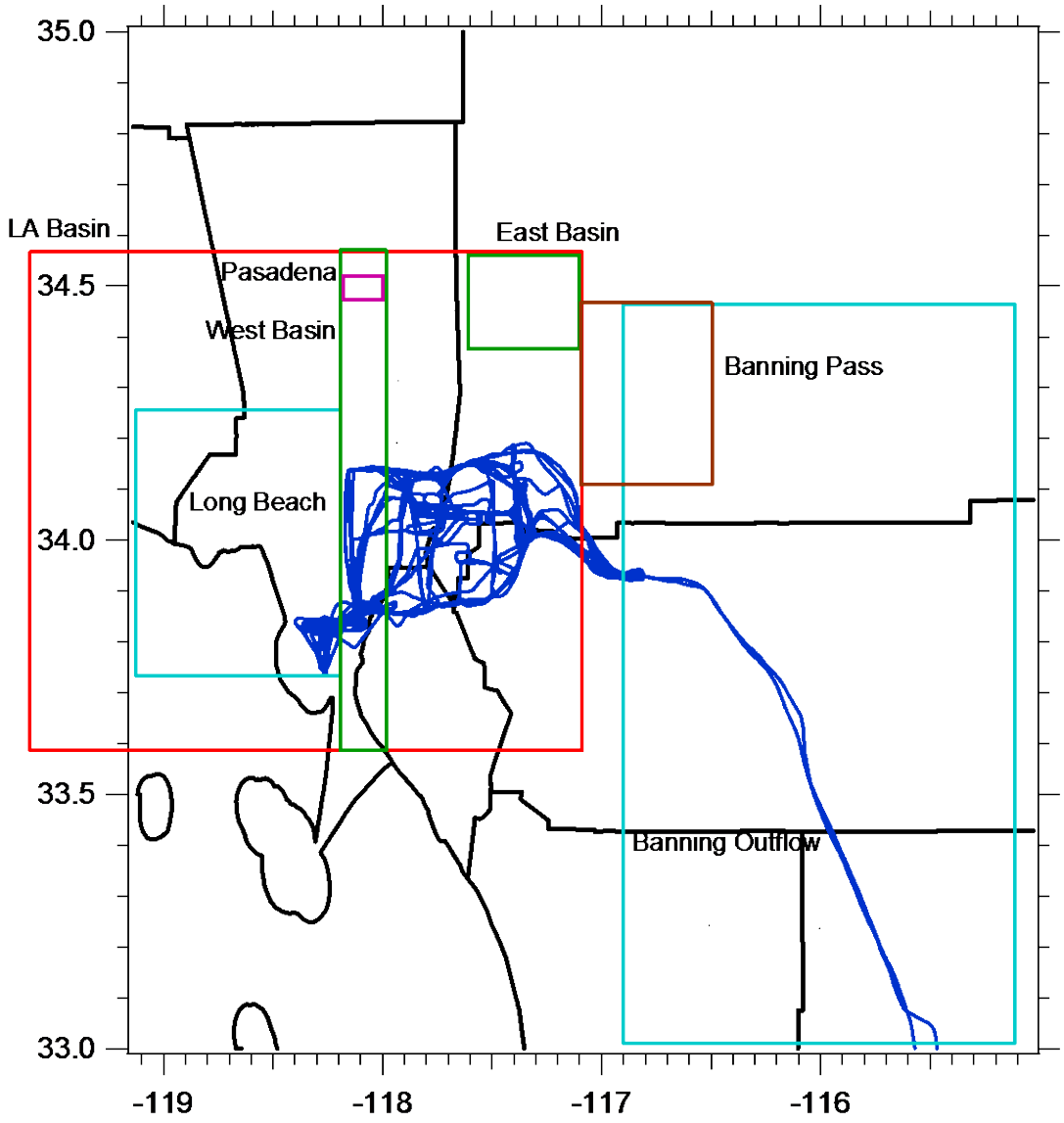

Figure 33: Different regions analyzed in detail are shown for CalNex. Flight paths with the A-ATOFMS are shown in blue.

To elucidate the magnitude of nitrate and sulfate in the same particle, a peak ion ratio of sulfate:nitrate was calculated by dividing the total RPA for each species by the other. These ratios form a distribution of values that represents all of the variance in magnitude of these species on particles. Since these ratios are calculated for a single particle, they are not dependent on laser fluence or matrix effects, assuming that the entire particle is completely ablated and that matrix effects suppress the selected ions equally [*Morrical et al.*, 1998; *Wenzel and Prather*, 2004]. Figure 35 shows the sulfate:nitrate single particle peak ratio distributions for every region. Ratios using data from the entire LA Basin have already been reported in Cahill et al. To summarize, most of the particles in the region are dominated by nitrate. Both east and west sections of the basin exhibit the same nitrogen dominated characteristic. Interestingly in Long

Beach, where ship emissions are high, particles are seen to contain a significant fraction of sulfate, contrary to the LA basin in general. These findings agree with ship based measurements made in the LA port regions and presented in Gaston et al. [2012]. It is clear that very different particulate chemistry exists near the port regions compared to the area as a whole. The fact that the surrounding area is dominated by nitrate suggests highly rapid replacement of sulfate after emission.

As particles travel eastward, from the west side of the basin to the Banning outflow, there is a shift in single particle peak ratios from mostly nitrate containing in the east to mostly sulfate containing in the outflow regions. However, as previously discussed, the flight to the outflow region was impacted by fresh local biomass burning. The fresh emissions would likely contain more sulfate, explaining the ATOFMS peak ratios. After sufficient time, it is expected that these particles would replace sulfate with nitrate as was seen in the rest of the area.

1.3.4.2.3 Vertical Profiles within CalNex

There were few changes in particulate chemistry measured by the ATOFMS above and below the boundary layer, evidenced by similar chemical fractions found at altitudes above and below 700 m (Figure 34). Soot was found at a slightly higher fraction at altitudes <700 m, 9 vs. 5% respectively, consistent with sampling closer to the source of these particles. Biomass burning occurred at slightly higher fractions, 19 vs. 16% respectively; however this can be explained by a local fire event occurring during the 13th, which was sampled at higher altitudes. The composite vertical profile over the CalNex study is shown in Figure 36. Note that high altitude sampling was not done with the ATOFMS onboard during CalNex. Vertical profiles from ~200 – 1200 meters were obtained by taking landing approaches to airports periodically during flights. In this way chemical differences close to the source and after transport towards the boundary layer were probed.

Passive Cavity Aerosol Spectrometer Probe (PCASP) number concentrations ranged from ~1700-2500 particles/cm^3 when below the boundary layer, and then decreased dramatically when sampling above the boundary layer. At low altitudes, soot was detected at its highest fractions, ~15%, compared to at altitudes at and above the boundary layer, ~5%. This is consistent with sampling soot closer to its source where it is relatively unprocessed. As altitude increases the particles become more processed, as evidenced by increased number fractions of HP particles. This is also demonstrated in Figure 37, which shows the number fractions of sulfate and nitrate containing particles as a function of altitude. At low altitudes, sulfate containing particles are seen at a higher fraction than nitrate particles, 54 and 29%, respectively. At ~400 m these fractions intersect and by ~600 m the number of nitrate containing particles has become significantly greater than the number of sulfate containing particles, 70 and 30%, respectively. Note that the increased fraction of biomass burning particles at altitudes between 1000-1200 m is due to local fires. As the only data for these altitudes were obtained while this contamination occurred, it was not removed. It is expected that as particles are lifted higher in altitude, they will become even more processed with sulfate and nitrate. These findings suggest that soot particles underwent rapid aging processes, acquiring significant amounts of nitrate and sulfate within a relatively short travel period while within the boundary layer.

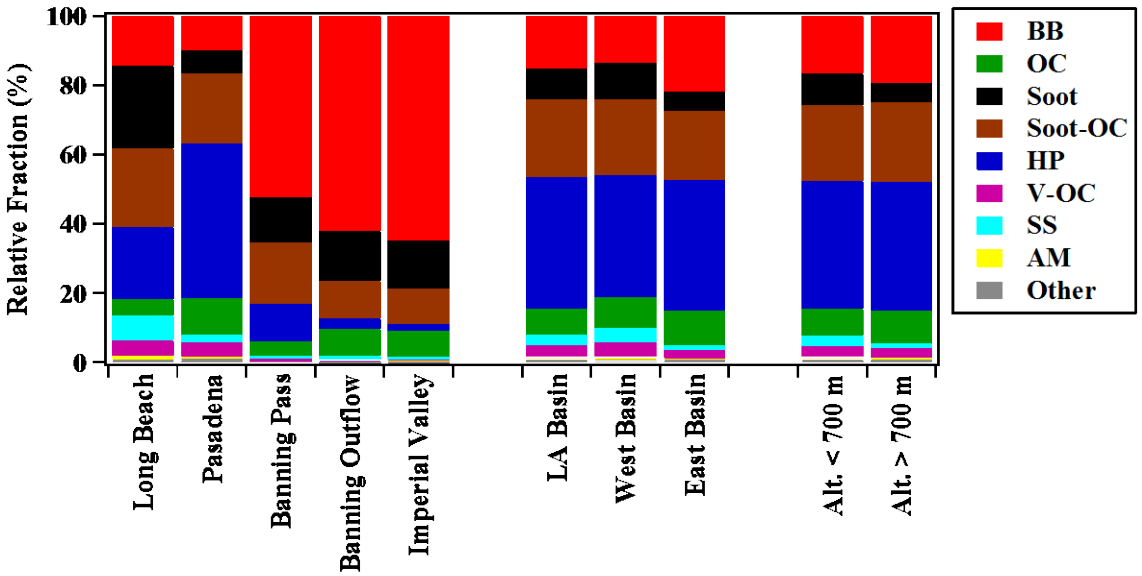

Figure 34: Relative number fractions of particle types in the regions analyzed by ATOFMS.

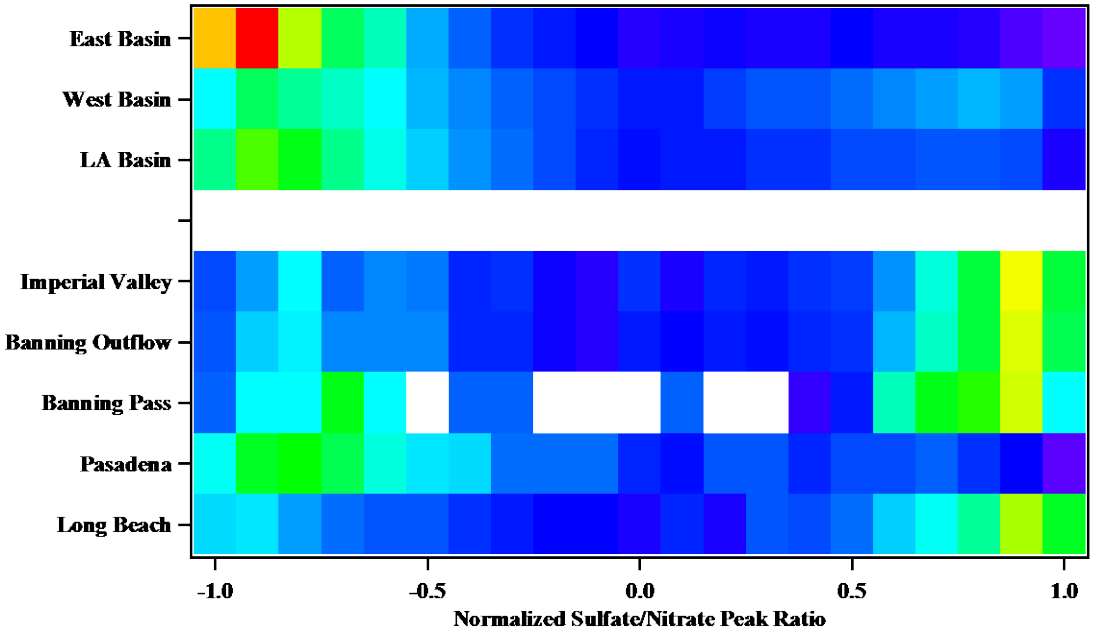

Figure 35: Sulfate/Nitrate peak ratio distributions for different regions measured during the CalNex study.

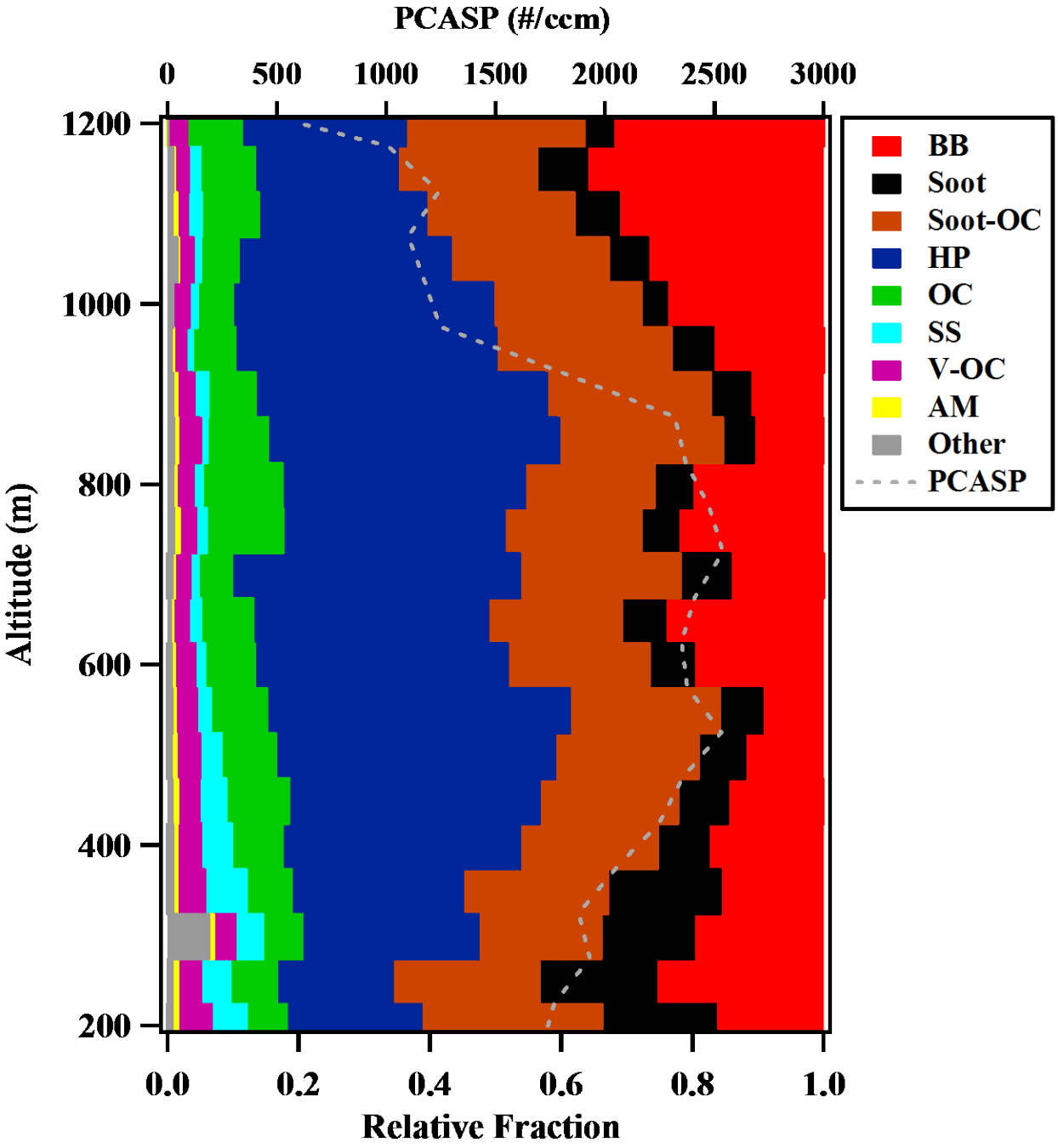

Figure 36: Vertical profile of relative compositional fractions measured by the ATOFMS during CalNex. PCASP number concentrations are shown in gray.

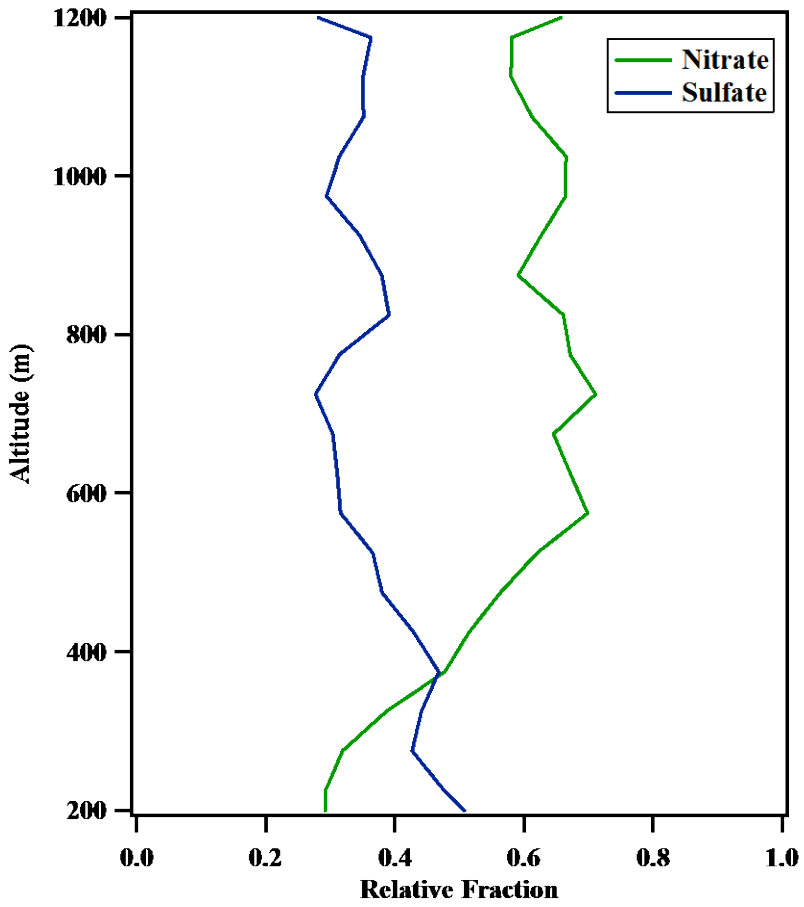

Figure 37: Relative fractions of nitrate (green) and sulfate (blue) containing particles as a function of altitude in CalNex.

1.3.4.2.4 Aerosol Hygroscopicity

To investigate the hygroscopicity of aerosols in the LA basin, 100-300 nm particles sampled with the ATOFMS were compared to Differential Aerosol Sizing and Hygroscopicity Spectrometer Probe (DASH-SP) results. This size range, 100-300 nm, was chosen to overlap with the DASH-SP sampling size range. The DASH-SP takes aerosols, dries them, size selects them (150, 175, 200, and 225 nm dry diameter), sends them through humidified chambers with 2 different RH values (74 and 92 %) and then sizes the resulting particles [*Sorooshian et al.*, 2008a]. The growth factor (GF) is calculated by taking the wet diameter size over the dry diameter size, which relates to how much the particles grew due to water uptake in the different RH conditions. A cloud condensation nuclei counter (CCNC) was used to calculate the fraction of aerosols that activate as cloud droplets. The CCNC works in a similar way to the DASH-SP, but exposes aerosols to RH above 100% or supersaturated conditions [*Roberts and Nenes*, 2005]. A single parameter for hygroscopicity, κ, as defined by Petters and Kreidenweis [2007] was used to relate subsaturated and supersaturated water uptake. For reference, an increase in κ corresponds to an increase in hygroscopicity.

Figure 38 shows a comparison between aerosol chemistry, GF-derived κ, and CCN-derived κ, reprinted from Hersey et al. [2013]. The flight on May 10, 2010 (Figure 38a) was impacted by a

biomass burning episode and the hygroscopicity of aerosols from that flight were compared to aerosols from five flights that were not affected by biomass burning events (Figure 38b). CCN derived κ increased in the East Basin samples, with lower values for both the West Basin and outflow regions; however, the GF-derived κ shows a decrease from west to east. This behavior is consistent for both the biomass burning influenced flight and the non-biomass burning flights. These results can possibly be explained by the presence of organic coatings which often inhibit the accretion of water in subsaturated regimes, while in supersaturated regimes, the water can make it through the coating to the more soluble under layers, thus taking up the water. Additionally, due to dilution in the outflow regions, semi-volatile secondary species can then evaporate from the particles, resulting in outflow regions having similar CCN-derived κ to the West Basin samples.

1.3.4.3 Conclusions

Regional analysis of flight data indicates very different particulate chemistry depending upon the area of the LA basin being sampled. Near Long Beach, particle chemistry was significantly influenced by port emissions, evidenced by increased fractions of soot and soot-OC particles. In addition, the secondary species associated with these particles differed from particles measured in the rest of CalNex, containing higher peak ratios of sulfate compared to nitrate. These results agree with ship-based measurements in the same region and explain the discrepancy between these two measurements as identified in Cahill et al. [2012] and Gaston et al. [2012].

The chemically resolved vertical profile of CalNex data shows higher number fractions of soot aerosol at lower altitudes, while particles at altitudes closer to the top of the boundary layer are more highly processed, indicating that particles acquire significant amounts of sulfate and nitrate coatings as they rise in altitude. When close to ground level, a higher fraction of particles contain sulfate than nitrate; however this quickly reverses as altitude increases with nitrate becoming more prevalent at higher altitudes.

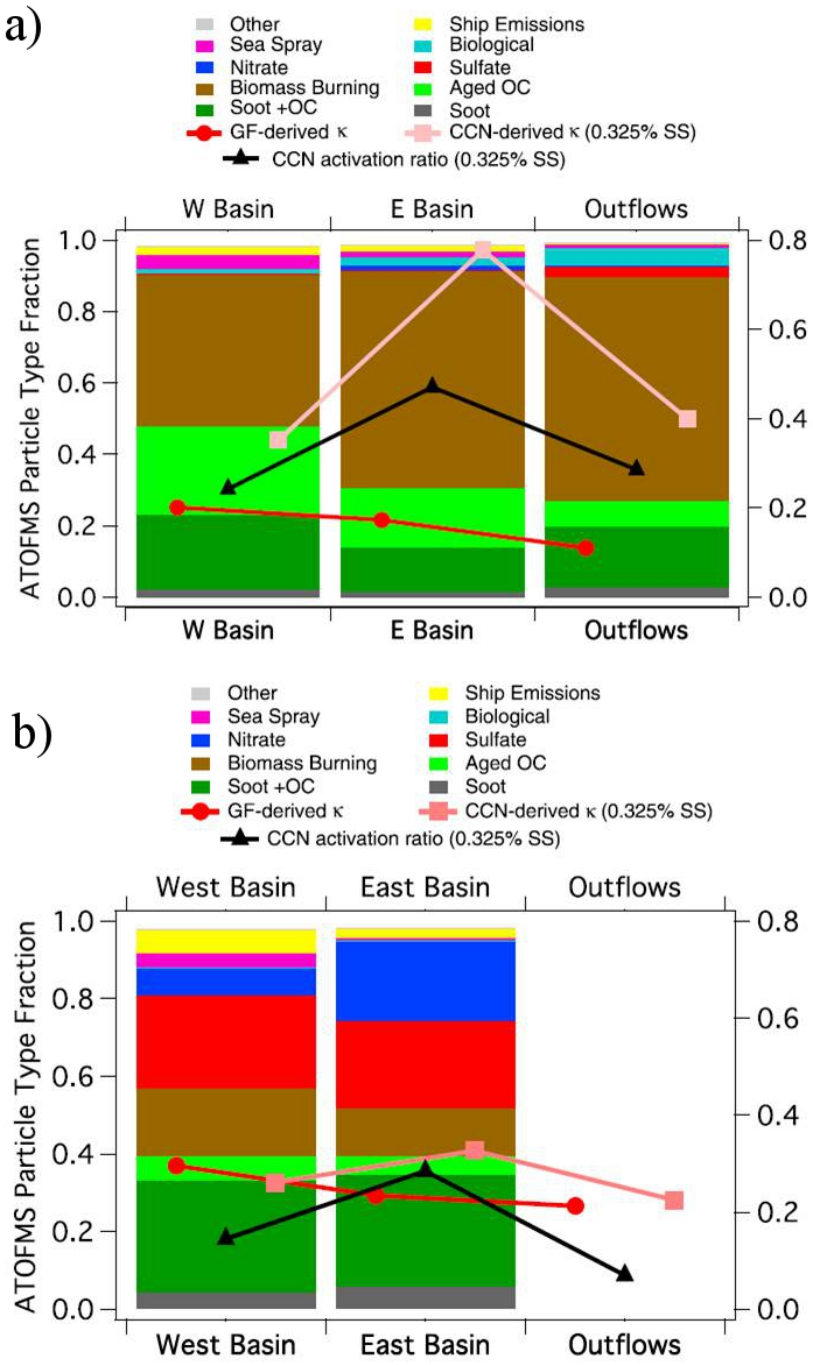

Figure 38: Comparison of ATOFMS particle type fraction, GF-derived k, CCN-derived k (0.325% SS), and activation ratio for (a) 13 May 2010 and (b) five non-biomass burning-influenced flights (6–7, 10, and 14–15 May 2010).

Conclusions and Recommendations

Conclusions

The results described in this report accomplished numerous objectives stated in the proposal. While some of the original questions of the proposal could not be addressed, due to aircraft measurements not reaching high altitudes, the dataset obtained in CalNex helped to answer many questions and fulfill the overall goal of the proposal "… to obtain detailed data on aerosol size and chemical mixing state during CalNex in May 2010 and link it with measured optical and hygroscopic properties". Towards this end, the ATOFMS data obtained in the CalNex study were used in the publication of six peer-reviewed papers [*Cahill et al.*, 2012; *Cazorla et al.*, 2013; *Gaston et al.*, 2012; *Hersey et al.*, 2013; *Weiss-Penzias et al.*, 2013; *Zaveri et al.*, 2012]. The revised questions as listed in the introduction were:

1. What are the major sources contributing to black carbon or soot aerosols in California?
2. What are the differences in aerosol sources and secondary chemistry between northern and southern California?
3. What are the differences in chemical mixing state across the LA basin?
4. How accurate are the optical retrievals from satellite measurements?
5. What is vertical profile of chemical mixing state within and just above the boundary layer?
6. How does aerosol mixing state impact hygroscopic properties?

For question (1), soot was found to be more predominant in southern California, with increased fractions found in regions near the ports in Long Beach. Throughout the rest of the LA Basin, soot number fractions were relatively constant, most likely due to vehicle emissions throughout the basin. In addition soot aerosol was mixed with large amounts of secondary species, even when sampled near the source. This has implications for radiative forcing calculations. Results 1.3.1, 1.3.2, and 1.3.4 helped to answer question (2) and (3) by measuring the chemical mixing state of aerosols over both northern and southern California as part of the CARES and CalNex campaigns. Aircraft measurements in northern California showed that particles were predominantly mixed with sulfate, while in southern California nitrate was the dominant secondary species present on particles. This contrasts with ship-based measurements which showed nitrate in the north and sulfate in the south. Upon closer examination of aircraft data, particles near the ports of LA contained significant amounts of sulfate. These particles quickly acquire nitrate as they move through the basin. In section 1.3.3, ATOFMS data from many flight campaigns helped to develop a methodology and determine its limitations to estimate absorbing aerosols speciation from spectral optical measurements. Optical measurements were able to classify secondary fossil fuel and biomass burning sources well; however the separation between biomass burning and fossil fuel sources have overlapping optical properties making them

difficult to classify. Aerosol speciation with this technique should be used with these limitations taken into account. Question (5) was addressed in section 1.3.4. The fractions of chemical types observed by the ATOFMS were relatively uniform except at low altitudes, where soot was present at an increased fraction due to closer proximity to the source. Finally, ATOFMS measurements in combination with in flight hygroscopicity measurements uncovered that biomass burning aerosol may be active cloud condensation nuclei, but relatively non-hygroscopic at sub-saturated RH. The opposing sub- and super-saturated trends occurred on non-biomass burning influenced periods as well. This could be due to the presence of an organic coating with variable water uptake depending on sub- or super-saturated conditions.

Recommendations

Unfortunately, the lack of high altitude measurements limit our ability to address specific questions outlined in the original proposal. High altitude sampling would allow for identification of the impact of long range transport of soot from other continents (i.e., Asia), as well as the distribution of soot vertically both as a function of concentration and mixing state. The data obtained within the LA basin suggests rapid aging of these aerosols. It is possible that their continued aging at higher altitudes may significantly change their optical properties, something that is still poorly understood in the scientific community.

The ATOFMS was on one flight (May 10, 2010) that sampled the outflow regions, but the region was contaminated by biomass burning aerosol on this particular day. Additional flights into the outflow region may shed more insight into hygroscopicity comparisons made in this report and Hersey et al. [2013]. A Lagrangian framework for flights into the outflow regions may provide more information on how quickly these particles age and acquire organic coatings.

Comparisons of satellite retrievals provided a unique look at the strengths and weaknesses in using optical data to predict aerosol chemistry and sources. Accurate satellite retrieval would significantly enhance our understanding of particulate chemistry by providing unprecedented regional coverage. Additional studies focusing on limiting the errors discussed in this report would be extremely beneficial.

The CalNex study was conducted in May 2010. An additional study during the winter season would provide interesting contrast with this dataset. It is important to determine the relative contributions of primary (soot, biomass burning, dust) and secondary species such a nitrate, sulfate, and amines for different seasons.

References

Ackerman, A.S., O.B. Toon, D.E. Stevens, A.J. Heymsfield, V. Ramanathan, and E.J. Welton, Reduction of tropical cloudiness by soot, *Science*, *288* (5468), 1042-1047, 2000.

Agrawal, H., Q.G.J. Malloy, W.A. Welch, J.W. Miller, and D.R. Cocker, In-use gaseous and particulate matter emissions from a modern ocean going container vessel, *Atmospheric Environment*, *42* (21), 5504-5510, 2008.

Ahlm, L., S. Liu, D.A. Day, L.M. Russell, R. Weber, D.R. Gentner, A.H. Goldstein, J.P. DiGangi, S.B. Henry, F.N. Keutsch, T.C. VandenBoer, M.Z. Markovic, J.G. Murphy, X. Ren, and S. Scheller, Formation and growth of ultrafine particles from secondary sources in Bakersfield, California, *J Geophys Res*, *117*, D00V08, doi:10.1029/2011JD017144, 2012.

Allen, J.O., YAADA software toolkit to analyze single-particle mass spectral data: Reference manual version 2.11., *Arizona State University*, http://www.yaada.org, 2002.

Anderson, T.L., and J.A. Ogren, Determining aerosol radiative properties using the TSI 3563 integrating nephelometer, *Aerosol Science and Technology*, *29* (1), 57-69, 1998.

Andreae, M.O., and A. Gelencser, Black carbon or brown carbon? The nature of light-absorbing carbonaceous aerosols, *Atmospheric Chemistry and Physics*, *6*, 3131-3148, 2006.

Angelino, S., D.T. Suess, and K.A. Prather, Formation of aerosol particles from reactions of secondary and tertiary alkylamines: Characterization by aerosol time-of-flight mass spectrometry, *Environ Sci Technol*, *35* (15), 3130-3138, 2001.

Ault, A.P., C.J. Gaston, Y. Wang, G. Dominguez, M.H. Thiemens, and K.A. Prather, Characterization of the Single Particle Mixing State of Individual Ship Plume Events Measured at the Port of Los Angeles, *Environ Sci Technol*, *44* (6), 1954-1961, 2010.

Ault, A.P., M.J. Moore, H. Furutani, and K.A. Prather, Impact of Emissions from the Los Angeles Port Region on San Diego Air Quality during Regional Transport Events, *Environ Sci Technol*, *43* (10), 3500-3506, 2009.

Ault, A.P., C.R. Williams, A.B. White, P.J. Neiman, J.M. Creamean, C.J. Gaston, F.M. Ralph, and K.A. Prather, Detection of Asian dust in California orographic precipitation, *Journal of Geophysical Research-Atmospheres*, *116*, 2011.

Bahadur, R., P.S. Praveen, Y.Y. Xu, and V. Ramanathan, Solar absorption by elemental and brown carbon determined from spectral observations, *Proceedings of the National Academy of Sciences of the United States of America*, *109* (43), 17366-17371, 2012.

Bahreini, R., E.J. Dunlea, B.M. Matthew, C. Simons, K.S. Docherty, P.F. DeCarlo, J.L. Jimenez, C.A. Brock, and A.M. Middlebrook, Design and Operation of a Pressure-Controlled Inlet for Airborne Sampling with an Aerodynamic Aerosol Lens, *Aerosol Science and Technology*, *42* (6), 465-471, 2008.

Barnaba, F., and G.P. Gobbi, Aerosol seasonal variability over the Mediterranean region and relative impact of maritime, continental and Saharan dust particles over the basin from MODIS data in the year 2001, *Atmospheric Chemistry and Physics*, *4*, 2367-2391, 2004.

Bateman, A.P., S.A. Nizkorodov, J. Laskin, and A. Laskin, Photolytic processing of secondary organic aerosols dissolved in cloud droplets, *Phys. Chem. Chem. Phys.*, *13*, 12199-12212, 2011.

Bates, T.S., P.K. Quinn, A.A. Frossard, L.M. Russell, J. Hakala, T. Petaja, M. Kulmala, D.S. Covert, C.D. Cappa, S.-M. Li, K. Hayden, I. Nuaaman, R. McLaren, P. Massoli, M.R.

Canagaratna, T.B. Onasch, D. Sueper, D. Worsnop, and W.C. Keene, Measurements of ocean derived aerosol off the coast of California, *J Geophys Res*, *117*, D00V15, doi:10.1029/2012JD017588, 2012.

Behnke, W., H.U. Kruger, V. Scheer, and C. Zetzsch, Formation of Atomic Cl from Sea Spray Via Photolysis of Nitryl Chloride - Determination of the Sticking Coefficient of N_2O_5 on NaCl Aerosol, *Journal of Aerosol Science*, *22*, S609-S612, 1991.

Bergstrom, R.W., P. Pilewskie, P.B. Russell, J. Redemann, T.C. Bond, P.K. Quinn, and B. Sierau, Spectral absorption properties of atmospheric aerosols, *Atmospheric Chemistry and Physics*, *7* (23), 5937-5943, 2007.

Bergstrom, R.W., P.B. Russell, and P. Hignett, Wavelength dependence of the absorption of black carbon particles: Predictions and results from the TARFOX experiment and implications for the aerosol single scattering albedo, *Journal of the Atmospheric Sciences*, *59* (3), 567-577, 2002.

Bhave, P.V., J.O. Allen, B.D. Morrical, D.P. Fergenson, G.R. Cass, and K.A. Prather, A field-based approach for determining ATOFMS instrument sensitivities to ammonium and nitrate, *Environ Sci Technol*, *36* (22), 4868-4879, 2002.

Bi, X.H., G.H. Zhang, L. Li, X.M. Wang, M. Li, G.Y. Sheng, J.M. Fu, and Z. Zhou, Mixing state of biomass burning particles by single particle aerosol mass spectrometer in the urban area of PRD, China, *Atmospheric Environment*, *45* (20), 3447-3453, 2011.

Bishop, G.A., B.G. Schuchmann, and D.H. Stedman, Emission changes resulting from the San Pedro Bay, California ports truck retirement program, *Environmental Science & Technology*, *46*, 551-558, 2012.

Blanchard, D.C., and A.H. Woodcock, Bubble formation and modification in the sea and its meteorological significance, *Tellus*, *9* (2), 145-158, 1957.

Bond, T.C., T.L. Anderson, and D. Campbell, Calibration and intercomparison of filter-based measurements of visible light absorption by aerosols, *Aerosol Science and Technology*, *30* (6), 582-600, 1999.

Bond, T.C., and R.W. Bergstrom, Light absorption by carbonaceous particles: An investigative review, *Aerosol Science and Technology*, *40* (1), 27-67, 2006.

Brands, M., M. Kamphus, T. Böttger, J. Schneider, F. Drewnick, A. Roth, J. Curtius, C. Voigt, A. Borbon, M. Beekmann, A. Bourdon, T. Perrin, and S. Borrmann, Characterization of a Newly Developed Aircraft-Based Laser Ablation Aerosol Mass Spectrometer (ALABAMA) and First Field Deployment in Urban Pollution Plumes over Paris During MEGAPOLI 2009, *Aerosol Science and Technology*, *45* (1), 46-64, 2010.

Cahill, J.F., K. Suski, J. Seinfeld, R.A. Zaveri, and K.A. Prather, The mixing state between northern and southern California measured during CARES and CalNEX 2010, *Atmospheric Chemistry and Physics*, *12*, 10989-11002, doi:10.5194/acp-12-10989-2012, 2012.

Cappa, C.D., D.L. Che, S.H. Kessler, J.H. Kroll, and K.R. Wilson, Variations in organic aerosol optical and hygroscopic properties upon heterogeneous OH oxidation, *Journal of Geophysical Research*, *116* (D15), 2011.

CARB, Final Regulation Order. Fuel Sulfur and Other Operational Requirements for Ocean-Going Vessels within California Waters and 24 Nautical Miles of the California Baseline, California Air Resources Board: Sacramento, CA, 2009.

Cazorla, A., R. Bahadur, K.J. Suski, J.F. Cahill, D. Chand, B. Schmid, V. Ramanathan, and K.A. Prather, Relating aerosol absorption due to soot, organic carbon, and dust to emission

sources determined from in-situ chemical measurements, *Atmospheric Chemistry and Physics*, *13* (18), 9337-9350, 2013.

Chang, W.L., P.V. Bhave, S.S. Brown, N. Riemer, J. Stutz, and D. Dabdub, Heterogeneous atmospheric chemistry, ambient measurements, and model calculations of N_2O_5: A review, *Aerosol Science and Technology*, *45* (6), 665-695, 2011.

Chen, L.W.A., J.G. Watson, J.C. Chow, and K.L. Magliano, Quantifying $PM_{2.5}$ source contributions for the San Joaquin Valley with multivariate receptor models, *Environmental Science & Technology*, *41* (8), 2818-2826, 2007.

Chow, J.C., L.W.A. Chen, J.G. Watson, D.H. Lowenthal, K.A. Magliano, K. Turkiewicz, and D.E. Lehrman, $PM_{2.5}$ chemical composition and spatiotemporal variability during the California Regional PM_{10}/$PM_{2.5}$ Air Quality Study (CRPAQS), *Journal of Geophysical Research-Atmospheres*, *111* (D10), D10S04, doi:10.1029/2005JD006457, 2006a.

Chow, J.C., J.G. Watson, P. Doraiswamy, L.W.A. Chen, D.A. Sodeman, D.H. Lowenthal, K. Park, W.P. Arnott, and N. Motallebi, Aerosol light absorption, black carbon, and elemental carbon at the Fresno Supersite, California, *Atmospheric Research*, *93* (4), 874-887, 2009.

Chow, J.C., J.G. Watson, D.H. Lowenthal, L.W.A. Chen, R.J. Tropp, K. Park, and K.A. Magliano, PM2.5 and PM10 mass measurements in California's San Joaquin Valley, *Aerosol Science and Technology*, *40* (10), 796-810, 2006b.

Chow, J.C., J.G. Watson, D.H. Lowenthal, P.A. Solomon, K.L. Magliano, S.D. Ziman, and L.W. Richards, Pm(10) and Pm(2.5) Compositions in California San Joaquin Valley, *Aerosol Science and Technology*, *18* (2), 105-128, 1993.

Chung, S.H., and J.H. Seinfeld, Global distribution and climate forcing of carbonaceous aerosols, *Journal of Geophysical Research-Atmospheres*, *107* (D19), 2002.

Coen, M.C., E. Weingartner, D. Schaub, C. Hueglin, C. Corrigan, S. Henning, M. Schwikowski, and U. Baltensperger, Saharan dust events at the Jungfraujoch: detection by wavelength dependence of the single scattering albedo and first climatology analysis, *Atmospheric Chemistry and Physics*, *4*, 2465-2480, 2004.

Corbett, J.J., and P. Fischbeck, Emissions from ships, *Science*, *278* (5339), 823-824, 1997.

Corbett, J.J., and H.W. Koehler, Updated emissions from ocean shipping, *Journal of Geophysical Research-Atmospheres*, *108* (D20), 4650, doi:10.1029/2003JD003751, 2003.

Creamean, J.M., A.P. Ault, J.E. Ten Hoeve, M.Z. Jacobson, G.C. Roberts, and K.A. Prather, Measurements of aerosol chemistry during new particle formation events at a remote rural mountain site, *Environmental Science & Technology*, *45* (19), 8208-8216, 2011.

Creamean, J.M., K.J. Suski, D. Rosenfeld, A. Cazorla, P.J. DeMott, R.C. Sullivan, A.B. White, F.M. Ralph, P. Minnis, J.M. Comstock, J.M. Tomlinson, and K.A. Prather, Dust and Biological Aerosols from the Sahara and Asia Influence Precipitation in the Western U.S., *Science*, *339* (6127), 1572-1578, 2013.

Dall'Osto, M., R.M. Harrison, D.C.S. Beddows, E.J. Freney, M.R. Heal, and R.J. Donovan, Single-particle detection efficiencies of aerosol time-of-flight mass spectrometry during the North Atlantic marine boundary layer experiment, *Environmental Science & Technology*, *40* (16), 5029-5035, 2006.

Docherty, K.S., E.A. Stone, I.M. Ulbrich, P.F. DeCarlo, D.C. Snyder, J.J. Schauer, R.E. Peltier, R.J. Weber, S.M. Murphy, J.H. Seinfeld, B.D. Grover, D.J. Eatough, and J.L. Jimenez, Apportionment of primary and secondary organic aerosols in Southern California during

the 2005 Study of Organic Aerosols in Riverside (SOAR-1), *Environmental Science & Technology*, *42* (20), 7655-7662, 2008.

Draxler, R.R., and G.D. Rolph, HYSPLIT (HYbrid Single-Particle Lagrangian Integrated Trajectory) Model access via NOAA ARL READY Website (http://ready.arl.noaa.gov/HYSPLIT.php), *NOAA Air Resources Laboratory*, Silver Spring, MD, 2011.

Dubovik, O., B. Holben, T.F. Eck, A. Smirnov, Y.J. Kaufman, M.D. King, D. Tanre, and I. Slutsker, Variability of absorption and optical properties of key aerosol types observed in worldwide locations, *Journal of the Atmospheric Sciences*, *59* (3), 590-608, 2002.

Duong, H.T., A. Sorooshian, J.S. Craven, S.P. Hersey, A.R. Metcalf, X. Zhang, R.J. Weber, H.H. Jonsson, R.C. Flagan, and J.H. Seinfeld, Water-soluble organic aerosol in the Los Angeles Basin and outflow regions: Airborne and ground measurements during the 2010 CalNex field campaign, *Journal of Geophysical Research*, *116*, D00V04, doi:10.1029/2011JD016674, 2011.

Eatough, D.J., B.D. Grover, W.R. Woolwine, N.L. Eatough, R. Long, and R. Farber, Source apportionment of 1 h semi-continuous data during the 2005 Study of Organic Aerosols in Riverside (SOAR) using positive matrix factorization, *Atmospheric Environment*, *42* (11), 2706-2719, 2008.

Eck, T.F., B.N. Holben, J.S. Reid, O. Dubovik, A. Smirnov, N.T. O'Neill, I. Slutsker, and S. Kinne, Wavelength dependence of the optical depth of biomass burning, urban, and desert dust aerosols, *Journal of Geophysical Research-Atmospheres*, *104* (D24), 31333-31349, 1999.

Facchini, M.C., S. Decesari, M. Rinaldi, C. Carbone, E. Finessi, M. Mircea, S. Fuzzi, F. Moretti, E. Tagliavini, D. Ceburnis, and C.D. O'Dowd, Important source of marine secondary organic aerosol from biogenic amines, *Environmental Science & Technology*, *42* (24), 9116-9121, 2008a.

Facchini, M.C., M. Rinaldi, S. Decesari, C. Carbone, E. Finessi, M. Mircea, S. Fuzzi, D. Ceburnis, R. Flanagan, E.D. Nilsson, G. de Leeuw, M. Martino, J. Woeltjen, and C.D. O'Dowd, Primary submicron marine aerosol dominated by insoluble organic colloids and aggregates, *Geophysical Research Letters*, *35*, L17814, doi:10.1029/2008GL034210, 2008b.

Fast, J.D., W.I. Gustafson, L.K. Berg, W.J. Shaw, M. Pekour, M. Shrivastava, J.C. Barnard, R.A. Ferrare, C.A. Hostetler, J.A. Hair, M. Erickson, B.T. Jobson, B. Flowers, M.K. Dubey, S. Springston, R.B. Pierce, L. Dolislager, J. Pederson, and R.A. Zaveri, Transport and mixing patterns over Central California during the carbonaceous aerosol and radiative effects study (CARES), *Atmospheric Chemistry and Physics*, *12* (4), 1759-1783, 2012.

Fergenson, D.P., M.E. Pitesky, H.J. Tobias, P.T. Steele, G.A. Czerwieniec, S.C. Russell, C.B. Lebrilla, J.M. Horn, K.R. Coffee, A. Srivastava, S.P. Pillai, M.T.P. Shih, H.L. Hall, A.J. Ramponi, J.T. Chang, R.G. Langlois, P.L. Estacio, R.T. Hadley, M. Frank, and E.E. Gard, Reagentless detection and classification of individual bioaerosol particles in seconds, *Anal Chem*, *76* (2), 373-378, 2004.

Fialho, P., A.D.A. Hansen, and R.E. Honrath, Absorption coefficients by aerosols in remote areas: a new approach to decouple dust and black carbon absorption coefficients using seven-wavelength Aethalometer data, *Journal of Aerosol Science*, *36* (2), 267-282, 2005.

Fitzgerald, J.W., Marine aerosols: A review, *Atmos. Environ. A-Gen. Topics*, *25* (3-4), 533-545, 1991.

Fraser, M.P., and G.R. Cass, Detection of excess ammonia emissions from in-use vehicles and the implications for fine particle control, *Environmental Science & Technology*, *32*, 1053-1057, 1998.

Furutani, H., M. Dallosto, G. Roberts, and K. Prather, Assessment of the relative importance of atmospheric aging on CCN activity derived from field observations, *Atmospheric Environment*, *42* (13), 3130-3142, 2008.

Gard, E., J.E. Mayer, B.D. Morrical, T. Dienes, D.P. Fergenson, and K.A. Prather, Real-time analysis of individual atmospheric aerosol particles: Design and performance of a portable ATOFMS, *Anal Chem*, *69* (20), 4083-4091, 1997.

Gard, E.E., M.J. Kleeman, D.S. Gross, L.S. Hughes, J.O. Allen, B.D. Morrical, D.P. Fergenson, T. Dienes, M.E. Galli, R.J. Johnson, G.R. Cass, and K.A. Prather, Direct observation of heterogeneous chemistry in the atmosphere, *Science*, *279* (5354), 1184-1187, 1998.

Gaston, C.J., H. Furutani, S.A. Guazzotti, K.R. Coffee, T.S. Bates, P.K. Quinn, L.I. Aluwihare, B.G. Mitchell, and K.A. Prather, Unique ocean-derived particles serve as a proxy for changes in ocean chemistry, *Journal of Geophysical Research-Atmospheres*, *116*, D18310, doi:10.1029/2010JD015289, 2011.

Gaston, C.J., K.A. Pratt, X.Y. Qin, and K.A. Prather, Real-Time Detection and Mixing State of Methanesulfonate in Single Particles at an Inland Urban Location during a Phytoplankton Bloom, *Environ Sci Technol*, *44* (5), 1566-1572, 2010.

Gaston, C.J., P.K. Quinn, B.S. Timothy, and K.A. Prather, Differences in Northern and Southern California particle chemistry and insight into the mixing-state of carbonaceous aerosol in California observed during the CalNex 2010 campaign, *In Preparation*, 2012.

Giles, D.M., B.N. Holben, T.F. Eck, A. Sinyuk, A. Smirnov, I. Slutsker, R.R. Dickerson, A.M. Thompson, and J.S. Schafer, An analysis of AERONET aerosol absorption properties and classifications representative of aerosol source regions, *Journal of Geophysical Research-Atmospheres*, *117*, 2012.

Giles, D.M., B.N. Holben, S.N. Tripathi, T.F. Eck, W.W. Newcomb, I. Slutsker, R.R. Dickerson, A.M. Thompson, S. Mattoo, S.H. Wang, R.P. Singh, A. Sinyuk, and J.S. Schafer, Aerosol properties over the Indo-Gangetic Plain: A mesoscale perspective from the TIGERZ experiment, *Journal of Geophysical Research-Atmospheres*, *116*, 2011.

Gross, D.S., M.E. Galli, P.J. Silva, and K.A. Prather, Relative sensitivity factors for alkali metal and ammonium cations in single particle aerosol time-of-flight mass spectra, *Anal Chem*, *72* (2), 416-422, 2000.

Grover, B.D., N.L. Eatough, W.R. Woolwine, J.P. Cannon, D.J. Eatough, and R.W. Long, Semi-continuous mass closure of the major components of fine particulate matter in Riverside, CA, *Atmospheric Environment*, *42*, 250-260, 2008.

Guazzotti, S.A., K.R. Coffee, and K.A. Prather, Continuous measurements of size-resolved particle chemistry during INDOEX-Intensive Field Phase 99, *Journal of Geophysical Research-Atmospheres*, *106* (D22), 28607-28627, 2001.

Gyawali, M., W.P. Arnott, K. Lewis, and H. Moosmuller, In situ aerosol optics in Reno, NV, USA during and after the summer 2008 California wildfires and the influence of absorbing and non-absorbing organic coatings on spectral light absorption, *Atmospheric Chemistry and Physics*, *9* (20), 8007-8015, 2009.

Hand, J.L., and W.C. Malm, Review of aerosol mass scattering efficiencies from ground-based measurements since 1990, *Journal of Geophysical Research-Atmospheres*, *112* (D18), 2007.

Hatch, L.E., J.M. Creamean, A.P. Ault, J.D. Surratt, M.N. Chan, J.H. Seinfeld, E.S. Edgerton, Y. Su, and K.A. Prather, Measurements of Isoprene-Derived Organosulfates in Ambient Aerosols by Aerosol Time-of-Flight Mass Spectrometry - Part 1: Single Particle Atmospheric Observations in Atlanta, *Environ Sci Technol, 45* (12), 5105-5111, 2011.

Hawkins, L.N., L.M. Russell, D.S. Covert, P.K. Quinn, and T.S. Bates, Carboxylic acids, sulfates, and organosulfates in processed continental organic aerosol over the southeast Pacific Ocean during VOCALS-REx 2008, *Journal of Geophysical Research-Atmospheres, 115*, D13201, doi:10.1029/2009JD013276, 2010.

Haywood, J.M., and K.P. Shine, The Effect of Anthropogenic Sulfate and Soot Aerosol on the Clear-Sky Planetary Radiation Budget, *Geophysical Research Letters, 22* (5), 603-606, 1995.

Healy, R.M., I.P. O'Connor, S. Hellebust, A. Allanic, J.R. Sodeau, and J.C. Wenger, Characterization of single particles from in-port ship emissions, *Atmos Environ, 43*, 6408-6414, 2009.

Hegg, D.A., The importance of liquid-phase oxidation of SO_2 in the troposphere, *Journal of Geophysical Research, 90* (D2), 3773-3779, 1985.

Hegg, D.A., and M.B. Baker, Nucleation in the atmosphere, *Reports on Progress in Physics, 72* (5), doi:10.1088/0034-4885/72/5/056801, 2009.

Hegg, D.A., D.S. Covert, H. Jonsson, and P.A. Covert, Determination of the transmission efficiency of an aircraft aerosol inlet, *Aerosol Science and Technology, 39* (10), 966-971, 2005.

Hering, S.V., and S.K. Friedlander, Origins of aerosol sulfur size distributions in the Los Angeles Basin, *Atmos Environ, 16* (11), 2647-2656, 1982.

Hersey, S.P., J.S. Craven, A.R. Metcalf, J. Lin, T. Lathem, K.J. Suski, J.F. Cahill, H.T. Duong, A. Sorooshian, H.H. Jonsson, M. Shiraiwa, A. Zuend, A. Nenes, K.A. Prather, R.C. Flagan, and J.H. Seinfeld, Composition and hygroscopicity of the Los Angeles Aerosol: CalNex, *Journal of Geophysical Research-Atmospheres, 118* (7), 3016-3036, 2013.

Higurashi, A., and T. Nakajima, Detection of aerosol types over the East China Sea near Japan from four-channel satellite data, *Geophysical Research Letters, 29* (17), 2002.

Hoffer, A., A. Gelencser, P. Guyon, G. Kiss, O. Schmid, G.P. Frank, P. Artaxo, and M.O. Andreae, Optical properties of humic-like substances (HULIS) in biomass-burning aerosols, *Atmospheric Chemistry and Physics, 6*, 3563-3570, 2006.

Holben, B.N., T.F. Eck, I. Slutsker, D. Tanre, J.P. Buis, A. Setzer, E. Vermote, J.A. Reagan, Y.J. Kaufman, T. Nakajima, F. Lavenu, I. Jankowiak, and A. Smirnov, AERONET - A federated instrument network and data archive for aerosol characterization, *Remote Sensing of Environment, 66* (1), 1-16, 1998.

Holecek, J.C., M.T. Spencer, and K.A. Prather, Analysis of rainwater samples: Comparison of single particle residues with ambient particle chemistry from the northeast Pacific and Indian oceans, *Journal of Geophysical Research-Atmospheres, 112* (D22), doi:10.1029/2006JD008269, 2007.

Hopkins, R.J., Y. Desyaterik, A.V. Tivanski, R.A. Zaveri, C.M. Berkowitz, T. Tyliszczak, M.K. Gilles, and A. Laskin, Chemical speciation of sulfur in marine cloud droplets and particles: Analysis of individual particles from the marine boundary layer over the California Current, *Journal of Geophysical Research-Atmospheres, 113* (D4), D04209, doi:10.1029/2007JD008954, 2008.

Hudson, P.K., D.M. Murphy, D.J. Cziczo, D.S. Thomson, J.A. de Gouw, C. Warneke, J. Holloway, J.R. Jost, and G. Hubler, Biomass-burning particle measurements: Characteristic composition and chemical processing, *Journal of Geophysical Research-Atmospheres*, *109* (D23), 2004.

Hughes, L.S., J.O. Allen, P. Bhave, M.J. Kleeman, G.R. Cass, D.Y. Liu, D.F. Fergenson, B.D. Morrical, and K.A. Prather, Evolution of atmospheric particles along trajectories crossing the Los Angeles basin, *Environmental Science & Technology*, *34* (15), 3058-3068, 2000.

Hughes, L.S., J.O. Allen, L.G. Salmon, P.R. Mayo, R.J. Johnson, and G.R. Cass, Evolution of nitrogen species air pollutants along trajectories crossing the Los Angeles area, *Environmental Science & Technology*, *36* (18), 3928-3935, 2002.

Jacobson, M.C., H.C. Hansson, K.J. Noone, and R.J. Charlson, Organic atmospheric aerosols: Review and state of the science, *Reviews of Geophysics*, *38* (2), 267-294, 2000.

Jacobson, M.Z., Isolating nitrated and aromatic aerosols and nitrated aromatic gases as sources of ultraviolet light absorption, *Journal of Geophysical Research-Atmospheres*, *104* (D3), 3527-3542, 1999.

Jacobson, M.Z., Strong radiative heating due to the mixing state of black carbon in atmospheric aerosols, *Nature*, *409* (6821), 695-697, 2001.

Jeong, M.J., and Z.Q. Li, Quality, compatibility, and synergy analyses of global aerosol products derived from the advanced very high resolution radiometer and Total Ozone Mapping Spectrometer, *Journal of Geophysical Research-Atmospheres*, *110* (D10), 2005.

Kalapureddy, M.C.R., D.G. Kaskaoutis, P.E. Raj, P.C.S. Devara, H.D. Kambezidis, P.G. Kosmopoulos, and P.T. Nastos, Identification of aerosol type over the Arabian Sea in the premonsoon season during the Integrated Campaign for Aerosols, Gases and Radiation Budget (ICARB), *Journal of Geophysical Research-Atmospheres*, *114*, 2009.

Kanakidou, M., J.H. Seinfeld, S.N. Pandis, I. Barnes, F.J. Dentener, M.C. Facchini, R. Van Dingenen, B. Ervens, A. Nenes, C.J. Nielsen, E. Swietlicki, J.P. Putaud, Y. Balkanski, S. Fuzzi, J. Horth, G.K. Moortgat, R. Winterhalter, C.E.L. Myhre, K. Tsigaridis, E. Vignati, E.G. Stephanou, and J. Wilson, Organic aerosol and global climate modelling: a review, *Atmospheric Chemistry and Physics*, *5*, 1053-1123, 2005.

Kaskaoutis, D.G., P. Kosmopoulos, H.D. Kambezidis, and P.T. Nastos, Aerosol climatology and discrimination of different types over Athens, Greece, based on MODIS data, *Atmospheric Environment*, *41* (34), 7315-7329, 2007.

Kasper, A., S. Aufdenblatten, A. Forss, M. Mohr, and H. Burtscher, Particulate emissions from a low-speed marine diesel engine, *Aerosol Science and Technology*, *41* (1), 24-32, 2007.

Kaufman, Y.J., O. Boucher, D. Tanre, M. Chin, L.A. Remer, and T. Takemura, Aerosol anthropogenic component estimated from satellite data, *Geophysical Research Letters*, *32* (17), 2005.

Khalizov, A.F., R.Y. Zhang, D. Zhang, H.X. Xue, J. Pagels, and P.H. McMurry, Formation of highly hygroscopic soot aerosols upon internal mixing with sulfuric acid vapor, *Journal of Geophysical Research-Atmospheres*, *114* (D5), 2009.

Kim, J., J. Lee, H.C. Lee, A. Higurashi, T. Takemura, and C.H. Song, Consistency of the aerosol type classification from satellite remote sensing during the Atmospheric Brown Cloud-East Asia Regional Experiment campaign, *Journal of Geophysical Research-Atmospheres*, *112* (D22), 2007.

Kirchstetter, T.W., T. Novakov, and P.V. Hobbs, Evidence that the spectral dependence of light absorption by aerosols is affected by organic carbon, *Journal of Geophysical Research-Atmospheres*, *109* (D21), 2004.

Kleeman, M.J., and G.R. Cass, Source contributions to the size and composition distribution of urban particulate air pollution, *Atmospheric Environment*, *32* (16), 2803-2816, 1998.

Kloster, S., F. Dentener, J. Feichter, F. Raes, U. Lohmann, E. Roeckner, and I. Fischer-Bruns, A GCM study of future climate response to aerosol pollution reductions, *Climate Dynamics*, *34* (7-8), 1177-1194, 2010.

Koch, D., Y. Balkanski, S.E. Bauer, R.C. Easter, S. Ferrachat, S.J. Ghan, C. Hoose, T. Iversen, A. Kirkevag, J.E. Kristjansson, X. Liu, U. Lohmann, S. Menon, J. Quaas, M. Schulz, O. Seland, T. Takemura, and N. Yan, Soot microphysical effects on liquid clouds, a multi-model investigation, *Atmospheric Chemistry and Physics*, *11* (3), 1051-1064, 2011.

Koch, D., T.C. Bond, D. Streets, N. Unger, and G.R. van der Werf, Global impacts of aerosols from particular source regions and sectors, *Journal of Geophysical Research-Atmospheres*, *112* (D2), 2007.

Kulmala, M., How particles nucleate and grow, *Science*, *302* (5647), 1000-1001, 2003.

Lack, D.A., and C.D. Cappa, Impact of brown and clear carbon on light absorption enhancement, single scatter albedo and absorption wavelength dependence of black carbon, *Atmospheric Chemistry and Physics*, *10* (9), 4207-4220, 2010.

Lack, D.A., J.J. Corbett, T. Onasch, B. Lerner, P. Massoli, P.K. Quinn, T.S. Bates, D.S. Covert, D. Coffman, B. Sierau, S. Herndon, J. Allan, T. Baynard, E. Lovejoy, A.R. Ravishankara, and E. Williams, Particulate emissions from commercial shipping: Chemical, physical, and optical properties, *Journal of Geophysical Research-Atmospheres*, *114*, D00F04, doi:10.1029/2008JD011300, 2009.

Langridge, J.M., D. Lack, C.A. Brock, R. Bahreini, A.M. Middlebrook, J.A. Neuman, J.B. Nowak, A.E. Perring, J.P. Schwarz, J.R. Spackman, J.S. Holloway, I.B. Pollack, T.B. Ryerson, J.M. Roberts, C. Warneke, J.A. de Gouw, M.K. Trainer, and D.M. Murphy, Evolution of aerosol properties impacting visibility and direct climate forcing in an ammonia-rich urban environment, *Journal of Geophysical Research-Atmospheres*, *117*, 2012.

Laskin, A., R.C. Moffet, M.K. Gilles, J.D. Fast, R.A. Zaveri, B. Wang, P. Nigge, and J. Shutthanandan, Tropospheric chemistry of internally mixed sea salt and organic particles: Surprising reactivity of NaCl with weak organic acids, *Journal of Geophysical Research*, *117*, D15302, doi:10.1029/2012JD017743, 2012.

Leibensperger, E.M., L.J. Mickley, D.J. Jacob, W.T. Chen, J.H. Seinfeld, A. Nenes, P.J. Adams, D.G. Streets, N. Kumar, and D. Rind, Climatic effects of 1950-2050 changes in US anthropogenic aerosols - Part 2: Climate response, *Atmospheric Chemistry and Physics*, *12* (7), 3349-3362, 2012.

Liu, D.-Y., K.A. Prather, and S.V. Herring, Variations in the size and chemical composition of nitrate-containing particles in Riverside, CA, *Aerosol Science and Technology*, *33* (1-2), 71-86, 2000.

Liu, P., P.J. Ziemann, D.B. Kittelson, and P.H. Mcmurry, Generating Particle Beams of Controlled Dimensions and Divergence .1. Theory of Particle Motion in Aerodynamic Lenses and Nozzle Expansions, *Aerosol Science and Technology*, *22* (3), 293-313, 1995a.

Liu, P., P.J. Ziemann, D.B. Kittelson, and P.H. Mcmurry, Generating Particle Beams of Controlled Dimensions and Divergence .2. Experimental Evaluation of Particle Motion in

Aerodynamic Lenses and Nozzle Expansions, *Aerosol Science and Technology*, *22* (3), 314-324, 1995b.

Magi, B.I., P. Ginoux, Y. Ming, and V. Ramaswamy, Evaluation of tropical and extratropical Southern Hemisphere African aerosol properties simulated by a climate model, *Journal of Geophysical Research-Atmospheres*, *114*, 2009.

Magliano, K.L., V.M. Hughes, L.R. Chinkin, D.L. Coe, T.L. Haste, N. Kumar, and F.W. Lurmann, Spatial and temporal variations in PM_{10} and $PM_{2.5}$ source contributions and comparison to emissions during the 1995 integrated monitoring study, *Atmospheric Environment*, *33* (29), 4757-4773, 1999.

Maricq, M.M., Chemical characterization of particulate emissions from diesel engines: A review, *Journal of Aerosol Science*, *38* (11), 1079-1118, 2007.

Mayol-Bracero, O.L., P. Guyon, B. Graham, G. Roberts, M.O. Andreae, S. Decesari, M.C. Facchini, S. Fuzzi, and P. Artaxo, Water-soluble organic compounds in biomass burning aerosols over Amazonia - 2. Apportionment of the chemical composition and importance of the polyacidic fraction, *Journal of Geophysical Research-Atmospheres*, *107* (D20), 8091, doi:10.1029/2001JD000522, 2002.

McLafferty, F.W., and F. Turecek, *Interpretation of Mass Spetra*, University Science Books, Sausalito, CA, 1993.

Meloni, D., A. di Sarra, G. Pace, and F. Monteleone, Aerosol optical properties at Lampedusa (Central Mediterranean). 2. Determination of single scattering albedo at two wavelengths for different aerosol types, *Atmospheric Chemistry and Physics*, *6*, 715-727, 2006.

Meng, Z., and J.H. Seinfeld, On the source of the submicrometer droplet mode of urban and regional aerosols, *Aerosol Science and Technology*, *20*, 253-265, 1994.

Metcalf, A.R., J.S. Craven, J.J. Ensberg, J. Brioude, W. Angevine, A. Sorooshian, H.T. Duong, H.H. Jonsson, R.C. Flagan, and J.H. Seinfeld, Black carbon aerosol over the Los Angeles Basin during CalNex, *J. Geophys. Res.*, *117*, D00V13, 2012.

Mickley, L.J., E.M. Leibensperger, D.J. Jacob, and D. Rind, Regional warming from aerosol removal over the United States: Results from a transient 2010-2050 climate simulation, *Atmospheric Environment*, *46*, 545-553, 2012.

Mielonen, T., A. Arola, M. Komppula, J. Kukkonen, J. Koskinen, G. de Leeuw, and K.E.J. Lehtinen, Comparison of CALIOP level 2 aerosol subtypes to aerosol types derived from AERONET inversion data, *Geophysical Research Letters*, *36*, 2009.

Mochida, M., M. Kuwata, T. Miyakawa, N. Takegawa, K. Kawamura, and Y. Kondo, Relationship between hygroscopicity and cloud condensation nuclei activity for urban aerosols in Tokyo, *Journal of Geophysical Research-Atmospheres*, *111* (D23), 2006.

Moffet, R.C., Y. Desyaterik, R.J. Hopkins, A.V. Tivanski, M.K. Gilles, Y. Wang, V. Shutthanandan, L.T. Molina, R.G. Abraham, K.S. Johnson, V. Mugica, M.J. Molina, A. Laskin, and K.A. Prather, Characterization of aerosols containing Zn, Pb, and Cl from an industrial region of Mexico City, *Environmental Science & Technology*, *42* (19), 7091-7097, 2008.

Moffet, R.C., T. Henn, A. Laskin, and M.K. Gilles, Automated Chemical Analysis of Internally Mixed Aerosol Particles Using X-ray Spectromicroscopy at the Carbon K-Edge, *Anal Chem*, *82* (19), 7906-7914, 2010.

Moffet, R.C., and K.A. Prather, In-situ measurements of the mixing state and optical properties of soot with implications for radiative forcing estimates, *Proceedings of the National Academy of Sciences of the United States of America*, *106* (29), 11872-7, 2009.

Monahan, E.C., C.W. Fairall, K.L. Davidson, and P.J. Boyle, Observed interrelations between 10m winds, ocean whitecaps and marine aerosols, *Quarterly Journal of the Royal Meteorological Society*, *109* (460), 379-392, 1983.

Morrical, B.D., D.P. Fergenson, and K.A. Prather, Coupling two-step laser desorption/ionization with aerosol time-of-flight mass spectrometry for the analysis of individual organic particles, *Journal of the American Society for Mass Spectrometry*, *9* (10), 1068-1073, 1998.

Murphy, D.M., D.J. Cziczo, P.K. Hudson, and D.S. Thomson, Carbonaceous material in aerosol particles in the lower stratosphere and tropopause region, *Journal of Geophysical Research*, *112* (D4), 2007.

Murphy, D.M., and D.S. Thomson, Laser Ionization Mass Spectroscopy of Single Aerosol Particles, *Aerosol Science and Technology*, *22* (3), 237-249, 1995.

Murphy, S.M.A., H.; Sorooshian, A.; Padro, L. T.; Gates,, S.W. H.; Hersey, W. A.; Jung, H.; Miller, J. W.; Cocker, D. R.;, and A.J. Nenes, H. H.; Flagan, R. C.; Seinfeld, J. H., Comprehensive simultaneous shipboard and airborne characterization of exhaust from a modern container ship at sea., *Environmental Science & Technology*, *43* (13), 4626-4640, 2009.

Myhre, G., C.R. Hoyle, T.F. Berglen, B.T. Johnson, and J.M. Haywood, Modeling of the solar radiative impact of biomass burning aerosols during the Dust and Biomass-burning Experiment (DABEX), *Journal of Geophysical Research-Atmospheres*, *113*, 2008.

Na, K., A.A. Sawant, C. Song, and D.R. Cocker, Primary and secondary carbonaceous species in the atmosphere of Western Riverside County, California, *Atmos Environ*, *38*, 1345-1355, 2004.

Naoe, H., S. Hasegawa, J. Heintzenberg, K. Okada, A. Uchiyama, Y. Zaizen, E. Kobayashi, and A. Yamazaki, State of mixture of atmospheric submicrometer black carbon particles and its effect on particulate light absorption, *Atmospheric Environment*, *43* (6), 1296-1301, 2009.

Neubauer, K.R., M.V. Johnston, and A.S. Wexler, On-line analysis of aqueous aerosols by laser desorption ionization, *International Journal of Mass Spectrometry and Ion Processes*, *163* (1-2), 29-37, 1997.

Neubauer, K.R., M.V. Johnston, and A.S. Wexler, Humidity effects on the mass spectra of single aerosol particles, *Atmospheric Environment*, *32* (14-15), 2521-2529, 1998.

Ng, N.L., A.J. Kwan, J.D. Surratt, A.W.H. Chan, P.S. Chhabra, A. Sorooshian, H.O.T. Pye, J.D. Crounse, P.O. Wennberg, R.C. Flagan, and J.H. Seinfeld, Secondary organic aerosol (SOA) formation from reaction of isoprene with nitrate radicals (NO_3), *Atmospheric Chemistry and Physics*, *8* (14), 4117-4140, 2008.

Nguyen, T.B., P.J. Roach, J. Laskin, A. Laskin, and S.A. Nizkorodov, Effect of humidity on the composition of isoprene photooxidation secondary organic aerosol, *Atmospheric Chemistry and Physics*, *11*, 6931-6944, 2011.

Noble, C.A., and K.A. Prather, Real-time measurement of correlated size and composition profiles of individual atmospheric aerosol particles, *Environ Sci Technol*, *30* (9), 2667-2680, 1996.

O'Dowd, C.D., and G. De Leeuw, Marine aerosol production: a review of the current knowledge, *Philosophical Transactions of the Royal Society a-Mathematical Physical and Engineering Sciences*, *365* (1856), 1753-1774, 2007.

Ogren, J.A., Comment on oCalibration and Intercomparison of Filter-Based Measurements of Visible Light Absorption by Aerosolso, *Aerosol Science and Technology*, *44* (8), 589-591, 2010.

Ovadnevaite, J., C. O'Dowd, M. Dall'Osto, D. Ceburnis, D.R. Worsnop, and H. Berresheim, Detecting high contributions of primary organic matter to marine aerosol: A case study, *Geophysical Research Letters*, *38*, L02807, doi:10.1029/2010GL046083, 2011.

Pastor, S.H., J.O. Allen, L.S. Hughes, P. Bhave, G.R. Cass, and K.A. Prather, Ambient single particle analysis in Riverside, California by aerosol time-of-flight mass spectrometry during the SCOS97-NARSTO, *Atmospheric Environment*, *37*, 239-258, 2003.

Petters, M.D., and S.M. Kreidenweis, A single parameter representation of hygroscopic growth and cloud condensation nucleus activity, *Atmospheric Chemistry and Physics*, *7* (8), 1961-1971, 2007.

Petters, M.D., A.J. Prenni, S.M. Kreidenweis, P.J. DeMott, A. Matsunaga, Y.B. Lim, and P.J. Ziemann, Chemical aging and the hydrophobic-to-hydrophilic conversion of carbonaceous aerosol, *Geophysical Research Letters*, *33* (24), 2006.

Poschl, U., Atmospheric aerosols: composition, transformation, climate and health effects, *Angewandte Chemie*, *44* (46), 7520-40, 2005.

Prather, K.A., C.D. Hatch, and V.H. Grassian, Analysis of atmospheric aerosols, *Annu Rev Anal Chem (Palo Alto Calif)*, *1* (1), 485-514, 2008.

Prather, K.A., T. Nordmeyer, and K. Salt, Real-Time Characterization of Individual Aerosol-Particles Using Time-of-Flight Mass-Spectrometry, *Analytical Chemistry*, *66* (9), 1403-1407, 1994.

Pratt, K.A., L.E. Hatch, and K.A. Prather, Seasonal volatility dependence of ambient particle phase amines, *Environmental Science & Technology*, *43* (14), 5276-5281, 2009a.

Pratt, K.A., A.J. Heymsfield, C.H. Twohy, S.M. Murphy, P.J. DeMott, J.G. Hudson, R. Subramanian, Z.E. Wang, J.H. Seinfeld, and K.A. Prather, In Situ Chemical Characterization of Aged Biomass-Burning Aerosols Impacting Cold Wave Clouds, *Journal of the Atmospheric Sciences*, *67* (8), 2451-2468, 2010.

Pratt, K.A., J.E. Mayer, J.C. Holecek, R.C. Moffet, R.O. Sanchez, T.P. Rebotier, H. Furutani, M. Gonin, K. Fuhrer, Y. Su, S. Guazzotti, and K.A. Prather, Development and Characterization of an Aircraft Aerosol Time-of-Flight Mass Spectrometer, *Anal Chem*, *81* (5), 1792-1800, 2009b.

Pratt, K.A., and K.A. Prather, Real-Time, Single-Particle Volatility, Size, and Chemical Composition Measurements of Aged Urban Aerosols, *Environ Sci Technol*, *43* (21), 8276-8282, 2009.

Pratt, K.A., and K.A. Prather, Aircraft measurements of vertical profiles of aerosol mixing states, *Journal of Geophysical Research*, *115* (D11), 2010.

Pratt, K.A., and K.A. Prather, Mass spectrometry of atmospheric aerosols—Recent developments and applications. Part II: On-line mass spectrometry techniques, *Mass Spectrometry Reviews*, DOI 10.1002/mas.20330, 2011.

Qin, X., K.A. Pratt, L.G. Shields, S.M. Toner, and K.A. Prather, Seasonal Comparisons of Single-Particle Chemical Mixing State in Riverside, CA, *Submitted to Atmospheric Environment*, 2012.

Qin, X.Y., P.V. Bhave, and K.A. Prather, Comparison of two methods for obtaining quantitative mass concentrations from aerosol time-of-flight mass spectrometry measurements, *Analytical Chemistry*, *78* (17), 6169-6178, 2006.

Qin, X.Y., and K.A. Prather, Impact of biomass emissions on particle chemistry during the California Regional Particulate Air Quality Study, *International Journal of Mass Spectrometry*, *258* (1-3), 142-150, 2006.

Ramanathan, V., and G. Carmichael, Global and regional climate changes due to black carbon, *Nature Geoscience*, *1* (4), 221-227, 2008.

Ramanathan, V., M.V. Ramana, G. Roberts, D. Kim, C. Corrigan, C. Chung, and D. Winker, Warming trends in Asia amplified by brown cloud solar absorption, *Nature*, *448* (7153), 575-8, 2007.

Rebotier, T.P., and K.A. Prather, Aerosol time-of-flight mass spectrometry data analysis: a benchmark of clustering algorithms, *Analytica chimica acta*, *585* (1), 38-54, 2007.

Reid, J.S., R. Koppmann, T.F. Eck, and D.P. Eleuterio, A review of biomass burning emissions part II: intensive physical properties of biomass burning particles, *Atmospheric Chemistry and Physics*, *5*, 799-825, 2005.

Riemer, N., M. West, R. Zaveri, and R. Easter, Estimating black carbon aging time-scales with a particle-resolved aerosol model, *Journal of Aerosol Science*, *41* (1), 143-158, 2010.

Roberts, G.C., and A. Nenes, A continuous-flow streamwise thermal-gradient CCN chamber for atmospheric measurements, *Aerosol Science and Technology*, *39* (3), 206-221, 2005.

Rollins, A.W., E.C. Browne, K.-E. Min, S.E. Pusede, P.J. Wooldridge, D.R. Gentner, A.H. Goldstein, S. Liu, D.A. Day, L.M. Russell, and R.C. Cohen, Evidence for NO_x control over nighttime SOA formation, *Science*, *337* (6099), 1210-1212, 2012.

Rosenfeld, D., and A. Givati, Evidence of orographic precipitation suppression by air pollution-induced aerosols in the western United States, *Journal of Applied Meteorology and Climatology*, *45* (7), 893-911, 2006.

Rudich, Y., Laboratory perspectives on the chemical transformations of organic matter in atmospheric particles, *Chemical Reviews*, *103* (12), 5097-5124, 2003.

Rudich, Y., N.M. Donahue, and T.F. Mentel, Aging of organic aerosol: bridging the gap between laboratory and field studies, *Annu Rev Phys Chem*, *58* (1), 321-52, 2007.

Russell, L.M., R. Bahadur, and P.J. Ziemann, Identifying organic aerosol sources by comparing functional group composition in chamber and atmospheric particles, *Proceedings of the National Academy of Sciences of the United States of America*, doi:10.1073/pnas.1006461108, 2011.

Russell, L.M., L.N. Hawkins, A.A. Frossard, P.K. Quinn, and T.S. Bates, Carbohydrate-like composition of submicron atmospheric particles and their production from ocean bubble bursting, *Proceedings of the National Academy of Sciences of the United States of America*, *107* (15), 6652-6657, 2010.

Russell, L.M., K.J. Noone, R.J. Ferek, R.A. Pockalny, R.C. Flagan, and J.H. Seinfeld, Combustion organic aerosol as cloud condensation nuclei in ship tracks, *American Meteorological Society*, 2591-2606, 2000.

Russell, L.M., S. Takahama, S. Liu, L.N. Hawkins, D.S. Covert, P.K. Quinn, and T.S. Bates, Oxygenated fraction and mass of organic aerosol from direct emission and atmospheric processing measured on the R/V Ronald Brown during TEXAQS/GoMACCS 2006, *Journal of Geophysical Research-Atmospheres*, *114*, D00F05, doi:10.1029/2008JD011275, 2009.

Russell, S.C., Microorganism characterization by single particle mass spectrometry, *Mass spectrometry reviews*, *28* (2), 376-87, 2009.

Schade, G.W., and P.J. Crutzen, Emission of aliphatic amines from animal husbandry and their reactions: Potential source of N_2O and HCN, *Journal of Atmospheric Chemistry, 22* (3), 319-346, 1995.

Schmid, B., R. Ferrare, C. Flynn, R. Elleman, D. Covert, A. Strawa, E. Welton, D. Turner, H. Jonsson, J. Redemann, J. Eilers, K. Ricci, A.G. Hallar, M. Clayton, J. Michalsky, A. Smirnov, B. Holben, and J. Barnard, How well do state-of-the-art techniques measuring the vertical profile of tropospheric aerosol extinction compare?, *Journal of Geophysical Research-Atmospheres, 111* (D5), 2006.

Schnaiter, M., C. Linke, O. Mohler, K.H. Naumann, H. Saathoff, R. Wagner, U. Schurath, and B. Wehner, Absorption amplification of black carbon internally mixed with secondary organic aerosol, *Journal of Geophysical Research-Atmospheres*, *110* (D19), 2005.

Schultz, P., and T.T. Warner, Characteristics of Summertime Circulations and Pollutant Ventilation in the Los-Angeles Basin, *Journal of Applied Meteorology, 21* (5), 672-682, 1982.

Schuster, G.L., O. Dubovik, and B.N. Holben, Angstrom exponent and bimodal aerosol size distributions, *Journal of Geophysical Research-Atmospheres*, *111* (D7), 2006.

Schwarz, J.P., J.R. Spackman, D.W. Fahey, R.S. Gao, U. Lohmann, P. Stier, L.A. Watts, D.S. Thomson, D.A. Lack, L. Pfister, M.J. Mahoney, D. Baumgardner, J.C. Wilson, and J.M. Reeves, Coatings and their enhancement of black carbon light absorption in the tropical atmosphere, *Journal of Geophysical Research-Atmospheres*, *113* (D3), 2008.

Setyan, A., Q. Zhang, M. Merkel, W.B. Knighton, Y. Sun, C. Song, J.E. Shilling, T.B. Onasch, S.C. Herndon, D. Worsnop, J.D. Fast, R.A. Zaveri, L.K. Berg, A. Wiedensohler, B.A. Flowers, M.K. Dubey, and R. Subramanian, Characterization of submicron particles influenced by mixed biogenic and anthropogenic using high-resolution aerosol mass spectrometry: Results from CARES, *Atmospheric Chemistry and Physics*, *12*, 8131-8156, 2012.

Shields, L.G., D.T. Suess, and K.A. Prather, Determination of single particle mass spectral signatures from heavy-duty diesel vehicle emissions for $PM_{2.5}$ source apportionment, *Atmospheric Environment*, *41* (18), 3841-3852, 2007.

Silva, P.J., D.Y. Liu, C.A. Noble, and K.A. Prather, Size and chemical characterization of individual particles resulting from biomass burning of local Southern California species, *Environ Sci Technol*, *33* (18), 3068-3076, 1999.

Silva, P.J., and K.A. Prather, Interpretation of Mass Spectra from Organic Compounds in Aerosol Time-of-Flight Mass Spectrometry, *Anal Chem*, *72* (15), 3553-3562, 2000.

Singh, M., P.A. Jaques, and C. Sioutas, Size distribution and diurnal characteristics of particle-bound metals in source and receptor sites of the Los Angeles Basin, *Atmospheric Environment*, *36* (10), 1675-1689, 2002.

Smirnov, A., B.N. Holben, D.M. Giles, I. Slutsker, N.T. O'Neill, T.F. Eck, A. Macke, P. Croot, Y. Courcoux, S.M. Sakerin, T.J. Smyth, T. Zielinski, G. Zibordi, J.I. Goes, M.J. Harvey, P.K. Quinn, N.B. Nelson, V.F. Radionov, C.M. Duarte, R. Losno, J. Sciare, K.J. Voss, S. Kinne, N.R. Nalli, E. Joseph, K.K. Moorthy, D.S. Covert, S.K. Gulev, G. Milinevsky, P. Larouche, S. Belanger, E. Horne, M. Chin, L.A. Remer, R.A. Kahn, J.S. Reid, M. Schulz, C.L. Heald, J. Zhang, K. Lapina, R.G. Kleidman, J. Griesfeller, B.J. Gaitley, Q. Tan, and T.L. Diehl, Maritime aerosol network as a component of AERONET - first results and comparison with global aerosol models and satellite retrievals, *Atmospheric Measurement Techniques*, *4* (3), 583-597, 2011.

Smirnov, A., B.N. Holben, Y.J. Kaufman, O. Dubovik, T.F. Eck, I. Slutsker, C. Pietras, and R.N. Halthore, Optical properties of atmospheric aerosol in maritime environments, *Journal of the Atmospheric Sciences*, *59* (3), 501-523, 2002.

Smith, J.N., M.J. Dunn, T.M. VanReken, K. Iida, M.R. Stolzenburg, P.H. McMurry, and L.G. Huey, Chemical composition of atmospheric nanoparticles formed from nucleation in Tecamac, Mexico: Evidence for an important role for organic species in nanoparticle growth, *Geophysical Research Letters*, *35* (4), L04808, doi:10.1029/2007GL032523, 2008.

Sodeman, D.A., S.M. Toner, and K.A. Prather, Determination of single particle mass spectral signatures from light-duty vehicle emissions, *Environmental Science & Technology*, *39* (12), 4569-4580, 2005.

Solomon, S., D. Qin, M. Manning, Z. Chen, M. Marquis, K.B. Averyt, M. Tignor, and H.L. Miller, Climate Change 2007: The Physical Science Basis. Contribution of Working Group I to the Fourth Assesmnet Report of the Intergovernmental Panel on Climate Change, Cambridge University Press, 2007.

Song, X.H., P.K. Hopke, D.P. Fergenson, and K.A. Prather, Classification of single particles analyzed by ATOFMS using an artificial neural network, ART-2A, *Anal Chem*, *71* (4), 860-865, 1999.

Sorooshian, A., S. Hersey, F.J. Brechtel, A. Corless, R.C. Flagan, and J.H. Seinfeld, Rapid, size-resolved aerosol hygroscopic growth measurements: Differential aerosol sizing and hygroscopicity spectrometer probe (DASH-SP), *Aerosol Science and Technology*, *42* (6), 445-464, 2008a.

Sorooshian, A., S.N. Murphy, S. Hersey, H. Gates, L.T. Padro, A. Nenes, F.J. Brechtel, H. Jonsson, R.C. Flagan, and J.H. Seinfeld, Comprehensive airborne characterization of aerosol from a major bovine source, *Atmospheric Chemistry and Physics*, *8* (17), 5489-5520, 2008b.

Sorooshian, A., L.T. Padro, A. Nenes, G. Feingold, A. McComiskey, S.P. Hersey, H. Gates, H.H. Jonsson, S.D. Miller, G.L. Stephens, R.C. Flagan, and J.H. Seinfeld, On the link between ocean biota emissions, aerosol, and maritime clouds: Airborne, ground, and satellite measurements off the coast of California, *Global Biogeochemical Cycles*, *23*, GB4007, doi:10.1029/2009GB003464, 2009.

Spencer, M.T., and K.A. Prather, Using ATOFMS to determine OC/EC mass fractions in particles, *Aerosol Science and Technology*, *40* (8), 585-594, 2006.

Spencer, M.T., L.G. Shields, D.A. Sodeman, S.M. Toner, and K.A. Prather, Comparison of oil and fuel particle chemical signatures with particle emissions from heavy and light duty vehicles, *Atmospheric Environment*, *40* (27), 5224-5235, 2006.

Srivastava, A., M.E. Pitesky, P.T. Steele, H.J. Tobias, D.P. Fergenson, J.M. Horn, S.C. Russell, G.A. Czerwieniec, C.S. Lebrilla, E.E. Gard, and M. Frank, Comprehensive assignment of mass spectral signatures from individual Bacillus atrophaeus spores in matrix-free laser desorption/ionization bioaerosol mass spectrometry, *Analytical Chemistry*, *77* (10), 3315-3323, 2005.

Steele, P.T., H.J. Tobias, D.P. Fergenson, M.E. Pitesky, J.M. Horn, G.A. Czerwieniec, S.C. Russell, C.B. Lebrilla, E.E. Gard, and M. Frank, Laser power dependence of mass spectral signatures from individual bacterial spores in bioaerosol mass spectrometry, *Anal Chem*, *75* (20), 5480-5487, 2003.

Sullivan, R.C., and K.A. Prather, Recent advances in our understanding of atmospheric chemistry and climate made possible by on-line aerosol analysis instrumentation, *Analytical Chemistry*, *77* (12), 3861-3885, 2005.

Toner, S.M., L.G. Shields, D.A. Sodeman, and K.A. Prather, Using mass spectral source signatures to apportion exhaust particles from gasoline and diesel powered vehicles in a freeway study using UF-ATOFMS, *Atmospheric Environment*, *42* (3), 568-581, 2008.

Torres, O., P.K. Bhartia, A. Sinyuk, E.J. Welton, and B. Holben, Total Ozone Mapping Spectrometer measurements of aerosol absorption from space: Comparison to SAFARI 2000 ground-based observations, *Journal of Geophysical Research-Atmospheres*, *110* (D10), 2005.

Twohy, C.H., M.D. Petters, J.R. Snider, B. Stevens, W. Tahnk, M. Wetzel, L. Russell, and F. Burnet, Evaluation of the aerosol indirect effect in marine stratocumulus clouds: Droplet number, size, liquid water path, and radiative impact, *Journal of Geophysical Research-Atmospheres*, *110* (D8), doi:10.1029/2004JD005116, 2005.

Ulrickson, B.L., and C.F. Mass, Numerical Investigation of Mesoscale Circulations over the Los-Angeles Basin .2. Synoptic Influences and Pollutant Transport, *Monthly Weather Review*, *118* (10), 2162-2184, 1990.

Vogt, R., P.J. Crutzen, and R. Sander, A mechanism for halogen release from sea-salt aerosol in the remote marine boundary layer, *Nature*, *383* (6598), 327-330, 1996.

Wang, J., M.J. Cubison, A.C. Aiken, J.L. Jimenez, and D.R. Collins, The importance of aerosol mixing state and size-resolved composition on CCN concentration and the variation of the importance with atmospheric aging of aerosols, *Atmospheric Chemistry and Physics*, *10* (15), 7267-7283, 2010.

Weiss-Penzias, P.S., E.J. Williams, B.M. Lerner, T.S. Bates, C. Gaston, K. Prather, A. Vlasenko, and S.M. Li, Shipboard measurements of gaseous elemental mercury along the coast of Central and Southern California, *Journal of Geophysical Research-Atmospheres*, *118* (1), 208-219, 2013.

Wenzel, R.J., D.Y. Liu, E.S. Edgerton, and K.A. Prather, Aerosol time-of-flight mass spectrometry during the Atlanta Supersite Experiment: 2. Scaling procedures, *Journal of Geophysical Research-Atmospheres*, *108* (D7), 8427,doi:10.1029/2001JD001563, 2003.

Wenzel, R.J., and K.A. Prather, Improvements in ion signal reproducibility obtained using a homogeneous laser beam for on-line laser desorption/ionization of single particles, *Rapid Communications in Mass Spectrometry*, *18* (13), 1525-1533, 2004.

Whiteaker, J.R., D.T. Suess, and K.A. Prather, Effects of meteorological conditions on aerosol composition and mixing state in Bakersfield, CA, *Environ Sci Technol*, *36* (11), 2345-2353, 2002.

Ying, Q., and M.J. Kleeman, Source contributions to the regional distribution of secondary particulate matter in California, *Atmospheric Environment*, *40* (4), 736-752, 2006.

Yu, H.B., M. Chin, L.A. Remer, R.G. Kleidman, N. Bellouin, H.S. Bian, and T. Diehl, Variability of marine aerosol fine-mode fraction and estimates of anthropogenic aerosol component over cloud-free oceans from the Moderate Resolution Imaging Spectroradiometer (MODIS), *Journal of Geophysical Research-Atmospheres*, *114*, 2009.

Zaremba, L.L., and J.J. Carroll, Summer wind flow regimes over the Sacramento Valley, *Journal of Applied Meteorology*, *38* (10), 1463-1473, 1999.

Zaveri, R.A., J.C. Barnard, R.C. Easter, N. Riemer, and M. West, Particle-resolved simulation of aerosol size, composition, mixing state, and the associated optical and cloud condensation

nuclei activation properties in an evolving urban plume, *Journal of Geophysical Research-Atmospheres*, *115*, 2010.

Zaveri, R.A., W.J. Shaw, D.J. Cziczo, B. Schmid, R.A. Ferrare, M.L. Alexander, M. Alexandrov, R.J. Alvarez, W.P. Arnott, D.B. Atkinson, S. Baidar, R.M. Banta, J.C. Barnard, J. Beranek, L.K. Berg, F. Brechtel, W.A. Brewer, J.F. Cahill, B. Cairns, C.D. Cappa, D. Chand, S. China, J.M. Comstock, M.K. Dubey, R.C. Easter, M.H. Erickson, J.D. Fast, C. Floerchinger, B.A. Flowers, E. Fortner, J.S. Gaffney, M.K. Gilles, K. Gorkowski, W.I. Gustafson, M. Gyawali, J. Hair, R.M. Hardesty, J.W. Harworth, S. Herndon, N. Hiranuma, C. Hostetler, J.M. Hubbe, J.T. Jayne, H. Jeong, B.T. Jobson, E.I. Kassianov, L.I. Kleinman, C. Kluzek, B. Knighton, K.R. Kolesar, C. Kuang, A. KubC!tovC, A.O. Langford, A. Laskin, N. Laulainen, R.D. Marchbanks, C. Mazzoleni, F. Mei, R.C. Moffet, D. Nelson, M.D. Obland, H. Oetjen, T.B. Onasch, I. Ortega, M. Ottaviani, M. Pekour, K.A. Prather, J.G. Radney, R.R. Rogers, S.P. Sandberg, A. Sedlacek, C.J. Senff, G. Senum, A. Setyan, J.E. Shilling, M. Shrivastava, C. Song, S.R. Springston, R. Subramanian, K. Suski, J. Tomlinson, R. Volkamer, H.W. Wallace, J. Wang, A.M. Weickmann, D.R. Worsnop, X.Y. Yu, A. Zelenyuk, and Q. Zhang, Overview of the 2010 Carbonaceous Aerosols and Radiative Effects Study (CARES), *Atmos. Chem. Phys.*, *12* (16), 7647-7687, 2012.

Zelenyuk, A., and D. Imre, Single particle laser ablation time-of-flight mass spectrometer: An introduction to SPLAT, *Aerosol Science and Technology*, *39* (6), 554-568, 2005.

Zelenyuk, A., D. Imre, M. Earle, R. Easter, A. Korolev, R. Leaitch, P. Liu, A.M. Macdonald, M. Ovchinnikov, and W. Strapp, In situ characterization of cloud condensation nuclei, interstitial, and background particles using the single particle mass spectrometer, SPLAT II, *Anal Chem*, *82* (19), 7943-51, 2010.

Zhang, Q., C.O. Stanier, M.R. Canagaratna, J.T. Jayne, D.R. Worsnop, S.N. Pandis, and J.L. Jimenez, Insights into the chemistry of new particle formation and growth events in Pittsburgh based on aerosol mass spectrometry, *Environmental Science & Technology*, *38* (18), 4797-4809, 2004.

Publications

1. The impact of shipping, agricultural, and urban emissions on single particle chemistry observed aboard the R/V Atlantis during CalNex. C. J. Gaston, P. K. Quinn, T. S. Bates, J. B. Gilman, D. M. Bon, W. C. Kuster, and K. A. Prather. *Journal of Geophysical Research-Atmospheres*, 118, 5003–5017, 2013.
2. The mixing state of carbonaceous aerosol particles in northern and southern California measured during CARES and CalNex 2010. J. F. Cahill, K. Suski, J. H. Seinfeld, R. A. Zaveri, and K. A. Prather. *Atmos. Chem. Phys.*, 12, 10989–11002, 2012.
3. Relating aerosol absorption due to soot, organic carbon, and dust to emission sources determined from in-situ chemical measurements. A. Cazorla, R. Bahadur, K. J. Suski, J. F. Cahill, D. Chand, B. Schmid, V. Ramanathan, and K. Prather. *Atmos. Chem. Phys.* 13, 9337-9350, 2013.
4. Composition and hygroscopicity of the Los Angeles Aerosol: CalNex. S.P. Hersey, J.S. Craven, A.R. Metcalf, J. Lin, T. Lathem, K.J. Suski, J.F. Cahill, H.T. Duong, A. Sorooshian, H.H. Jonsson, M. Shiraiwa, A. Zuend, A. Nenes, K.A. Prather, R.C. Flagan, and J.H. Seinfeld. *Journal of Geophysical Research-Atmospheres*, 118, 3016-3036, 2013.
5. Overview of the 2010 Carbonaceous Aerosols and Radiative Effects Study (CARES). Zaveri, R.A., W.J. Shaw, D.J. Cziczo, B. Schmid, R.A. Ferrare, M.L. Alexander, M. Alexandrov, R.J. Alvarez, W.P. Arnott, D.B. Atkinson, S. Baidar, R.M. Banta, J.C. Barnard, J. Beranek, L.K. Berg, F. Brechtel, W.A. Brewer, J.F. Cahill, B. Cairns, C.D. Cappa, D. Chand, S. China, J.M. Comstock, M.K. Dubey, R.C. Easter, M.H. Erickson, J.D. Fast, C. Floerchinger, B.A. Flowers, E. Fortner, J.S. Gaffney, M.K. Gilles, K. Gorkowski, W.I. Gustafson, M. Gyawali, J. Hair, R.M. Hardesty, J.W. Harworth, S. Herndon, N. Hiranuma, C. Hostetler, J.M. Hubbe, J.T. Jayne, H. Jeong, B.T. Jobson, E.I. Kassianov, L.I. Kleinman, C. Kluzek, B. Knighton, K.R. Kolesar, C. Kuang, A. KubC!tovC, A.O. Langford, A. Laskin, N. Laulainen, R.D. Marchbanks, C. Mazzoleni, F. Mei, R.C. Moffet, D. Nelson, M.D. Obland, H. Oetjen, T.B. Onasch, I. Ortega, M. Ottaviani, M. Pekour, K.A. Prather, J.G. Radney, R.R. Rogers, S.P. Sandberg, A. Sedlacek, C.J. Senff, G. Senum, A. Setyan, J.E. Shilling, M. Shrivastava, C. Song, S.R. Springston, R. Subramanian, K. Suski, J. Tomlinson, R. Volkamer, H.W. Wallace, J. Wang, A.M. Weickmann, D.R. Worsnop, X.Y. Yu, A. Zelenyuk, and Q. Zhang. *Atmos. Chem. Phys.*, 12, 7647-7687, 2012.
6. Shipboard measurements of gaseous elemental mercury along the coast of Central and Southern California. Weiss-Penzias, P.S., E.J. Williams, B.M. Lerner, T.S. Bates, C. Gaston, K. Prather, A. Vlasenko, and S.M. Li. *Journal of Geophysical Research-Atmospheres*, 118, 208-219, 2013